RUPRECHT-KARLS-UNIVERSITÄT HEIDELBERG
FACULTY OF ENGINEERING SCIENCES

DISSERTATION

THE EMERGENT PROPERTIES OF PC12 POPULATIONS IN CONFINEMENT

To attain the academic degree
Doctor of Engineering Sciences
(Dr.-Ing.)

submitted by
Stephen Louis Casale, M. Sc.

Heidelberg, Thursday 8th May 2025

THE EMERGENT PROPERTIES OF PC12 POPULATIONS IN CONFINEMENT

Date of submission: Thursday 8th May 2025

1. Examiner: Prof. Dr. Christine Selhuber-Unkel
2. Examiner: Prof. Dr. Dr. Ada Cavalcanti-Adam

Abstract

This study explores neuron-like PC12 behavior in vitro with a focus on neuronal interactions within confined microenvironments, addressing a gap in neurobiological research related to spatially constrained neuron behavior. While previous studies have examined neuronal interactions with synthetic structures, how neuron populations selectively navigate confined areas has been underinvestigated. This work interrogates neuronal responses to spatial constraints by confining neuron-like PC12 cell populations inside 3D-printed microenvironments on glass substrates. The microenvironments enable localized interaction with neighboring cells and the printed structure. Key parameters analyzed include neurite outgrowth, migration, and cell proliferation in relation to confinement. The results reveal that PC12 cells in contact with structural features exhibit longer neurite outgrowth and a preference for maintaining contact rather than occupying open spaces within the confinement. Time-lapse imaging confirms PC12 cells actively seek structural interactions, a behavior not widely investigated up to now. These findings underscore the role played by spatial constraints in neuronal network formation and highlight how structural contact could guide neuronal behavior in confinement. The insights gained could enhance neurobiological modeling and tissue engineering, and suggest that a better understanding of spatially structured environments could improve neural tissue models. Future research could expand on these findings by varying confinement geometries and materials and investigating additional aspects of cellular behavior, to possibly advance bioengineering efforts that aim to create brain-like tissue structures and neural interfaces.

Abstract[1]

Diese Studie untersucht das neuronale Verhalten von PC12-Zellen in vitro mit Schwerpunkt auf neuronalen Interaktionen in geschlossenen Mikroumgebungen und schließt damit eine Lücke in der neurobiologischen Forschung im Zusammenhang mit räumlich begrenztem Neuronenverhalten. Während frühere Studien neuronale Interaktionen mit synthetischen Strukturen untersucht haben, wurde die Frage, wie Neuronenpopulationen selektiv in begrenzten Bereichen navigieren, bisher nur unzureichend erforscht. In dieser Arbeit werden neuronale Reaktionen auf räumliche Begrenzungen untersucht, indem neuronale PC12-Zellpopulationen in 3D-gedruckten Mikroumgebungen auf Glassubstraten eingeschlossen werden. Die Mikroumgebungen ermöglichen eine lokalisierte Interaktion mit benachbarten Zellen und der gedruckten Struktur. Zu den wichtigsten analysierten Parametern gehören Neuritenauswuchs, Migration und Zellproliferation in Bezug auf die räumliche Begrenzung. Die Ergebnisse zeigen, dass PC12-Zellen mit Kontakt zu strukturellen Komponenten einen längeren Neuritenauswuchs aufweisen und dazu neigen, eher den Kontakt aufrechtzuerhalten als offene Flächen innerhalb der räumlichen Begrenzung zu besetzen. Zeitrafferaufnahmen bestätigen, dass PC12-Zellen aktiv nach strukturellen Interaktionen suchen, ein Verhalten, das bisher nicht umfassend untersucht wurde. Diese Ergebnisse unterstreichen die Rolle räumlicher Einschränkungen bei der Bildung neuronaler Netzwerke und zeigen, wie struktureller Kontakt das neuronale Verhalten in der Enge lenken könnte. Die gewonnenen Erkenntnisse könnten die neurobiologische Modellierung und das Tissue Engineering verbessern und deuten darauf hin, dass ein besseres Verständnis räumlich strukturierter Umgebungen neuronale Gewebemodelle verbessern könnte. Zukünftige Forschungen könnten diese Erkenntnisse durch Variation der Abgrenzungsgeometrien und -materialien und die Untersuchung weiterer Aspekte des Zellverhaltens erweitern, um möglicherweise die Fortschritte im Bioengineering voranzutreiben, die darauf abzielen, gehirnähnliche Gewebestrukturen und neuronale Schnittstellen zu schaffen.

---

[1] English to German translation provided on 13-February-2025 via email by: Übersetzungsbüro ENGIN GmbH, Language Service; L 14, 16-17; 68161 Mannheim; T. 0621 / 12 94 90; F. 0621 / 12 94 929; `info@engin.de`; `www.engin.de`; Rechnung Nr.: MA25-036016

Table of Contents

1 Introduction

Engineered materials are being utilized to investigate a range of cellular behaviors, with an eye toward revealing novel biological phenomena and addressing specific questions related to cellular behavior. Advances in 3D printing unlock opportunities to create systems with sub-micron to micron resolution that can interact with cells at the cellular size scale. In addition, the growing demand of organ-on-a-chip systems to mimic disease states and perform pre-clinical drug screening as part of a regulatory process[1] intensifies the desire to understand exactly how these systems work, and the roles their components play. As these in vitro systems are tailored towards particular investigations, researchers are challenged to understand the role artificial structures play in impacting cell behavior. The study of neuronal differentiation and behavior in controlled environments, for example, has been advanced through the use of in vitro models, incorporating model neurons such as PC12 cells, that can replicate key aspects of neuronal development. The ability of PC12 cells to differentiate into neuron-like cells upon exposure to Nerve Growth Factor (NGF) has made them a helpful tool for studying neurodevelopmental processes, signaling pathways, and neuronal interactions. However, as neuronal cells develop and establish connections, the surrounding environment—including the physical structures they encounter—plays a critical role in shaping their behavior. This investigation focuses on understanding 1) how physical confinement within 3D-printed structures impacts differentiation, growth, and behavior of PC12 cells, and 2) how these cells navigate confinement, particularly in relation to their contact with surface modifications and neighboring cells.

1.1 PC12 Cells as a Model for Neuronal Differentiation

PC12 cells, a cell line derived from a rat pheochromocytoma, have long been established as a model in neuroscience research, particularly for studying neuronal differentiation. Since they were first isolated in 1975[2], PC12 cells have mainly been utilized due to their singular response to Nerve Growth Factor (NGF), a neurotrophic agent that promotes neurite outgrowth in these cells. Upon exposure to NGF, PC12 cells extend neurites, structures that resemble axons and dendrites, making these cells a highly qualified proxy for neuronal investigations[3]. In addition to this defining feature, PC12 cells express a variety of ion channels, neurotransmitter receptors, and proteins essential for synaptic function and signal transduction, making them a comprehensive model for studying neurobiology[4]. These characteristics, combined with their ability to differentiate into neuron-like cells in response to NGF, establish PC12 cells as a reliable in vitro model for investigating a variety of neuronal features and behaviors.

Neurons, the basic structural units of the nervous system, consist of four primary regions: the cell body (also known as the soma), dendrites, axon, and presynaptic terminals (Fig. 1.1.1). The soma acts as the metabolic center, housing the nucleus and the endoplasmic reticulum, which synthesizes proteins essential for neuronal function. Dendrites, branching out from the soma, serve as the primary recipients of incoming signals from other neurons. The axon, typically a long tubular structure, extends from the soma and transmits electrical signals, or action potentials, to other neurons. These signals, propagated along the axon at speeds of up to 100 m/s, are critical for the brain's ability to receive and convey information, such as sensory input and motor commands. The myelin sheath, which insulates the axon, enhances signal transmission by allowing the action potential to jump between the nodes of Ranvier, uninsulated points along the axon[5].

The work of Camillo Golgi and Santiago Ramón y Cajal was the earliest attempt to successfully identify a neuron's distinct morphological components. Golgi developed a silver staining technique, known as the "reazione nera," which allowed the visualization of neurons in their entirety, revealing critical structures such as the axon and dendrites. Golgi's observations, made between 1873 and 1885, uncovered heterogeneity in neuronal structure across different regions of the brain, such as the neocortex and hippocampus. He documented the complexity of dendritic arborizations and axonal branching, providing the foundational descriptions for understanding neuronal diversity and function[6].

Cajal, utilizing Golgi's staining technique, proposed the neuron doctrine, a revolutionary concept that contradicted a prevailing theory at the time. Cajal's neuron doctrine posited that the nervous system is composed of discrete cells (neurons) that communicate through synaptic connections. He further introduced the law of dynamic polarization, which established that information flows within each neuron from the dendrites toward the axon. Cajal's work laid the foundation for modern neuroscience, fundamentally changing our understanding of the organization and function of the nervous system[7].

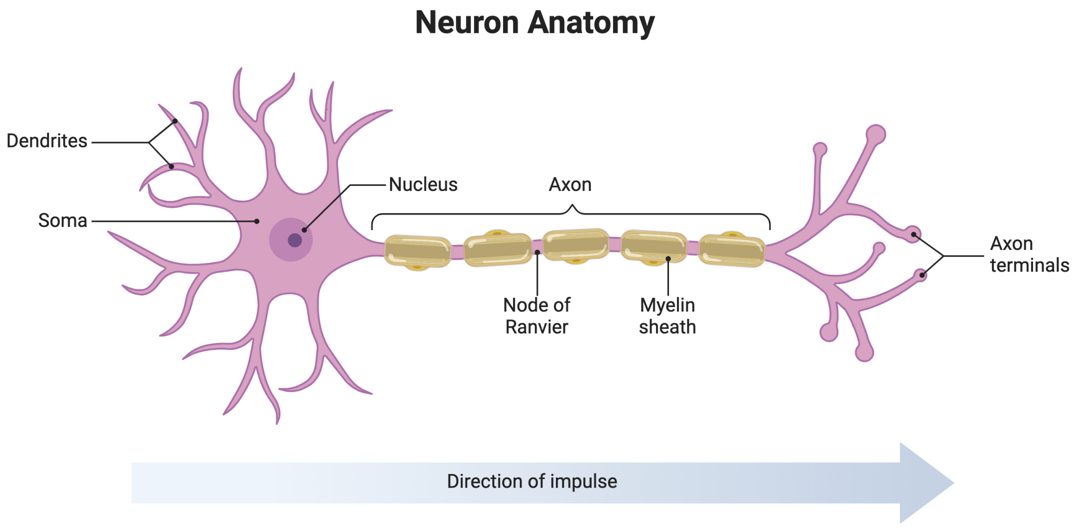

Figure 1.1.1: Neuron anatomy, created in https://BioRender.com.

Neuronal differentiation, the process by which progenitor cells develop into mature neurons, involves distinct morphological changes such as the formation of axons and dendrites. With respect to PC12 differentiation, NGF plays a pivotal role by initiating a cascade of intracellular signaling pathways that drive both morphological and functional changes. NGF binding to its high-affinity receptor, TrkA, triggers downstream signaling pathways such as the Ras-MAPK pathway, which is instrumental in promoting neurite outgrowth[8], and Ras-independent pathways involved in cytoskeletal formation[9]. Neurite outgrowth is further facilitated by microtubule-associated proteins, including Tau, which stabilizes axonal microtubules, and MAP2, which promotes dendritic growth[10].

The regulatory roles of MAP2 and Tau underscore their importance not only in the structural aspects of neuronal differentiation but also in the context of neurodegenerative diseases. Tau, for instance, is crucial for maintaining axonal stability and transport, and its dysregulation is a hallmark of diseases like Alzheimer's[10]. Similarly, abnormal MAP2 expression has been linked to Huntington's disease, suggesting its potential as a therapeutic target[11]. The expression of these proteins, along with other molecular changes induced by NGF, reflects the critical role of intracellular signaling in driving neuronal differentiation. With respect to PC12 cells, therefore, MAP2 and Tau are valid immunostaining targets used to verify a neuron-like phenotype. The adaptability of PC12 cells to different experimental conditions further enhances their utility for studying complex neuronal behaviors, toxicological effects, and potential neuroprotective compounds[12]. Taken together, the numerous features of PC12 cells, particularly their capacity to develop neuron-like properties through NGF-induced differentiation, make them an invaluable model for studying neurodevelopmental pathways, signaling mechanisms, and neuronal function.

1.2 Neurite Outgrowth and Guidance

Neurites are the long, thin processes that extend from the cell body, growing as a result of neuronal maturation and differentiation, involved in transmitting information in the brain. Neurite outgrowth is important to neuronal development and regeneration, where neurons extend processes that will form axons and dendrites, facilitating the establishment of functional neural networks. Neurite extension is regulated by a combination of intrinsic cellular mechanisms and extracellular cues. Internally, this process is governed by a process called dynamic instability[13], which comprises phases of both formation and disassembly of microtubules, heterodimeric structures composed of both α and β tubulin.[14]. Dynamic instability allows microtubules to search the intracellular environment with the intention of binding specific structures[13]. In addition, microtubules are involved in neuritogenesis, forming bundles that extend out of neuronal cells that are mostly spherical before undergoing differentiation[15]. Microtubule reorganization, therefore, is essential to neurite formation. Cell adhesion molecules such as laminin, found in the extracellular matrix of the nervous system, can also stimulate neurite formation[16]. Neurite outgrowth occurs in distinct stages, beginning with the formation of lamellipodia around the soma, followed by the formation of multiple neurites and their searching around the substrate, then, one neurite grows much faster than the others, followed by the growth and maturation of the other neurites and finally, the neurons mature and demonstrate functionality (Fig. 1.2.1)[17].

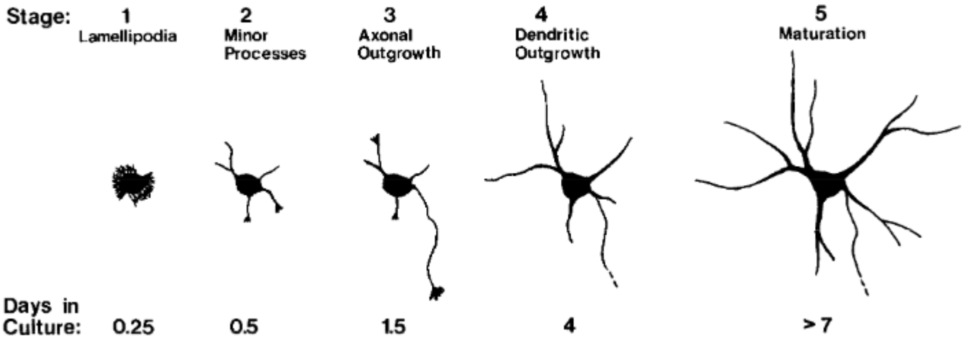

Figure 1.2.1: Stages of neuron differentiation as described by Dotti et al.[17] Reprinted with permission.

Interrogating neurite outgrowth may help to better understand neuronal differentiation and how external factors, such as microtopography, extracellular matrices, and spatial environments, affect neurite behavior. Attiah et al., focused on how PC12 cell differentiation is influenced by various substrates, with neurite outgrowth serving as a marker of successful neuronal differentiation[18].

Béduer et al. examined the influence of microgrooved polymers on human neural stem cell behavior, using neurite outgrowth as a metric to determine whether the patterned surfaces could guide and promote neurite extension in a predetermined direction. The investigation revealed that microgroove dimensions $(5-60\,\mu m)$ could significantly influence neurite outgrowth and alignment, indicating that topography can dictate the directionality and extent of neurite growth[19]. Similarly, Song et al. optimized micropattern dimensions $(40\,\mu m)$ on surfaces coated with laminin to enhance dorsal root ganglia neurite outgrowth rates and orientation, providing insights into the role of physical cues in guiding neurite growth[20]. Xu et al. used neurite outgrowth in rat hippocampal neurons to compare the differences in neuronal behavior between 3D collagen hydrogels and 2D surfaces, finding that while neurons in 2D extended longer neurites than those in 3D, the number of neurites extending from the cell body was similar in both 2D and 3D[21]. Length and number of neurites for cells under confinement could therefore be rational parameters worthy of analysis, and related findings are presented in secs. 4.12 (Path Lengths, All and Longest), 4.13 (Effect of Confined Cell Count on Neurite Length), 4.14 (Neurites Per Cell). How confinement impacts both neurite length and the number of neurites extended by a neuron can likely provide some insight into how confined microenvironments impact cell growth and differentiation.

1.2.1 Cell Classification in Neuronal Studies

Contact between neurons and mechanically stiff materials can guide neurite outgrowth, with the cells extending neurites along these features due to the physical constraints imposed by the surface. For instance, Johansson et al. used sympathetic and sensory ganglia neurons to demonstrate that axonal outgrowth was directed by the presence of patterned surfaces, such as nano-grooves, where axons showed a preference for growing along the ridges rather than within grooves located between ridges[22]. This form of contact guidance could provide insight into constructing systems that at least help understand how to tune neurite growth within the confines of 3D topological modifications.

In the presence of regular patterns of topological cues, neurite guidance results in the formation of more directed neuronal network formation. In an investigation involving the production of tubular structures produced via epitaxial deposition and mouse cortical neurons, neuronal behavior was influenced by spatial proximity to the structures, resulting in a greater density of neuronal processes in the proximity of the structures[23]. Synthetic features shape neurite growth by creating spatial cues that could influence cell behavior, guiding neurons to change how they form more organized and directed networks in response to physical interactions.

On flat surfaces without topographical features, isolated neurons tend to extend more neurites in multiple directions, reflecting a lack of directional guidance and leading to more disorganized growth. In one investigation, neuronal stem cells cultured on flat PDMS surfaces not only displayed more random branching but also extended longer neurites compared to those in narrow microchannels (Fig. 1.2.2)[19]. This suggests that, while isolated neurons can grow longer neurites, their growth remains less structured and lacks the organized, directional alignment observed in cells interacting with patterned environments.

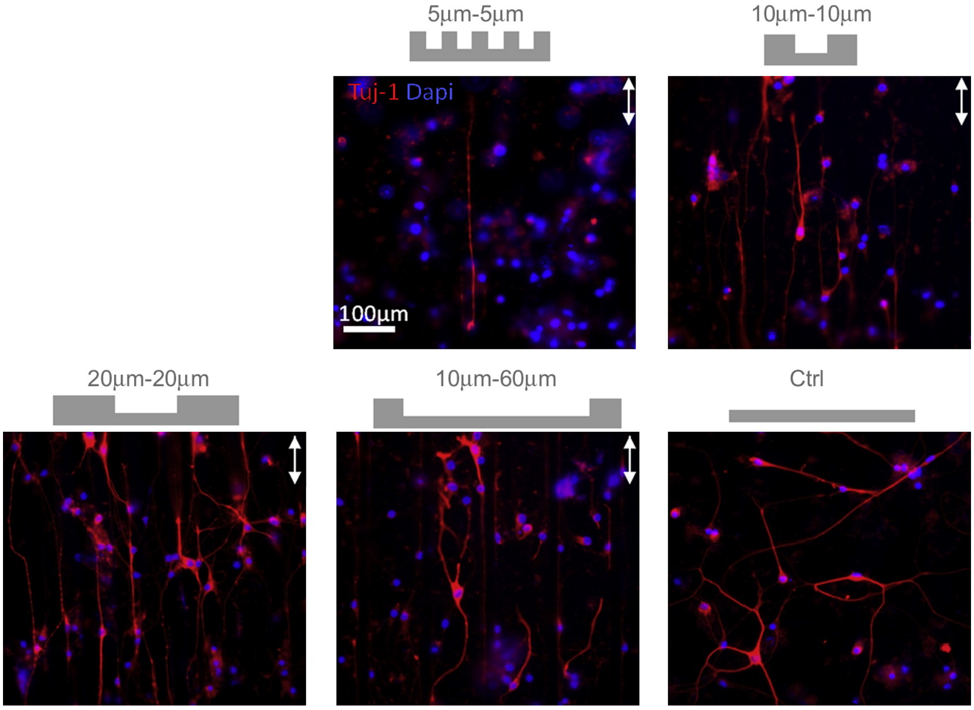

Figure 1.2.2: Neuronal stem cells (red: neuronal specific marker tuj-1, blue: DAPI nuclear stain) cultured on micropatterned PDMS microchannels of different terrace and groove widths[19]. Reprinted with permission.

Understanding the interactions between neurons and synthetic structures could help interpret the effects of confinement in neural studies, particularly when examining neurite outgrowth and network formation in tissue-engineered environments. In this investigation, the different spatial relationships cells have with the confinement structure are defined in sec. 4.7, Labeling Cells and Classifying Population Type. These classifications serve as the foundation for results presented in secs. 4.12 (Path Lengths, All and Longest), 4.13 (Effect of Confined Cell Count on Neurite Length), 4.14 (Neurites Per Cell), and 4.15 (Real Time Cell Behavior).

1.3 Cell Density Effects on Neuronal Behavior

Cell density influences a number of neuronal behaviors such as cell proliferation and protein expression. These density-dependent effects could provide insight into how neuronal cultures develop and respond to different environmental conditions. In one investigation using cerebellar granule neurons, intercellular distance was demonstrated to impact cell survival[24]. In another investigation, researchers found that the density of PC12 cultures was related to the expression of proteins tyrosine hydroxylase and dopamine β-hydroxylase, both involved in the production of neurotransmitters[25]. This highlights the importance of tuning cell density to alter neuronal growth. Such adjustments could provide the necessary cell-cell interactions to optimize—or at least clarify how to facilitate—functional neuronal development.

Cell density has also been linked to morphological differences in neuronal cultures. Parnas et al. demonstrated that increasing cell density in P19 neuronal cultures accelerates the maturation process, as evidenced by faster neurite outgrowth, earlier axon and dendrite segregation, and upregulation of synaptic proteins[26]. Ivenshitz et al. showed that as culture density changes, rat hippocampal neurons change their morphology and electrical activity to adapt to the presence – or lack – of nearby cells. Dendrites in sparse cultures extended branches farther away from their originating cell than dendrites in dense cultures. However, dendrites in dense cultures had much higher density of spines (protrusions from the main dendrite) than those in sparse cultures. Additionally, neurons in sparse cultures transmitted both higher excitatory currents and higher inhibitory currents, suggesting that at lower cell densities, synaptic connections are stronger[27]. These findings at least imply that culture density plays an important role in neuronal network formation and ultimately intercellular signaling.

Multiple neuronal phenomena show a relationship to cell density, suggesting that altering culture density could result in unique outcomes that govern how individual neurons, and the network as a functioning unit, behave. While there is an apparent connection between cell behavior and cell density, to our knowledge this relationship is underexplored for cells under confinement. Experimental results connecting cell density and a number of cellular phenomena are presented in secs. 4.11 (Proliferation and Cell Density), 4.12 (Path Lengths, All and Longest, 4.13 (Effect of Confined Cell Count on Neurite Length), and 4.14 (Neurites Per Cell).

1.4 Impact of Confinement on Neuronal Growth

Investigating the role of physical confinement on neuronal growth assists in replicating in vivo environments and developing effective in vitro models. In the nervous system, neurons rely on structural cues for directional growth, and this behavior can be mimicked in engineered systems through scaffold designs. Agrawal et al. demonstrated that dorsal root ganglia neurons cultured on confined nanogrid scaffolds showed enhanced axonal growth oriented along aligned nanofibers, compared to unconfined environments where neurite outgrowth was random and disorganized[28]. This finding highlights the role engineered structures could play in fostering organized neural networks, which is particularly relevant for tissue engineering applications aiming to replicate the physical characteristics of neural tissues.

Neuronal behavior is influenced by the physical restrictions imposed by 3D spatial constraints. Francisco et al. found that dorsal root ganglia neurons grown within fully confined 2D chambers demonstrated a decrease in axon formation due to the presence of spatial constraints in both lateral directions, limiting their ability to extend neurites. However, when neurons were placed in narrow channels with only partial confinement, axonal outgrowth was more easily facilitated (Fig. 1.4.1)[29]. These findings highlight the role that features of the physical environment can play in guiding neuronal growth and suggest that partially confined spaces enable more extensive neurite outgrowth than fully confined spaces.

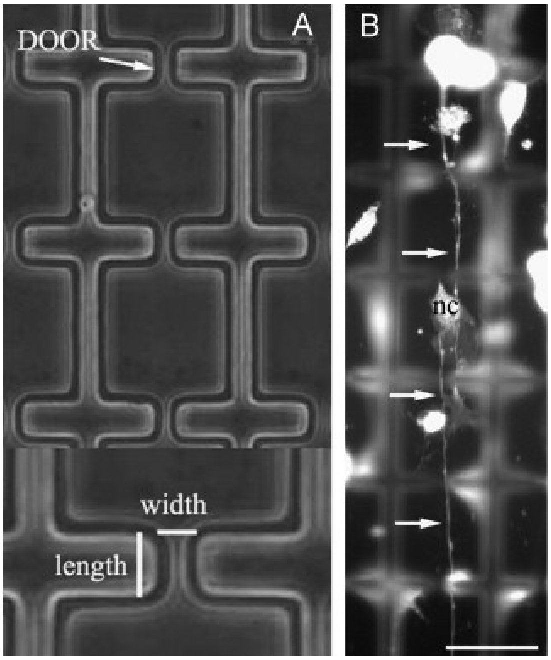

Figure 1.4.1: (A) Micropatterned features to investigate axonal extension (scale bar = 40 μm) in dorsal root ganglia neurons; (B) a neuron (indicated by arrows) extends its axon, navigating the microenvironment ("nc" label - non-neuronal cells); adapted[29]. Reprinted with permission.

The spacing between structural features also has a pronounced impact on neurite outgrowth. Microstructured scaffolds, such as those developed by Marino et al. offer 3D-printed ridges with submicron thickness that promote significant neurite extension in both PC12 and SH-SY5Y neuronal model cell lines. These ridges are meant to mimic the alignment of axonal architecture in vivo by providing spatial cues that guide neurite growth along the structures. As the spacing between these ridges decreased, increases in neurite extension were observed, with longer neurites growing within narrower ridges[30]. These findings at least highlight that neurons are capable of a range of behaviors that can be induced by tuning their surroundings. Understanding how neurons respond to confinement could enhance the design of scaffolds meant to reconstruct neural tissue phenomena in vitro. While these studies explore neuronal behavior in various geometries, it remains to be understood how a small population of confined cells respond to geometrical constraints. Results presented below (sec. 4.10, Experimental Reliability; sec. 4.11, Proliferation and Cell Density; sec. 4.12, Path Lengths, All and Longest; sec. 4.13, Effect of Confined Cell Count on Neurite Length; sec. 4.14, Neurites Per Cell; sec. 4.15, Real Time Cell Behavior) aim to accurately correlate each member of a confined neuron population with distinct behaviors.

1.5 Role of Laminin in Neuronal Behavior

In vivo, laminin plays a prominent role in maintaining the structure of various tissues, due to its ability to interact with cells. One type of basement membrane, the vascular basement membrane, found within the neural extracellular matrix (ECM), is comprised of four protein families, of which laminin is the second most abundant. Since the vascular membrane separates endothelial cells from neurons and glial cells, laminin's role is critical in helping to maintain the blood-brain-barrier. More specifically, laminin interacts with the transmembrane integrins expressed by multiple cell types around the blood brain barrier to help maintain the function of the blood-brain-barrier[31]. Laminin, therefore, has an important function in maintaining the nervous system.

Because laminin plays such a critical role in vivo, its function as a protein that reliably binds to certain cells has been explored in vitro. By incorporating laminin into an electrospun polymer, researchers were able to create a biomimetic scaffold that enhanced PC12 neurite growth and could serve as a platform to investigate nerve regeneration[32]. Biochemical cues from the ECM can also be complemented by topographical and mechanical features in the environment. For instance, researchers demonstrated that neurites of mesencephalic neurons can be guided by surface modifications, such as microcontact printed tracks comprised of laminin, which align the direction of outgrowth by providing physical constraints (Fig. 1.5.1)[33]. Surface features can direct neurite alignment and enhance the formation of neural circuits, indicating that both biochemical and topographical cues can orchestrate neurite guidance. Modulating neurite guidance and outgrowth underscores the importance of optimizing the physical properties of scaffolds or substrates used in neuronal tissue engineering. The roles played by biochemical signals, topographical features, and mechanical constraints in these engineered environments should therefore be considered when investigating neurite outgrowth and guidance.

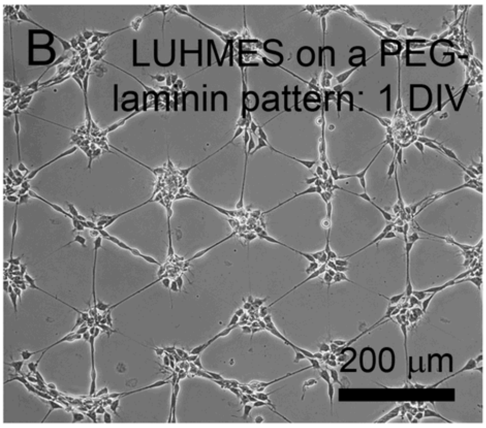

Figure 1.5.1: The neurites of mesencephalic neurons (LUHMES, as indicated) grow along laminin microcontact printed tracks[33], adapted. Reprinted with permission.

PC12 cells demonstrate predictable responsiveness to ECM proteins, particularly laminin and collagen, which mediate cellular attachment, neurite outgrowth, and differentiation through integrin interactions. Integrins are heterodimeric transmembrane proteins composed of two subunits, designated as alpha (α) and beta (β), and the specific $\alpha - \beta$ combinations confer distinct ligand-binding properties. In one study using PC12 cells, it was demonstrated that the β_1 integrin binds to laminin's P1 fragment and not to its E8 fragment[34]. However, another study using PC12 cells showed that laminin fragments E1, E1-4, and E8 promote both adhesion and neurite outgrowth by interacting with integrins $\alpha_1\beta_1$ (E1, E1-4) and $\alpha_3\beta_1$ (E8), suggesting that β_1 can mediate binding to E8 in the context of different integrin complexes[35]. One possible explanation for this discrepancy comes from work by Sonnenberg et al., although their study did not use PC12 cells. They found that while β_1 integrins bind to laminin's P1 fragment, the α_6 subunit in the $\alpha_6\beta_1$ complex is critical for E8-mediated adhesion in non-neuronal cells, suggesting a similar mechanism (e.g. involvement of an α subunit) could play a role in PC12 cell binding to laminin's E8[36]. Nevertheless, laminin has consistently been shown to support PC12 attachment more effectively than other ECM components, such as fibronectin[35]. Additionally, at least one of these integrin subtypes, $\alpha_3\beta_1$, has been implicated in promoting neuritogenesis in PC12 cells through its interaction with laminin[37]. Laminin also promotes the clustering of integrins within lipid rafts, further enhancing signaling interactions between integrins and growth factor receptors like TrkA, thereby supporting neuronal differentiation in both dorsal root ganglia neurons and PC12 cells[38]. While remodeling of the ECM is a typical cellular phenomenon involving secretion of various enzymes and protein production, and is carried out by fibroblasts and epithelial cells, for example, a search revealed no literature describing any such investigation connecting ECM remodeling with PC12 cells. Some neurons, however, play a role in ECM remodeling. For example, one investigation found that a selected population of secretagogin-expressing neurons release matrix metalloprotease-2, thus controlling neuroblast migration by restructuring the extracellular matrix in both rodents and humans[39].

Collagen also plays a supportive role in neurite outgrowth by interacting with PC12 cells via integrins containing the β_1, through which cell adhesion and neurite extension are enabled. However, collagen's effectiveness in promoting neurite outgrowth is less pronounced compared to laminin. This may at least partly be because, of the $\alpha_1\beta_1$ and $\alpha_3\beta_1$ integrins expressed by PC12 cells, only $\alpha_1\beta_1$ binds to collagen, while both $\alpha_1\beta_1$ and $\alpha_3\beta_1$ bind to laminin[35]. Studies involving PC12 cells cultured in three-dimensional collagen gels showed that while collagen supports neurite growth, laminin enhances this process more effectively. In particular, laminin-modified gels promoted robust neurite extension without the inhibitory trends seen in collagen-only environments, highlighting laminin's specialized role in facilitating neuronal differentiation and neuritogenesis[40].

Laminin, through its interactions with PC12 integrins $\alpha_1\beta_1$, and $\alpha_3\beta_1$, promotes neurite outgrowth and differentiation. This relationship between PC12 cells and specific ECM components highlights the importance of integrin-mediated signaling in neuronal development and underscores the varying effects of different ECM components in modulating cellular behavior. While there are some results herein that explored PC12 response to collagen type 1 and one laminin isoform, laminin 111 (sec. 4.3, PC12 Differentiation on Protein Coated Surfaces), the bulk of investigations in this study used laminin 111 as the sole surface coating (sec. 4.2, PC12 Characterization; sec. 4.6, Live Dead Assay; sec. 4.10, Experimental Reliability; sec. 4.11, Proliferation and Cell Density; sec. 4.12, Path Lengths, All and Longest; sec. 4.13, Effect of Confined Cell Count on Neurite Length; sec. 4.14, Neurites Per Cell; sec. 4.15, Real Time Cell Behavior).

1.6 3D Printed Structures in Tissue Engineering

3D-printed structures provide researchers with tools to study neuronal behavior in conditions that recreate phenomena found in vivo, where spatial confinement and physical cues are influential in guiding cell migration, growth, and differentiation. Xiao et al. used 3D-printed ordered graphene microstructures to interrogate cell-cell interactions between rat cortical neurons and astrocytes (Fig. 1.6.1). One of the main findings in this investigation was that neurons grown on ordered graphene aligned with the substrate[41]. In another investigation, researchers demonstrated that the growth cone area of hippocampal neurons increased as micropillar spacing increased.[42].

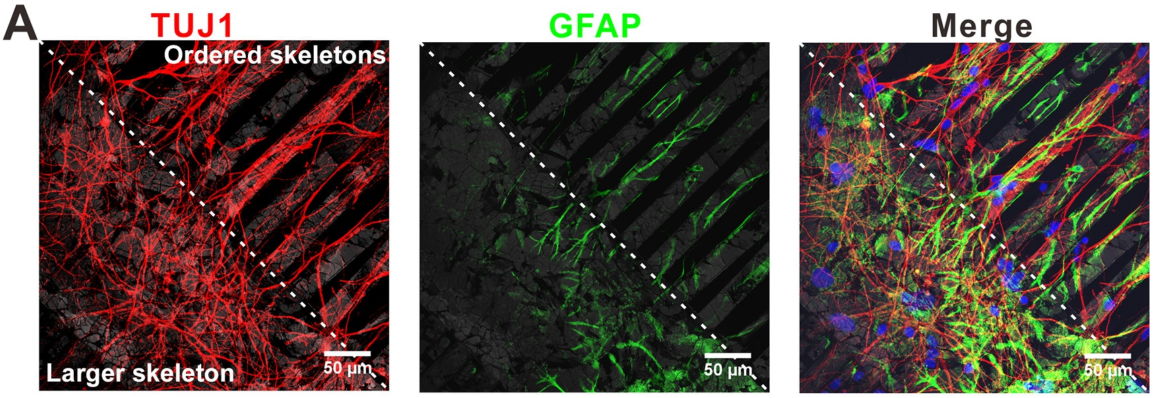

Figure 1.6.1: Stained rat cortical neurons growing along the graphene skeleton atop ordered graphene structures (above dashed line) and growing in random orientations on the flat, supporting graphene structure (below dashed line); adapted[41]. Reprinted with permission.

Spatial confinement within 3D-printed structures offers a controlled environment that influences cellular behavior, particularly in neurons. For instance, it was demonstrated that microgrooves made from laminin coated poly(lactide-co-glycolide) (PLGA) influenced neurite growth in PC12 cells[43]. In another investigation, nanogrooved 3D scaffolds were produced to modulate PC12 migration and axonal pathfinding, and one outcome was that focal adhesion (FA) size increased when FAs were aligned with the scaffold[44]. 3D printed structures demonstrate the potential of engineered topographical cues to guide growth and migration, and ultimately provide valuable insights into how neurons respond to modified physical environments.

In addition, the ability of 3D-printed structures to provide nanoscale topographical cues has been shown to significantly influence neuronal behavior. Xie et al. demonstrated that electrospun fibers can guide neuronal alignment and enhance neurite extension in dorsal root ganglia neurons, suggesting topographical features within these in vitro structures can direct growth in a manner similar to in vivo environments[45]. These findings are reinforced by an investigation by Chen et al., demonstrating that multiscale 3D-printed biomimetic scaffolds can enhance neurite elongation in PC12 cells through the sustained release of NGF via GelMA-based microspheres and by co-culture with NGF-releasing RSC96 Schwann cells[46]. These advancements highlight the fundamental role played by topography in neuronal development and the potential of 3D-printed structures to influence cell behavior through mechanical and biochemical interactions.

3D-printing technologies enable the creation of structures and scaffolds with customizable physical and biochemical properties, further enhancing their utility in tissue engineering. By tailoring features like inter-feature distances, structure diameter, and release of neurotrophic agents, researchers can create environments that promote specific cellular responses, such as directed neuronal migration and neurite extension. In the investigation presented herein, a variety of cell behaviors are explored to gain insight into how PC12 cells change their behavior as a direct result of their individual interactions in the presence of a 3D-printed structure that confines their migration and growth.

1.7 Fundamentals of Two Photon Polymerization

In a variety of experimental scenarios, coating a glass surface with a laminin solution will facilitate effective and replicable PC12 attachment. However, to investigate how neurons and their respective neurites might respond to external stimuli, the topology of the glass surface should first be modified to include a microscale structure. Adding a synthetic structure to a glass surface presents both a challenge and an opportunity: there is a technical hurdle which must be overcome to ensure that any microscale structure can be printed numerous times with consistent dimensions and is tightly adhered to the glass surface; and there is an opportunity to apply custom-made structures to glass surfaces which can uniquely influence cell growth. Two-photon polymerization (2PP) has emerged as a powerful tool for the fabrication of microscale and nanoscale structures, providing a high degree of precision useful for investigations into neuronal behavior. This technique offers a way to create environments for in vitro studies, where neurons can be confined and examined in controlled conditions. These 3D structures can provide a more accurate representation of biological systems than traditional in vitro cell culture devices, making 2PP an invaluable tool for neuroscience research. For example, Buchmann et al. used 2PP to develop a network of cavities and guidance structures meant to support a mesencephalic neuron-astrocyte coculture (Fig. 1.7.1). One of their findings was that a dopaminergic protein downregulation in neurons was induced as a result of coculture, and not the result of cell contact with the 3D printed structure, indicating that the 3D printed structure could effectively support coculture[47]. This suggests that 2PP can produce structures that guide cellular interactions without disrupting important biological function.

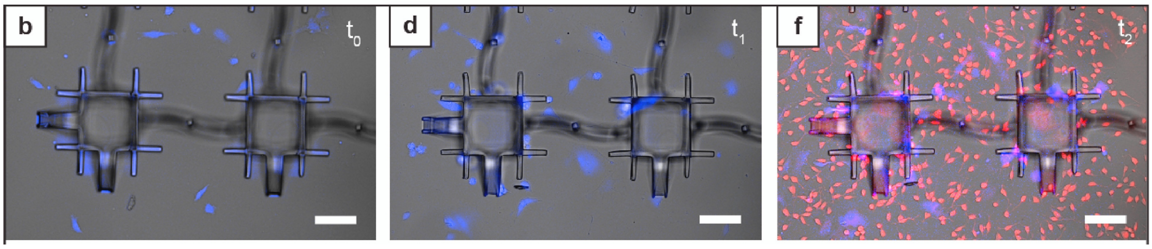

Figure 1.7.1: Cavities and channels created by 2PP meant to guide and support coculture of mesencephalic neurons and astrocytes; (b) low density astrocyte seeding, (d) astrocyte proliferation, (f) high density neuron seeding, scale bars 100 μm; adapted[47]. Reprinted with permission.

A key advantage of 2PP over traditional photolithography-based methods is its additive nature. Traditional photolithography requires the use of master masks, which are unalterable once fabricated. In contrast, 2PP starts with a computer-aided design and directly writes the structure by guiding a laser along the desired scanning path. This flexibility allows for the creation of intricate designs that can be adjusted as needed, providing submicron resolution, which is a significant improvement over other direct laser writing (DLW) techniques like UV laser stereolithography or selective laser sintering[48].

At the core of 2PP is the two-photon absorption (TPA) process. Unlike single-photon absorption, which requires higher-energy photons with wavelengths in the UV range, TPA involves the simultaneous absorption of two lower-energy photons each with wavelengths typically near infrared. As seen in Fig. 1.7.2, this process excites an electron in a target molecule (known as a photoinitiator) to a higher energy state. Once excited by the combined energy of two photons, an electron in the photoinitiator returns to the ground state through non-radiative decay, transferring energy to nearby monomer molecules. This initiates a chain reaction of polymerization, where free radicals are generated, leading to the solidification of the monomer into the desired 3D structure. This entire process, from initiation to termination of polymerization, occurs within the volumetric element defined by the focal point of the laser, known as a voxel[49]. This makes 2PP an intrinsically additive manufacturing technique[48].

As illustrated in Fig. 1.7.3 (left), single-photon absorption typically spreads energy over a large volume, which can result in less precise structures. In contrast, two-photon absorption is highly localized (right, indicated with arrow, Fig. 1.7.3), allowing the transferred energy to be confined to the voxel. The use of a femtosecond laser is essential for this process because its pulse duration, on the order of 10–100 femtoseconds (1 femtosecond $= 1 \times 10^{-15}$ s), creates the high photon density necessary for TPA to occur[49]. This high photon flux, combined with the small voxel size (200–500 nm laterally and 1–2 microns axially), allows for the creation of sub-diffraction limit structures, useful for applications in fields such as micro-optics, photonics, and, importantly, neurobiology[49].

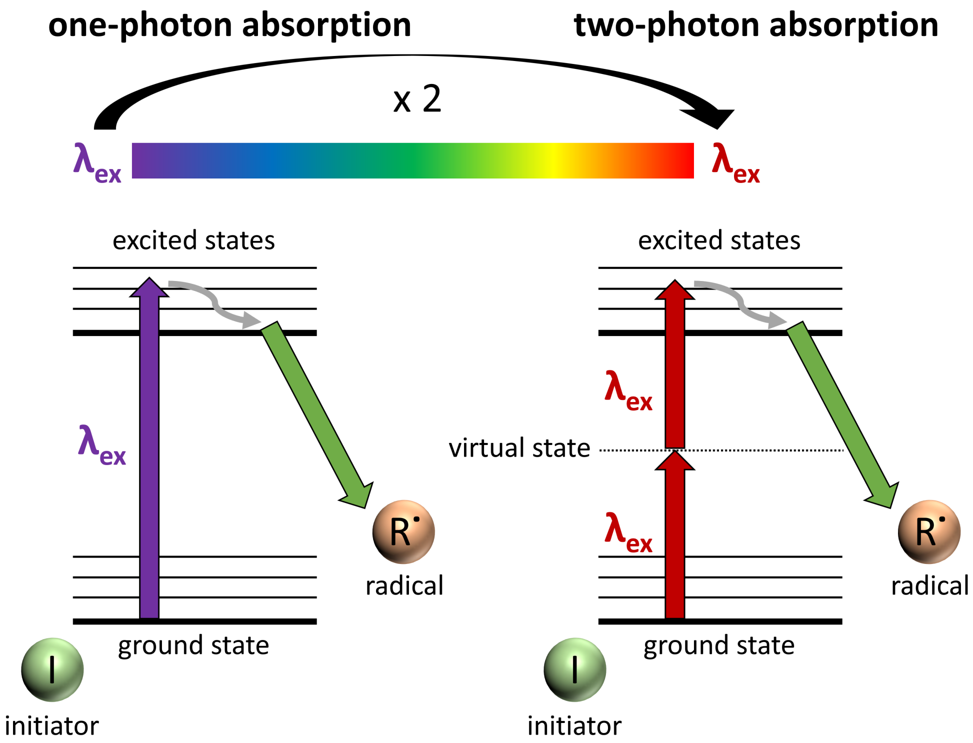

Figure 1.7.2: Jablonski diagram illustrating two-photon absorption and subsequent relaxation pathways, which trigger polymerization in the presence of a photoinitiator[50]. Reprinted with permission.

The resolution of 2PP is controlled by several parameters, including the laser power, exposure time, and numerical aperture of the focusing optics. Adjusting these factors enables tuning of the voxel size, allowing for precise control over the structure's dimensions. Lower laser power produces smaller voxels, improving resolution but increasing print time, while higher power speeds up the process but may sacrifice some level of detail[48]. Voxel shape is influenced by the Gaussian beam profile of the femtosecond laser and the numerical aperture of the objective lens.

Photoinitiators used in 2PP must meet several requirements to ensure efficient polymerization. These include solubility in the monomer resin, a low bandgap for excitation via two-photon absorption, and compatibility with near-infrared light in the 700–1100 nm range. The photoinitiator should also have a high two-photon absorption cross-section, which is measured in Göppert Mayer units ($10^{-50}\,\mathrm{cm}^4\,\mathrm{s\,photon}^{-1}$), and a high quantum yield for generating free radicals. The use of femtosecond lasers enhances the likelihood of nonlinear absorption, ensuring that polymerization occurs only at the focal point, reducing heat buildup, and enabling fine control over the fabrication process[49]. Furthermore, photoinitiators must be stable, non-toxic, and biocompatible, particularly for applications in biomedical research.

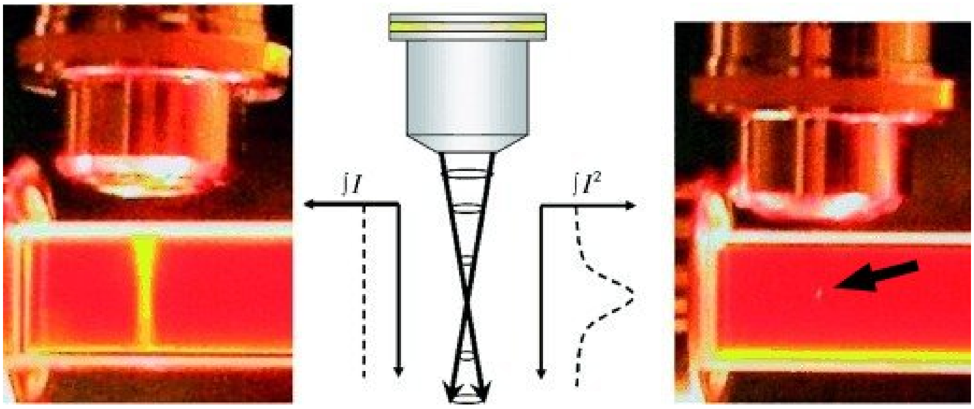

Figure 1.7.3: Comparison of single-photon absorption, which spreads energy over a large volume where absorption rate is linearly dependent on intensity (left), versus two-photon absorption, which confines energy to a small focal point using femtosecond laser pulses where absorption rate is proportional to intensity squared (right, indicated with arrow), adapted.[51]. Reprinted with permission.

Two-photon polymerization has proven to be a highly versatile technique, offering the ability to create intricate 3D structures with sub-micron precision. This method is useful in fields such as neuronal research, where it allows for the creation of tailored environments for studying cellular behavior. This investigation relies on 2PP DLW to make structures used in a range of investigations where maturing neuronal populations are laterally confined. By optimizing laser parameters and choosing an appropriate photoinitiator, 2PP provides a flexible platform for designing and fabricating complex structures, advancing both fundamental research and practical applications in neuroscience and beyond. For a discussion of the specific features of the structure used in this investigation, please refer to sec. 4.4, 3D Printed Confinement Microstructures; for results describing the biocompatibility of the structure used in this investigation, please refer to sec. 4.6, Live Dead Assay; discussions describing structures used in other investigations are found in sec. 4.4, 3D Printed Confinement Microstructures and 1.4, Impact of Confinement on Neuronal Growth.

1.8 Summary

PC12 cells, known for their ability to differentiate into neuron-like cells upon exposure to nerve growth factor can be used as part of an in vitro model for studying neuronal differentiation and function. Neurite outgrowth, a critical aspect of neuronal development, is influenced by environmental factors such as the ECM and topographical cues. Recognizing how these factors could influence neurite extension underscores the importance of spatial relationships and cell interactions in neuronal studies. While previous investigations into neurite outgrowth, guidance, network formation, and interaction with synthetic topology have yielded meaningful conclusions, further investigation should focus on how these phenomena simultaneously influence the development of neuronal networks. More specifically, no study we are aware of has 1) interrogated how specific spatial relationships of neurons under lateral confinement differentially influence neuronal morphology and 2) interrogated localized neuronal migration in confinement, given the presence of other cells and a tightly confined environment. Physical confinement influences neurite extension, neurite guidance, cell-cell interactions, and neuronal differentiation, which all play a role in neuronal network formation. Developing an understanding of how these phenomena work together could be relevant to the development of in vitro models and tissue engineering applications, where mimicking the spatial constraints of in vivo environments can lead to more functional and biologically relevant neural networks.

Cell density and physical confinement could be significant determinants of neuronal behavior, particularly within engineered environments. By categorizing PC12 cells based on their membrane contact with structure walls and neighboring cells, we aim to elucidate how physical and environmental factors direct cell fate and growth patterns. Despite extensive studies on neurite outgrowth, neurite guidance, neuronal interaction with topological cues, and the effects of confinement, there is still a need to 1) understand how specific spatial relationships within 3D-printed structures influence neuronal behavior and 2) interrogate localized neuronal migration in confinement, given the presence of other cells and physical barriers. In addition, no study we are aware of incorporates neuronal migration under confinement with network formation.

This work aims to investigate how possible intercellular relationships—between neurons and the physical structures that confine them, as well as between neighboring cells—affect neuronal behavior. Results presented below describe how the confinement structure used in this investigation influences cell viability (4.6, Live Dead Assay), cell proliferation (4.11, Proliferation and Cell Density), neurite outgrowth (4.12, Path Lengths, All and Longest, 4.13, Effect of Confined Cell Count on Neurite Length, 4.14, Neurites Per Cell), and migration (4.15, Real Time Cell Behavior). The aim of the results below, therefore, is to present data that strongly argues that cells in confinement demonstrate novel behaviors that could be relevant to the design of in vitro neuronal tissue models, neuronal networks, and possibly any other work that seeks to guide neuronal behavior.

Using additive manufacturing techniques to create and interrogate biological models can provide insight into how particular features of cellular behavior might be tuned. Employing 2PP direct laser writing enables the creation of microscale 3D structures with precision at the cellular scale. These structures are customizable microenvironments that could also lead to greater understanding of in vitro models for tissue engineering. By exploring how physical confinement within these 3D printed structures impacts the differentiation, growth, and behavior of PC12 cells, this research aims to deepen existing understanding of in vitro and in vivo neuronal development.

2 State of the Art

2.1 Advanced 3D Printing Techniques in Neuronal Tissue Engineering

There have been significant developments in neuronal tissue engineering as a result of the integration of advanced 3D printing technologies, which allow for more precise modeling of the brain's complex cellular architecture. 3D printing innovations enable the creation of intricate structures that closely replicate in vivo conditions, fostering neuronal growth, differentiation, and synaptic connectivity. As a result, 3D printing has emerged as a powerful tool in the development of neural constructs, providing new avenues for studying neurological diseases and testing therapeutic interventions.

One major advancement in 3D printing is the use of scaffolds to promote neural differentiation from human pluripotent stem cells. Koroleva et al. used iPSC-derived neurons to demonstrate that 3D-printed scaffolds could support the formation of functional neural networks, enabling the development of synapses and long-term cell viability. These constructs maintained their structure and functionality for over 120 days in vitro, creating an extended window for studying neuronal activity and offering potential for applications in drug discovery and neurodegenerative disease modeling[52]. This approach highlights the ability of 3D scaffolds to facilitate the study of neural tissue behavior in a controlled environment over prolonged periods.

Kajtez et al. presented another innovation in neuronal tissue engineering with the biofabrication of SHAPE (Self-Healing Annealable Particle Extracellular matrix), a novel composite material. SHAPE uses hydrogel microparticles and an extracellular matrix-based continuous phase to create a supportive environment for human neural stem cells (hNSCs) (Fig. 2.1.1). Its unique rheological properties ensure stable printing of complex neuronal structures, promoting neuronal maturation and synaptic activity[53]. This method could enable the creation of 3D neural constructs with potential applications in disease modeling and regenerative medicine, providing new tools for long-term neural tissue studies.

A recent study introduces the use of tetrapod-shaped ZnO (t-ZnO) microparticles as dopamine (DA) sensors within 3D-printed neural constructs. By embedding t-ZnO particles in a bio-ink with human SH-SY5Y cells, researchers developed a 3D neural tissue platform that allows for real-time, non-invasive monitoring of dopamine release[54]. Integration of neurochemical sensing with 3D-printed tissues represents a significant advancement in neuronal tissue engineering, as it enables both structural integrity and functional monitoring within engineered constructs, paving the way for future applications in neurochemical research and drug testing.

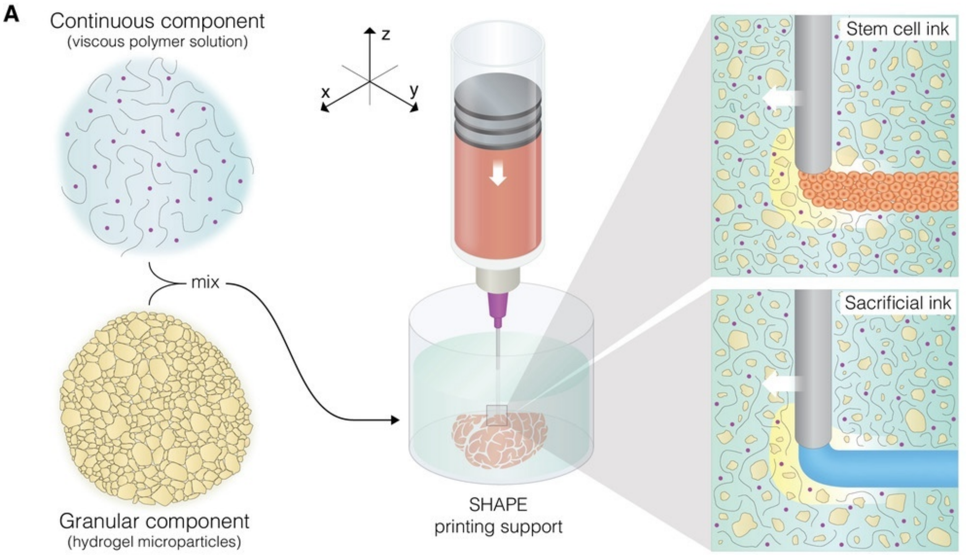

Figure 2.1.1: SHAPE support material - a viscous polymer solution consisting of ECM macromolecules and a solution of soft hydrogel microparticles are combined. Each of the stem cell ink and sacrificial ink can be printed into the polymer solution. The polymer solution promotes neural stem cell differentiation, while the hydrogel microparticles provide physical support for cell growth upon annealing; adapted[53]. Open access article.

Advances in 3D printing for neuronal tissue engineering have introduced new possibilities for creating complex, functional neural systems that mimic the brain's natural environment. These developments enhance the study of neuronal function and disease and offer potential breakthroughs in regenerative medicine and drug discovery, revolutionizing how researchers model and treat neurological conditions.

2.2 Neurite Outgrowth and Guidance

Neurite outgrowth and guidance are critical aspects of neural development and regeneration, particularly in engineered microenvironments designed for tissue engineering. By manipulating the physical properties of substrates, researchers can direct the growth and organization of neurons. Micro- and nano-scale surface topographies, such as grooves or ridges, create physical cues that neurons respond to, altering their growth patterns and behavior. These engineered environments can mimic the extracellular matrix (ECM) and provide insight into how neurons naturally extend, branch, and form networks. This understanding could open new possibilities for designing biomaterials aimed at neural repair and regeneration.

Engineered patterns on substrates can effectively guide the growth of neurons, offering important insights for neural tissue engineering. Using techniques like grayscale lithography (GSL) and UV nano-imprint lithography (UV-NIL), researchers created parallel grooved microstructures that influence how murine cerebellar granule cells (MCGCs, a type of neuron) grow. Neurons exhibited three distinct behaviors (Fig. 2.2.1): they grew in random directions when seeded in shallow grooves; they aligned with the groove edges of the microstructures and formed networks; and, in other cases, higher features acted as barriers, preventing outgrowth[55]. By investigating how neurons respond differentially to the changing heights of raised structures, researchers are potentially able to understand at least one key factor related to design of synthetic neural tissue.

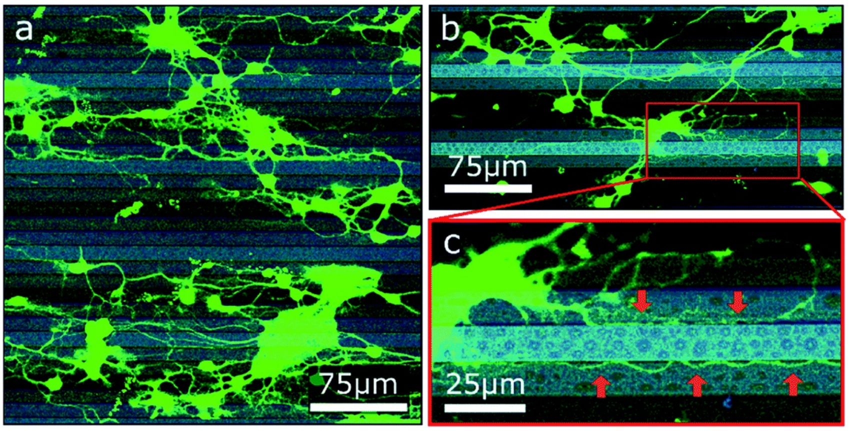

Figure 2.2.1: Confocal images of murine cerebellar neurons growing in and around lithographically structured grooves (red arrows indicated neurites guided along edges); adapted[55]. Open access article.

Engineered vibrational patterns can significantly influence neuronal growth, both in terms of direction and length. Maruyama et al. used a petri dish with an attached ultrasonic transducer (Fig. 2.2.2) to demonstrate that applying low-frequency ultrasound vibrations (78 kHz) to cultured PC12 cells enabled neurite outgrowth in specific orientations. Neurites grew along the directions where vibrational amplitude remained constant, and higher ultrasound voltages enhanced this alignment. Additionally, ultrasound stimulation almost doubled the average neurite length and activated key genes involved in neuronal differentiation[56]. These findings suggest that ultrasonic methods could be valuable for manipulating neuronal networks in bioengineering and regenerative medicine.

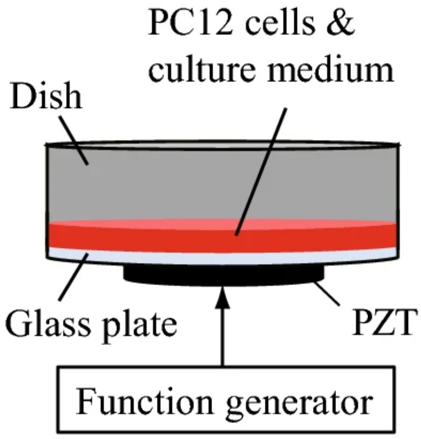

Figure 2.2.2: Petri dish incorporating ultrasound functionality (dish ϕ: 35 mm, "PZT": lead zirconate titanate); adapted[56]. Open access article.

Engineered nanoscale topographies can strongly influence neuronal growth, impacting both the directionality and length of neurites. For instance, Omidinia-Anarkoli et al. demonstrated that among smooth, porous, and grooved fibers, only grooved fibers increased dorsal root ganglia neurite alignment, while inter-fiber distances were increased to 50 μm. This suggests neurons exhibit a "memory" of topographical cues, leading to more directed growth even after leaving the structured areas. One claim made to clarify the use of the term memory is that cell behavior in this instance could be attributed to focal adhesions and nuclear YAP translocation, because YAP translocation has been demonstrated to reflect prior culture conditions[57]. Aligned neurite extension, when considered in light of possible cellular memory, could be useful when designing in vitro systems for neural tissue investigations.

As advancements in microfabrication and topographical engineering continue, the potential to guide neuronal networks more precisely becomes increasingly feasible. These engineered platforms, which combine physical and vibrational cues, hold great promise for developing synthetic tissues and optimizing in vitro models. Such approaches could contribute to innovations in neuroprosthetics, brain-computer interfaces, and neural regeneration therapies, enabling the seamless integration of artificial and biological systems.

2.3 Structured Neuronal Networks

The human brain's extraordinary capacity to process vast amounts of information with speed and efficiency has long inspired advancements in artificial intelligence and neuroscience. A key characteristic of biological neuronal networks is their ability to self-organize into structured systems, allowing for efficient information processing through a balance of local specialization and global integration[58]. As a result, understanding and replicating these structured networks in artificial systems has become a focus of research into neuromorphic computing. By modeling neuronal architectures that reflect the brain's inherent modularity and flexibility, scientists are pushing the boundaries of brain-inspired technology, aiming to develop networks capable of sophisticated and adaptive information processing.

The development of artificial networks that can mimic the brain's information processing capabilities is a major step in neuroscience and neuromorphic computing. Shirai et al. created a self-organizing artificial neuronal network that exhibits key properties similar to those found in the brain, such as a scale-free topology and a power-law distribution of node degrees. This structure, using Sn nanoparticles distributed between Au electrodes, where a few highly connected hubs dominate the network, is critical for efficient information processing—a hallmark of biological neuronal systems. The network's ability to self-organize and cross the percolation threshold demonstrates that it can transition from a non-conducting to a conducting state, much like how the brain achieves optimal information flow. The solid lines connecting the Sn nanoparticle clusters from one electrode to another represent an Ohmic conduction pathway, governed by Ohm's law; the corresponding dashed lines represent a tunneling pathway, governed by the quantum tunneling of electrons (Fig. 2.3.1, A). An electron micrograph (Fig. 2.3.1, B) of the Sn nanoparticle network is colorized to reflect network connectivity - particles with the same or similar colors are considered to be connected to one another[59]. These findings suggest that by applying information processing theories to artificially developed neuronal networks, researchers can create systems that function similarly to the brain, opening new avenues for brain-inspired computing technologies.

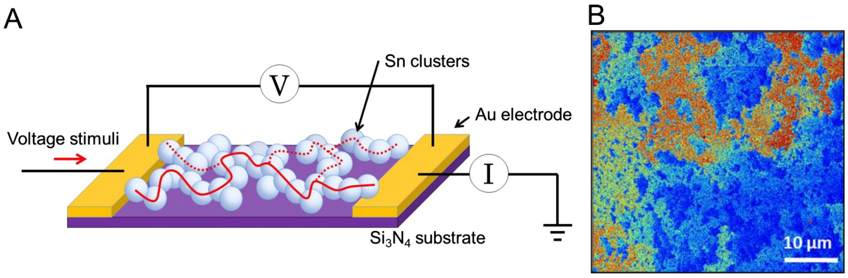

Figure 2.3.1: Schematic of a Sn nanoparticle network, showing both solid and dashed lines traversing the Au electrodes, meant to represent an Ohmic conduction pathway and a tunneling pathway, respectively (A) and an electron micrograph of the Sn nanoparticle network, with colorization used to indicate connectivity (B); adapted[59]. Open access article.

Modularity plays a critical role in enhancing a structured network's ability to process information by balancing local segregation with global integration. By organizing neurons into distinct modules, each with high internal correlations and reduced inter-module interactions, the network achieves more efficient and diverse activity. Sato et al. found that in modular networks, primary cortical rat neurons within the same module were highly synchronized, while interactions between different modules were less correlated. This arrangement contrasts with random networks, where high correlations are uniform across the entire network, leading to less complex and more homogeneous activity. Modular networks were also shown to exhibit higher complexity scores through 10-14 days in culture, as they allow for specialized processing within modules while maintaining sufficient communication between them[60]. These findings underscore the role modularity plays in structured neuronal networks, suggesting that this organization enables more flexible and adaptive information processing, mirroring dynamics found in the brain.

In information processing theory, modularity allows for local specialization and global integration, making systems more adaptable and efficient. Yamamoto et al. focused on how modularity influences dynamic richness and the balance between local and global activity in biological neuronal networks using primary cortical rat neurons. Their study compared neurons grown for 10 days in culture in three configurations—merged, triple-bond, and single-bond networks—and found that the most modular configuration (single-bond) showed the most flexibility in switching between localized and global firing patterns[58]. This suggests that the more modular a network, the better suited it is to handle complex tasks and adapt to changing conditions due to its increased flexibility. These findings highlight the importance of modularity for efficient information processing in biological systems and for designing more adaptable and robust artificial networks.

2.4 Biocompatible Materials for Neuronal Interfaces

Biocompatible materials are vital for neural interfaces, supporting neuron growth while minimizing inflammation. Mimicking the brain's extracellular matrix (ECM) is a promising approach, and Moon et al. demonstrated that ulvan (ULV), an algal derivative, combined with chitosan (CHT) in layer-by-layer (LbL) films, significantly improved rat hippocampal neuronal adhesion and neurite outgrowth compared to poly-d-lysine (PDL) surfaces (Fig.2.4.1). Additionally, these films selectively suppressed astrocyte adhesion, helping to prevent glial scar formation[61]. Suppressing astrocyte adhesion is meaningful because astrocytes form a glial scar at injury sites and play a role in inhibiting neuronal regeneration by secreting axon-repulsive proteoglycans[62]. Therefore, surfaces that support neuronal growth while minimizing astrocyte adhesion are optimal for in vivo neuronal interfaces. The dual functionality of these ULV-based films, combined with the adaptability of LbL assembly, highlights their potential for neural implants and other biomedical applications.

Figure 2.4.1: Schematic of layer-by-layer film fabrication (ULV - Ulvan, an algal derivative, CHT-Chitosan, a marine-derived polysaccharide); adapted[61]. Reprinted with permission.

Creating neural interfaces that match the mechanical properties of biological tissues is essential for minimizing tissue damage and enhancing long-term functionality. Yang et al. presented a novel approach using bacterial cellulose (BC), a biocompatible material, as a substrate for neural interfacing electrodes. The study shows that BC's mechanical properties closely resemble those of brain and peripheral nerve tissues, significantly reducing the bending stiffness and making it more conformable than conventional materials like polyimide. The Au-coated BC electrodes demonstrated high durability, maintaining over 95% conductivity after 100 cycles of bending, and exhibited excellent biocompatibility with reduced inflammatory response compared to traditional materials[63]. These findings suggest that BC-based electrodes hold great potential for applications in neural implants and other biomedical devices requiring soft, flexible interfacing.

PEDOT:PSS is a well-known conductive polymer used to interface with cells, however, preparation can be cytotoxic due to the solvents used for self-assembly and it can result in a brittle hydrogel. One attempt to use PEDOT:PSS while simultaneously addressing these challenges is to incorporate a multifunctional polyzwitterion, poly(sulfobetaine). Researchers introduced poly(sulfobetaine) as a covalent cross-linker into a PEDOT:PSS hydrogel, creating a multifunctional hydrogel. The multifunctional hydrogel was able to be patterned using photolithography due to the UV-sensitivity of poly(sulfobetaine). In addition, it was also found that at certain poly(sulfobetaine) precursor concentrations, the multifunctional hydrogel demonstrated a Young's modulus comparable to neural tissue[64]. Modifying the material properties of PEDOT:PSS by creating a multifunctional hydrogel increases the likelihood that an established conductive polymer can be used as a neural tissue interface.

Materials meant to act as conducting polymers are faced with challenges related to their ability to maintain contact with electrodes as well. Kleber et al. blended a synthetic hydrogel (P(DMAA-co-5%MABP-co-2,5%SSNa)) with PEDOT, to act as a coating material for a neural interface. Due to the properties of the synthetic hydrogel, the blended, conductive material was covalently bonded to a chemically coated electrode surface. In addition, they demonstrated that the synthetic hydrogel and PEDOT formed an interpenetrating network, confirming the preferred, homogenous distribution of PEDOT throughout the hydrogel matrix[65]. While the electrical properties of PEDOT are useful when interfacing with cells, there are engineering challenges associated with the production of neural interfaces that can be addressed by blending PEDOT with another polymer with specific material and chemical properties.

Silk-based bionic interfaces could also hold significant promise for advancing neural interfacing technologies due to their excellent biocompatibility, flexibility, and ability to support neuron growth. In one study, researchers explored the use of silk substrates to create a favorable environment for neuron-electrode interactions, which are essential for effective signal communication. They found that primary rat dorsal root ganglia neurons, a key cell type in the central and peripheral nervous systems, demonstrated significantly better attachment and extended neurite outgrowth on silk substrates compared to traditional polyimide surfaces. Further, human neural stem cells (hNSC) also showed improved proliferation on silk, with a 50% increase in cell numbers after five days of culture compared to polyimide, and minimal signs of toxicity[66]. These results highlight silk's potential as a neural interface material, offering both biocompatibility and functional support for neural development.

The development of biocompatible materials for neural interfaces is evolving, with innovative approaches demonstrating improved neuron adhesion, reduced inflammation, enhanced mechanical compatibility with neural tissues, and improved adhesion to electrodes. Ulvan-based films, bacterial cellulose, and silk fibroin are emerging as promising candidates, offering both biocompatibility and the mechanical properties necessary to create stable, long-lasting neural interfaces. These materials facilitate better neuron growth and functionality and reveal new possibilities for the design of next-generation biomedical devices that can seamlessly integrate with the nervous system. While PEDOT:PSS remains a useful conductive polymer, modifications to its functionality via the incorporation of other materials are demonstrated to increase its utility. As research continues, the potential for these materials to revolutionize neural interfacing technologies becomes increasingly apparent.

3 Goals of This Thesis

Despite indications that cell-cell interactions and topographical cues influence neuronal behavior[18–21], it remains unclear how these factors work together to influence behavior when cells are confined. Specifically, few studies have characterized the impact of neuronal location within such microenvironments on neuronal differentiation and migration as well as neurite extension. While several investigations have explored changes in neurite outgrowth and guidance[43,45,46], the outcomes induced simultaneously by cell density and cell-structure contact on neuronal morphology and localized migration have yet to be fully elucidated.

To address this gap, we propose that both cell density and physical confinement within precisely engineered 3D-printed microstructures drive neuronal differentiation, morphology, and migration in ways that have not previously been captured or examined using in vitro systems (Fig. 3.1). Specifically, we hypothesize that (1) cell densities under confinement will impact neuronal differentiation and proliferation, (2) individual cells demonstrate behaviors that correlate with their spatial relationship to the confinement structure, and (3) the presence of a confinement microstructure influences differentiation, proliferation, and migration. By examining the density, location, and neurite length of PC12 cells within these microstructures, we aim to unveil how confinement influences fundamental neuronal behavior, thereby affording the synthetic structure some degree of control over the emergent properties of developing neuronal networks.

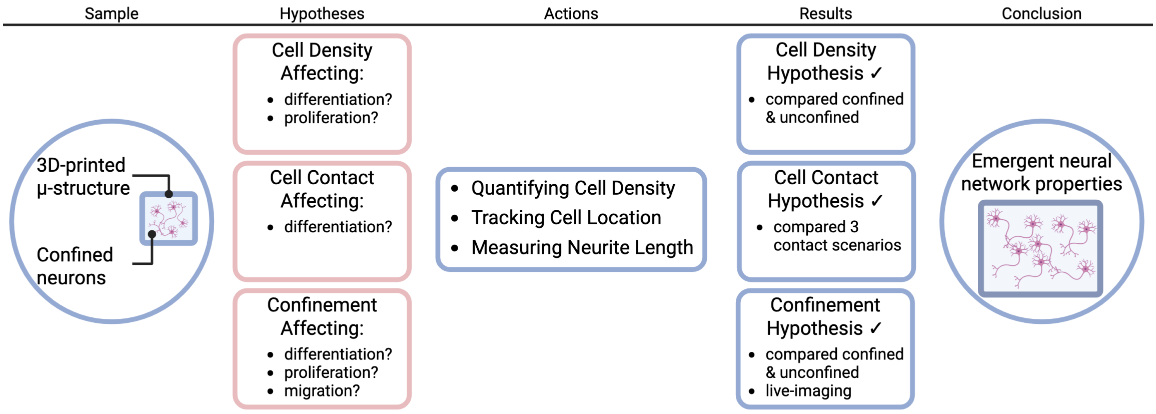

Figure 3.1: Project overview. Schematic depiction of how PC12 cells confined within 3D-printed microstructures are examined for cell density, cell location, and neurite length to test hypotheses related to differentiation, proliferation and migration in confined microenvironments. Created in https://BioRender.com.

4 Results and Discussion

4.1 Introduction

The results presented here demonstrate various aspects of PC12 behavior within a 3D printed confinement structure. Neuron-like PC12 cells are seeded on substrates coated with laminin, containing 3D printed confinement structures, and cellular behavior is interrogated over a period of 5 days. When possible, a comparison between previously published literature and the results obtained in this project is presented. Not all results from published literature allow for direct comparison. In some cases, previously published outcomes utilize alternative experimental approaches and data gathering strategies, and possibly provide insightful explanations for the results obtained in this project.

First, PC12 cells are characterized, confirming a neuron-like phenotype, and their behavior on various substrates is explored. Next, the 3D printed microenvironment is presented, along with a discussion rationalizing the experimental setup (microenvironment details, cell classification and data gathering) from both an engineering and biological perspective. The remaining results provide experimental data that assess multiple aspects of PC12 behavior within 3D printed confinement structures. The purpose of the results presented is to strongly argue that confined neurons demonstrate unique behaviors that result from confinement which could be relevant to the development of in vitro neuronal tissue models, neuronal networks, and efforts to guide neuronal behavior.

4.2 PC12 Characterization

The immunostaining of PC12 cells demonstrates successful differentiation into a neuron-like phenotype (Fig. 4.2.1). Cells stained after 14 days in vitro with DAPI reveal nuclei (Fig. 4.2.1, (i)), while Tau[67] (Fig. 4.2.1, (ii)) and MAP2[68] (Fig. 4.2.1, (iii)) highlight axons and dendrites[10], respectively. The merged image (Fig. 4.2.1, (iv)) illustrates the co-localization of these features, confirming that the PC12 cells have developed both dendritic and axonal neurites. This is indicative of neuronal differentiation, a well-established outcome when PC12 cells are treated with nerve growth factor (β-NGF) to mimic neuronal behavior[69].

Differentiated PC12 cells show a distribution of cytoskeletal markers similar to that presented in Jeon et al.[70], providing sufficient evidence of typical PC12 cell fate upon β-NGF exposure. The presence of MAP2 in dendrites and Tau in axons also aligns with the findings of Kanai et al., who used mouse spinal cord neurons to demonstrate that MAP2 is overexpressed in dendrites while Tau is predominantly localized in axons[71]. This staining pattern is a hallmark of neuronal morphology and is consistent with mature, differentiated neurons.

The comparison to rat hippocampal neurons from Dehmelt et al. further supports the validity of this model. In hippocampal neurons, MAP2 and Tau exhibit similar staining patterns, reflecting the characteristic organization of neurons[72]. By demonstrating comparable immunostaining profiles, this figure suggests that PC12 cells can serve as a reliable proxy for studying neuronal biology, offering a functional and morphological model for investigating neurodevelopment, neuronal network formation and in vitro neuronal behavior. These results reinforce the reliability of PC12 cells as a neuronal model system and provide a foundation for further exploration of neuronal functions, structures, and pathologies.

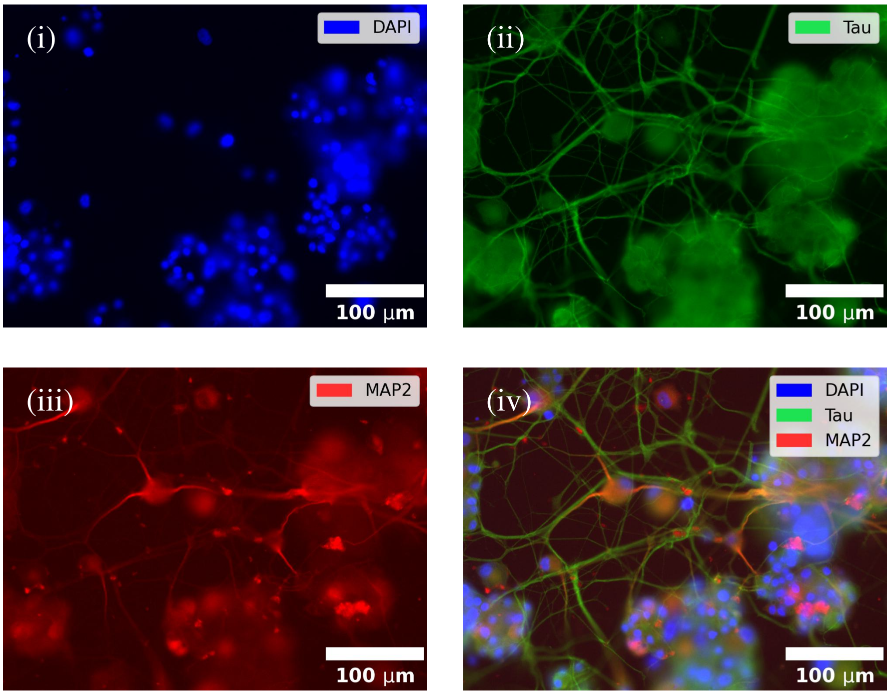

Figure 4.2.1: Representative images of PC12 characterization after 14 days *in vitro* on a 10 μg/ml laminin 111 coated glass surface. Nuclear staining via DAPI (i); DAPI is a commonly used fluorescent dye that preferably binds A-T rich regions of dsDNA; anti-Tau staining (ii); Tau, a microtubule-associated protein, is responsible for microtubule bundling in the axon[10]; anti-MAP2 staining (iii); MAP2, a microtubule-associated protein, is responsible for microtubule bundling in dendrites[10]; colocalization of nuclei and proteins (iv). Tau and MAP2 are therefore rational biomarker targets to assess a neuronal phenotype. Similar neuronal cytoskeletal markers have been observed in other investigations[70–72].

4.3 PC12 Differentiation on Protein Coated Surfaces

PC12 cells were cultured for 4 days on different substrates (1 mg/ml poly-L-lysine, uncoated glass as a (-) control, 10 μg/ml collagen type 1, and 10 μg/ml laminin; representative images in Figs. 4.3.1, i - iv, respectively) and their adhesion and differentiation was qualitatively compared.

After 4 days in vitro, the cells exhibit distinct morphologies, providing insights into how each surface treatment influences PC12 adhesion and differentiation.

PC12 cells grown on poly-L-lysine (PLL) demonstrate an aggregated morphology with minimal/non-existent neurite extension (Fig. 4.3.1, i). PLL supports cell adhesion by providing a positively charged surface to interact with the anionic cell membrane, but it could lack the biological components required for PC12 differentiation. In a related investigation, PC12 cells were found to adhere and differentiate to a lesser extent on PLL, when compared to laminin[73]. This outcome suggests that when compared to laminin, PLL does not possess the signaling domains required by PC12 cells. This is likely explained by the fact that PLL is a synthetic, positively charged polymer. The (-) control condition, an uncoated surface, shows minimal neurite outgrowth and patches of spherical cells (Fig. 4.3.1, ii), similar to what is observed when cells are cultured in suspension (not shown). Upon gently tapping the (-) control sample, it was observed that cells readily wobbled, suggesting they were not attached to the surface, reinforcing the importance of pre-coating a surface to promote neuron-like characteristics. PC12 cells cultured on collagen type 1 demonstrated neurite growth and their cell body morphology suggests they readily adhere to the coated surface (Fig. 4.3.1, iii). In a related study, collagen type 1 promoted PC12 adhesion and differentiation, but collagen type 1's effects on PC12 differentiation may be sub-optimal[74]. On laminin coated surfaces, PC12 cells display extensive neurite outgrowth, with clear, long projections extending from the cell bodies (Fig. 4.3.1, iv). Laminin is known to promote neuronal differentiation by interacting with integrins and other surface receptors to facilitate axon guidance. PC12 cells express integrins $\alpha_1\beta_1$, which binds with laminin fragments E1-4 and E1, and $\alpha_3\beta_1$, which binds with laminin fragment E8[35]. This image confirms laminin's efficacy in promoting both cell attachment and differentiation. Laminin, therefore, was selected as the sole adhesion protein used for this study.

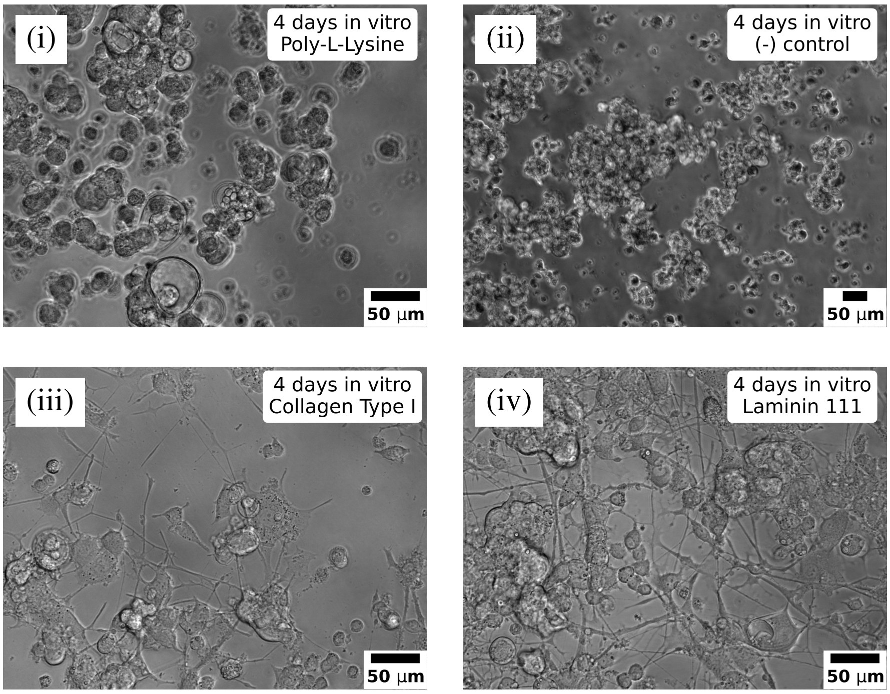

Figure 4.3.1: Representative images of β-NGF exposed PC12 cells after 4 days in vitro on glass surfaces coated with 1 mg/ml poly-L-lysine (i), uncoated glass ((-) control) (ii), 10 μg/ml collagen type I (iii), and 10 μg/ml laminin (iv). Cells seeded on poly-L-lysine surfaces adhere because their negatively charged membranes are electrostatically attracted to the positively charged polymer coating. Their morphology is aggregated, however there is minimal/non existent neurite extension. In contrast, in the absence of any surface treatment, PC12 cells do not adhere. Upon coating with collagen type 1 or laminin, cells adhere, form focal adhesions and differentiate. However, the less robust differentiation observed on collagen type 1 here may at least partly be explained by the fact that of the $\alpha_1\beta_1$ and $\alpha_3\beta_1$ integrins expressed by PC12 cells, only $\alpha_1\beta_1$ binds to collagen, while both $\alpha_1\beta_1$ and $\alpha_3\beta_1$ bind to laminin[35].

4.4 3D Printed Confinement Microstructures

The 3D printed confinement structure's shape is derived from a study on single-cell dynamics in migrating cancerous (MDA-MB-231) and non-cancerous cells (MCF10A) by Bruckner et al. where researchers sought to elucidate the behavioral dynamics of a single migrating cell by confining the cell in a microenvironment entailing two 37 x 37 μm square islands linked by a narrow channel (6-56 μm). This layout is rationalized by the idea that a minimal system will allow for an understanding of a migrating cell's behavioral dynamics[75]. In the system presented herein, a microenvironment was sought that allowed for confinement of a cell population. More specifically, the microenvironment used herein was designed to confine 1) neuronal formation of neurites resulting from differentiation and 2) neuronal migration. Guidance was taken from the microenvironment used by Bruckner et al. because there is a similar desire here for a system with minimal features, this time designed to guide a confined population of differentiating, migrating, and proliferating neurites. The dimensions of the structure, including the narrow midsection, are derived from three previous investigations: 1) 2PP 3D printed cell cavities used to confine neuronal populations in Buchmann et al., previously discussed in sec. 1.7 (110 x 110 μm, with a

10 μm channel for neurite extension; cf. herein: 95 x 200 μm with a 14 μm narrow channel for neurite guidance)[47], 2) the 200 x 200 μm micropatterned regions utilized by Yamamoto et al. to analyze neuronal dynamics[58], previously discussed in sec. 2.3 and 3) the modular primary rat cortical neuronal networks applied to collagen type 1 coated microelectrode arrays (each module was 200 x 200 μm connected via a 7 μm channel), briefly discussed in sec. 2.3[60]. The dimensions chosen for this investigation could therefore provide guidance for studies that seek to electrically excite confined or structured neuronal populations[60].

The 3D printed confinement structure's design is meant to expose cells in the same confined environment to curves, corners, straight edges, open space, and an obstacle in the form of a narrow opening. In addition, since structural features are raised off the glass surface, this gives cells the opportunity to laterally interact with structure walls. The small, protruding features outside the closed region of each structure ("feet", Fig. 4.4.1, ii, upper middle) are meant to reduce the likelihood that 1) structures will delaminate from the glass surface and 2) cells under confinement will interact with cells outside the confined area. Confining PC12 cells in these structures is intended to at least promote localized cell-cell interaction and cell-structure interaction.

IP-Visio, a commercially available non-cytotoxic, negative tone resin, was used as the sole 3D printing resin in this investigation. This decision was made because of both IP-Visio's inherent features and demonstrated performance in related work. One of its key features is that its photosensitivity is optimized for use with a 25X printing objective (which has a printing diameter of 400 μm)[76], enabling fabrication of the structures used in this investigation (140 μm $\times$ 265 μm) without any noticeable seams, thereby improving their structural integrity. In previous work, IP-Visio resin was used to create microenvironments that interact and guide mesencephalic neurons in a co-culture with astrocytes[47]. Additionally, the low-autofluorescence of IP-Visio structures[77] facilitates clear imaging, which assists with immunocytochemistry. IP-Visio was therefore an ideal choice because its features and previous performance align well with the aims of this investigation.

3D printed confinement structures were produced using the Nanoscribe Photonic Professional GT2 in conjunction with IP-Visio (Fig. 4.4.1).[1] A 3 x 3 array of 3D-printed confinement structures was fabricated (Fig. 4.4.1, i). Although the Young's Modulus of these structures was not specifically determined, at least one investigation found that, when exploring a range of printing parameters, the Young's modulus of IP-Visio was as low as ~40MPa and as high as ~280MPa (this is briefly discussed in appendix section A.5)[78]. Each confinement structure, an hourglass-like unit, is designed to support neuronal growth, migration, and network formation within its defined geometry. Scanning electron microscopy images[2] show that the mean width and length of the confinement area of each structure are 95.77 ± 0.78 μm (0.81%) and 200.2 ± 0.89 μm (0.45%, n = 9), respectively; supportive structures ("feet", as indicated) meant to maintain adhesion between the structure and glass are also labeled (Fig. 4.4.1, ii). Magnified views of the narrow midsection (Fig. 4.4.1, iii) and the wall height (Fig. 4.4.1, iv, imaged at a

---

[1] 3D printed structures were provided by Ms. Malin Schmidt, M.Sc.

[2] SEM images were provided by Mr. Sebastian Weber.

59.8° tilt angle) reveal fine details. Measurements of the narrow midsection of each structure in a printed array show a mean distance of 14.10 ± 0.34 μm (2.40%, n = 9). Similarly, measurements of the wall height in the printed array yield a mean height of 45.64 ± 1.15 μm (2.52%, n = 9, calculated from a measured distance of 39.45 ± 1.00 μm at a 59.8° tilt angle). Measurements of the confinement area yield a mean value of ~15,352.1 μm^2 ± 171.7 μm^2 (1.12%, n = 9). This architecture is intended for direct printing onto silanized boroscilicate glass substrates, providing a unique platform for examining neuronal dynamics within constrained microenvironments.

One aim of this investigation is to understand the behavioral changes induced in PC12 cells by confinement. The open space in this structure provides opportunities for cell migration, cell isolation, and cell-cell contact absent structural contact. The size and shape of the structure may also be conducive to guiding neurite outgrowth along specific pathways, which could enhance any investigation into the relationship between topology and cell behavior. In a related investigation, researchers found that when PC12 cells were seeded on patterned ridges and grooves of varying sizes, neurite outgrowth followed the ridged and grooved patterning. In addition to finding that anisotropic substratum features guided neurite growth, they also found that neurites responded to feature sizes as small as 70nm[79]. Furthermore, since neurons are known to respond to physical cues present in vivo[80], what could be meaningful about an analogous in vitro investigation is to interrogate and potentially induce similar behaviors. Qiu et al. demonstrated that when mouse hippocampal neurons were applied to arrays of high aspect ratio microtubes (structures had a maximum height of 130 µm and an aspect ratio of 16), the high aspect ratio microtubes increased neuronal proliferation and synaptic connections[81], somewhat paralleling the findings presented herein - interaction with the structure enhances some aspects of neuronal behavior. However, the effect of a confined environment containing ample open space on neuronal behavior remains an open question.

This confinement structure could be used to study cellular responses to physical constraints, such as how limited space influences neuronal differentiation, polarity, neurite extension and synaptic connectivity. The confinement structure used in this investigation provides a platform for studying PC12 growth and network formation in a controlled, microscale environment. The precise design and fabrication achieved with the Nanoscribe Photonic Professional GT2 enables the creation of structures that confine PC12 growth and provide insight into how cell-cell interactions and physical cues influence PC12 behavior. Results presented below utilize the confinement structure to explore the following: 1) biocompatibility (sec. 4.6)), confinement effectiveness (sec. 4.10), cell proliferation (sec. 4.11), neurite length (secs. 4.12, 4.13), neurite count (sec. 4.14), and migration (sec. 4.15).

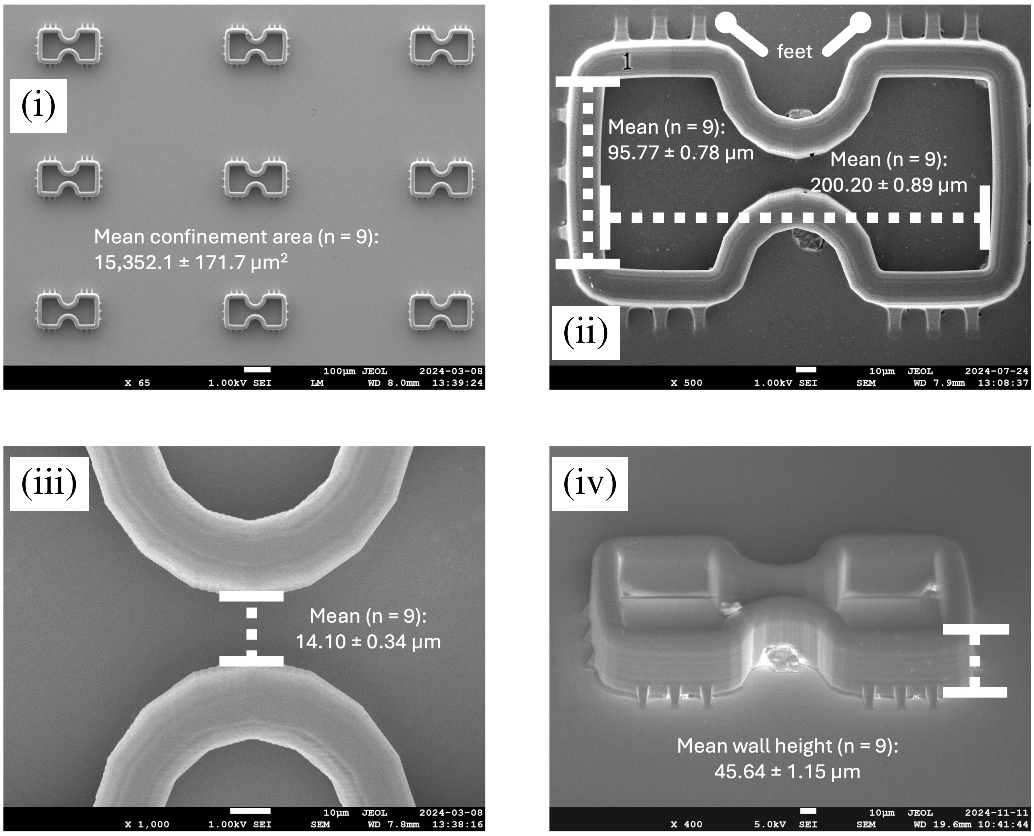

Figure 4.4.1: SEM of array of 2-photon polymerization (2PP) printed confinement structures fabricated using the Nanoscribe GT2 in conjunction with IP-Visio, a biocompatible polymerizable resin, with a mean confinement area of ~15,352.1 μm^2 ± 171.7 μm^2 (~1.12%, n = 9 printed structures) (i); confinement area lateral dimensions: mean width and length are 95.77 ± 0.78 μm (~0.81%) and 200.2 ± 0.89 μm (~0.45%, n = 9) respectively; supportive structures ("feet") are also indicated (upper middle of image) (ii); a magnified view of the narrow midsection, with a mean width of 14.10 ± 0.34 μm (n = 9) (iii); structure height imaged at a 59.8° tilt angle: mean wall height of 45.64 ± 1.15 μm (~1.66%, n = 9, calculated from a measured distance of 40.67 ± 0.67 μm) (iv). 3D printing courtesy of M. Schmidt, SEM courtesy of S. Weber.

4.5 Experimental Setup

In this investigation's experimental setup, microstructures were 3D-printed on glass and surrounded by a PDMS block with a central "donut hole" of 8 mm in diameter to minimize the volume of liquid media required, while simultaneously ensuring cell viability (supporting $\sim$ 150-200 μl of liquid), all placed inside a petri dish (Fig. 4.5.1). Fig. 4.5.1(i) illustrates the stepwise assembly of the system, showing 1) the coverslip with 2 separate 3x3 microstructure arrays which is glued into a petri dish with the bottom already removed, using biocompatible glue, then 2) the printed microstructure arrays are surrounded by a PDMS block which is glued into the petri dish using biocompatible glue. Fig. 4.5.1(ii) presents the final assembled product.

To interrogate the nuances of PC12 cell behavior under confinement, the assembly provides a number of advantages related to both the ease of fabrication and the robust environment it offers for cells to interact with 3D printed microstructures. PDMS can be readily fabricated at the benchtop, and its utility extends from simple prototypes to multifunctional, fully operational systems, providing immediate and predictable support for this investigation. PDMS was used due to its established biocompatibility and non-toxic properties, which support mammalian cell growth, as demonstrated in earlier studies[82]. Each feature in this system was included because it has previously demonstrated the ability to effectively support the interaction of neurons with 3D printed microstructures, providing at least some insight into how to construct complex, modular neural networks in vitro.

The experimental system presented herein combines the advantages of the ease of use and biocompatibility of PDMS with the microscale precision and versatility of 3D printing. The platform provides a useful environment within which to study PC12 behavior under confinement. The versatile and modular features of the experimental setup enabled repeatability, ultimately assisting in the facile and reliable observation of PC12 behavior over multiple days, as well as the collection of meaningful data.

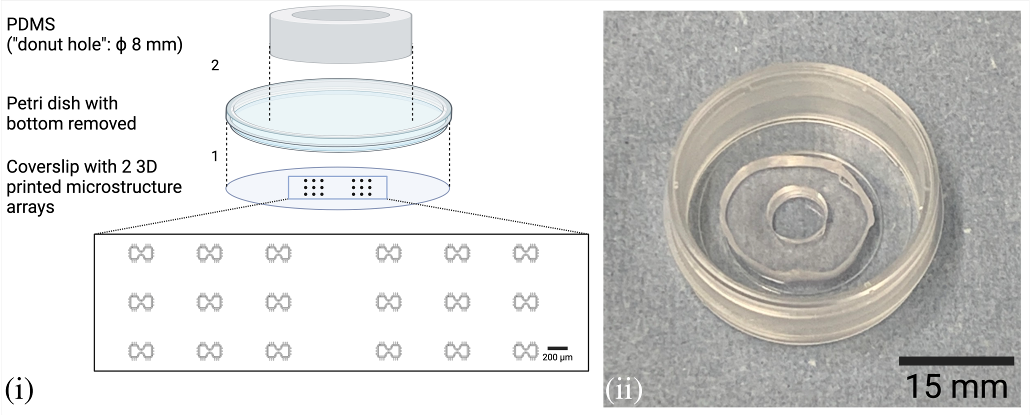

Figure 4.5.1: Schematic of the custom experimental setup, consisting of a petri dish with the bottom removed and a coverslip with 2 3D printed microstructure arrays glued into place (step 1) and a biopsy punched (ϕ: 8 mm) PDMS block glued onto the glass from above to create a 200 μl microwell (step 2) surrounding the printed arrays; a magnified view of the printed arrays (inset) (i), created in https://BioRender.com. A photograph of the assembled system (ii).

4.6 Live Dead Assay

A Live/Dead assay of PC12 cells cultured under different conditions for 7 days (Fig. 4.6.1) mainly provides insight into the influence of the 3D confinement structure on cell viability. The experimental condition (Fig. 4.6.1, (i)), where cells in medium are growing within the IP Visio 3D-printed hourglass structure (outer vertical edges of a single confinement structure are indicated by a white dashed line) shows mostly green fluorescence with a few red regions, indicating nearly all cells are viable. The center image (Fig. 4.6.1, (ii)) is of a live control group where cells are growing in medium, showing mostly green fluorescence and therefore nearly

100% cell viability. The right image (Fig. 4.6.1, (iii)) contains a (-) control group where all cells were incubated in 100% ethanol for 3 minutes prior to staining, showing all cells are non-viable. This assay uses standard live/dead markers, Calcein AM and Propidium Iodide, diluted in cell medium, to differentiate between living and dead cells.

Nearly all cells (> 90%) are alive when cultured in the presence of the 3D-printed structure, as indicated by widespread green fluorescence (Fig. 4.6.1, (i)). The cells appear to have adhered and proliferated in and around the confinement structure, suggesting polymerized IP-Visio is biocompatible with PC12 cells, and therefore does not inhibit cell viability. The presence of some red-stained cells indicates either a few instances of cell death or microscopic artifacts, both of which can be expected in long-term cultures, but overall viability appears high. This outcome aligns with previous research, where IP-Visio is meant to demonstrate low autofluorescence[77] and be biocompatible[47].

The live control group (Fig. 4.6.1, (ii)) shows nearly 100% of cells appearing alive and healthy, as indicated by green fluorescence. This comparison indicates that including a 3D-printed structure does not negatively impact cell viability when compared to a standard 2D culture, absent 3D-printed structures. Both groups exhibit pronounced growth, indicating that the experimental setup supports PC12 growth and proliferation.

The dead control group (Fig. 4.6.1, (iii)) shows exclusive red fluorescence, indicating that the cells have undergone extensive cell death. As a negative control, this image provides a clear contrast to the high cell viability observed in both the experimental and live control groups. Therefore, culture conditions in the experimental and live control groups are supportive of cellular health and survival over at least 7 days.

These findings suggest that the 3D-printed confinement structure effectively supports PC12 cell survival and growth, comparable to traditional 2D culture. The live/dead assay provides clear evidence that the structure's design and material composition are conducive to PC12 viability, making it a promising platform for studying differentiation, network formation, and cell behavior in response to cell-cell and cell-structure interaction.

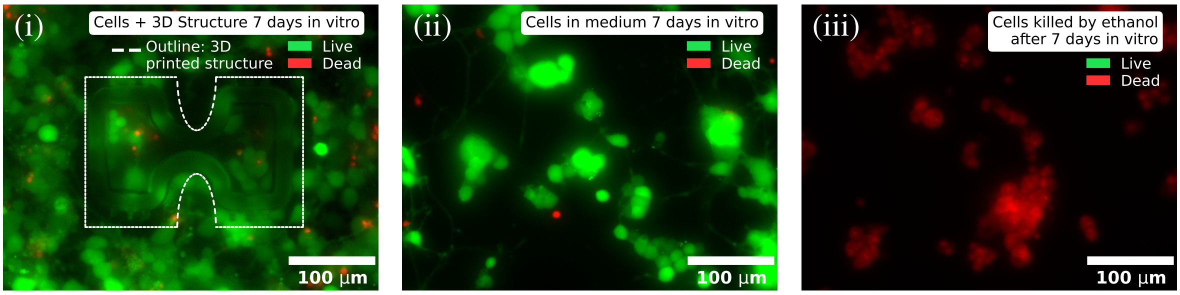

Figure 4.6.1: Live/Dead Assay: Cells cultured in medium and in the presence of an IP-Visio 3D printed structure (i, structure outline indicated by dashed white line), positive control (ii, cells cultured in medium, no structure), negative control (iii, cells incubated in 100% ethanol for 3 min., no structure), stained with Calcein AM and Propidium Iodide after 7 days in vitro. Results show that the 3D-printed confinement structure supports PC12 cell survival and growth, comparable to standard 2D culture absent 3D-printed structures. The presence of green fluorescence indicates high cell viability in both the experimental (i) and live control (ii). The structure's biocompatibility suggests it can effectively support PC12 differentiation and growth for at least 7 days.

4.7 Labeling Cells and Classifying Population Type

Cells under confinement can have one of three possible labels (Fig. 4.7.1, i). First, each cell is labeled based on its membrane interaction: cells whose membranes touch any part of the structure are labeled as **edge** cells, cells whose membranes touch no other cell and no part of the structure are labeled as **isolated** cells and cells whose membranes touch other cells but who are not also touching any part of the structure are labeled as **clustered** cells. This labeling scheme is drawn from strategies previously taken where cell-structure contact involving mesencephalic neurons and 3D printed structures[47], cell-cell contact utilizing PC12 cells[83], and isolated cell behavior using neural stem cells[19] were examined. Second, any respective neurite growing out of a given cell is given the same label (edge, isolated, clustered) as its originating cell. Labeling cells in this way aids in determining the relationship each cell has with neighboring cells and the surrounding structure. The idea that the presence or absence of physical contact with a topological modification may reveal distinct cell behaviors was previously discussed (Cell Classification in Neuronal Studies, subsec. 1.2.1). Introducing this labeling system helps determine the role that features of the microenvironment play in determining cell behavior, especially neurite growth.

Structures were also separated into three categories based on their respective cell population types (Fig. 4.7.1, ii). First, it is calculated that in the confinement area, approximately 26 cell bodies occupying the area would constitute 100% confinement. This calculation is based on an estimated cellular diameter of 27 um, assuming cell bodies are circular, and a measured hourglass-like confinement area of 15,352.1 μm^2 (result would be ~26 cells/confinement area). Accounting for numerous variations in overall packing efficiency (common scenarios include square packing or hexagonal/honeycomb packing), it was determined that there are three categories that can provide distinct population types: **sparse** (structures less than 20% occupied), **intermediate** (structures 20–50% occupied), and **dense** (structures more than 50% occupied). As outlined in table 4.1

below, these density values fall within ranges undertaken in previous studies that examined the effect of cell density on cell behavior in neuronal cultures. In addition, accounting for cell density when analyzing cell behavior in neuronal cultures follows strategies previously undertaken[25–27] and has been discussed herein (Cell Density Effects on Neuronal Behavior, sec. 1.3).

Cell Density (herein Population Type)	**Ivenshitz et al.[27]**	**Herein**	**Biffi et al.[84]**
Sparse	1.5×10^4 cells/cm^2	~3.3×10^4 cells/cm^2	9×10^4 cells/cm^2
Medium (herein Intermediate)	3×10^4 cells/cm^2	~6.5×10^4 cells/cm^2	18×10^4 cells/cm^2
Dense	4.5×10^4 cells/cm^2	~12.4×10^4 cells/cm^2	36×10^4 cells/cm^2

Table 4.1: Comparison of Cell Densities Across Studies

It is considered that within each of the population types, the factors influencing cell behavior differentially impact the cells under confinement. For example, in a sparsely populated structure, the conditions created by the presence of other cells is distinct: there is ample opportunity for cells to migrate, occupy open space, or occupy the structure edge. In contrast, in a densely populated structure, the impact made by the increased presence of other cells is likely to induce outcomes which contrast with the outcomes induced in sparsely populated confinement environments: there is less space available for cell movement and fewer opportunities for cells to interact directly with the structure. Classifying individual confinement structures by population type enables systematic investigations into how different cell counts may affect processes such as proliferation, differentiation, neurite growth, and cell migration, providing a valuable tool for studying neurodevelopmental mechanisms and the effect of spatial constraints on in vitro neuronal systems. Conclusions that relate varying population types to behavioral responses in neuron-like PC12 cells can then be drawn. Correlating cell behavior with population type, then, could provide insight into understanding some of the principles that inform design of synthetic microenvironments for the purpose of interrogating cellular systems in vitro.

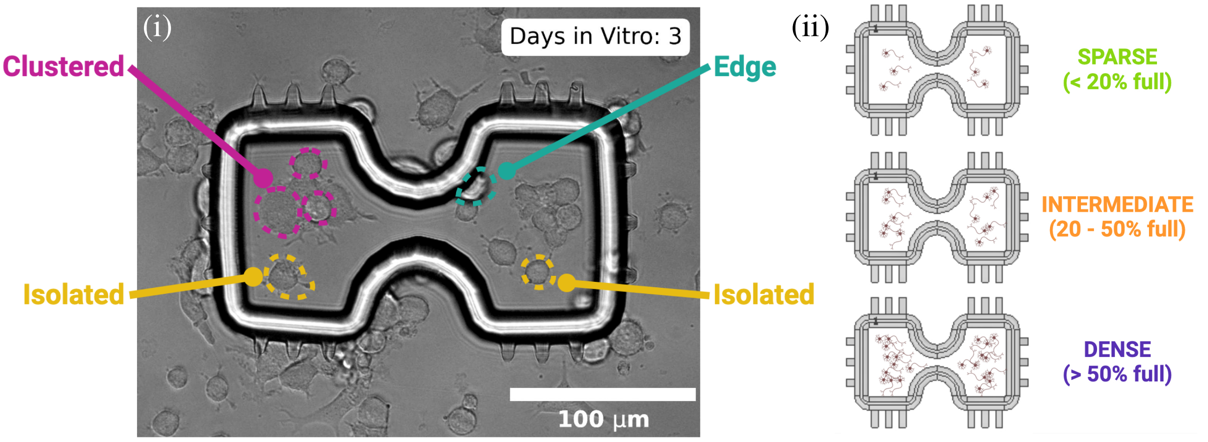

Figure 4.7.1: Labeling cells according to cell membrane contact with the structure or neighboring cells. Cells are given one of three labels based on their respective membrane interaction: **edge** cells (membranes touch any part of the structure), **isolated** cells (membranes touch no other cell or structure), and **clustered** cells (membranes touch other cells but not the structure). Neurites are given the same label, according to the label of their originating cell (i). Classifying population type. Population types fall into one of the three following categories: **sparse** (less than 20% occupied), **intermediate** (20–50% occupied), and **dense** (more than 50% occupied) (ii). Population type designations were determined by calculating that ~ 26 cells would constitute 100% occupancy in the confinement area, based on an estimated cell diameter of 27 μm and a total confinement area of 15,352.1 μm^2.

4.8 Raw Data Acquisition and Statistical Analysis

To begin the process of acquiring quantitative data from microscopic images, Fiji's `Simple Neurite Tracer`[85] (SNT) plugin is opened via `Neuroanatomy` in the `Plugins` dropdown menu (Fig. 4.8.1, 1); images are uploaded to Fiji, adjusted for proper scaling, and then opened in `SNT` (Fig. 4.8.1, 2); cellular features are then annotated, recorded on the image of interest, and compiled in the `Path Manager` window (Fig. 4.8.1, 3); when all desired cellular features have been identified, the data from `Path Manager` can be saved in three desired file formats for later use: `*.traces`, `*.swc`, and `*.csv` (Fig. 4.8.1, 4). Options in `Path Manager` allow for precise annotation of different structures (any tracings are recorded both in `Path Manager` and on the image (see inset photos, 4.8.1, 3). As shown in Table 4.2, the various file types are used for different purposes in the data acquisition and analysis workflow. A detailed, step-by-step guide to raw data acquisition is provided in A.6, Raw Data Acquisition and Analysis.

Throughout this investigation, where notations are indicated on plots, datasets are compared using the Mann Whitney U test (also known as the Mann-Whitney-Wilcoxon test or Wilcoxon rank-sum test). This test was used because it does not require data to be normally distributed (i.e. distributed in the shape of a bell curve). Additional explanation of how this test works is provided in appendix sec. A.7 (Mann Whitney U test) below. In addition, throughout this investigation, datasets are represented by their respective median values and the range of data within datasets is represented by a 95% confidence interval. An explanation discussing this approach is provided in Use of Median and Confidence Interval (Appendix A.8) below.

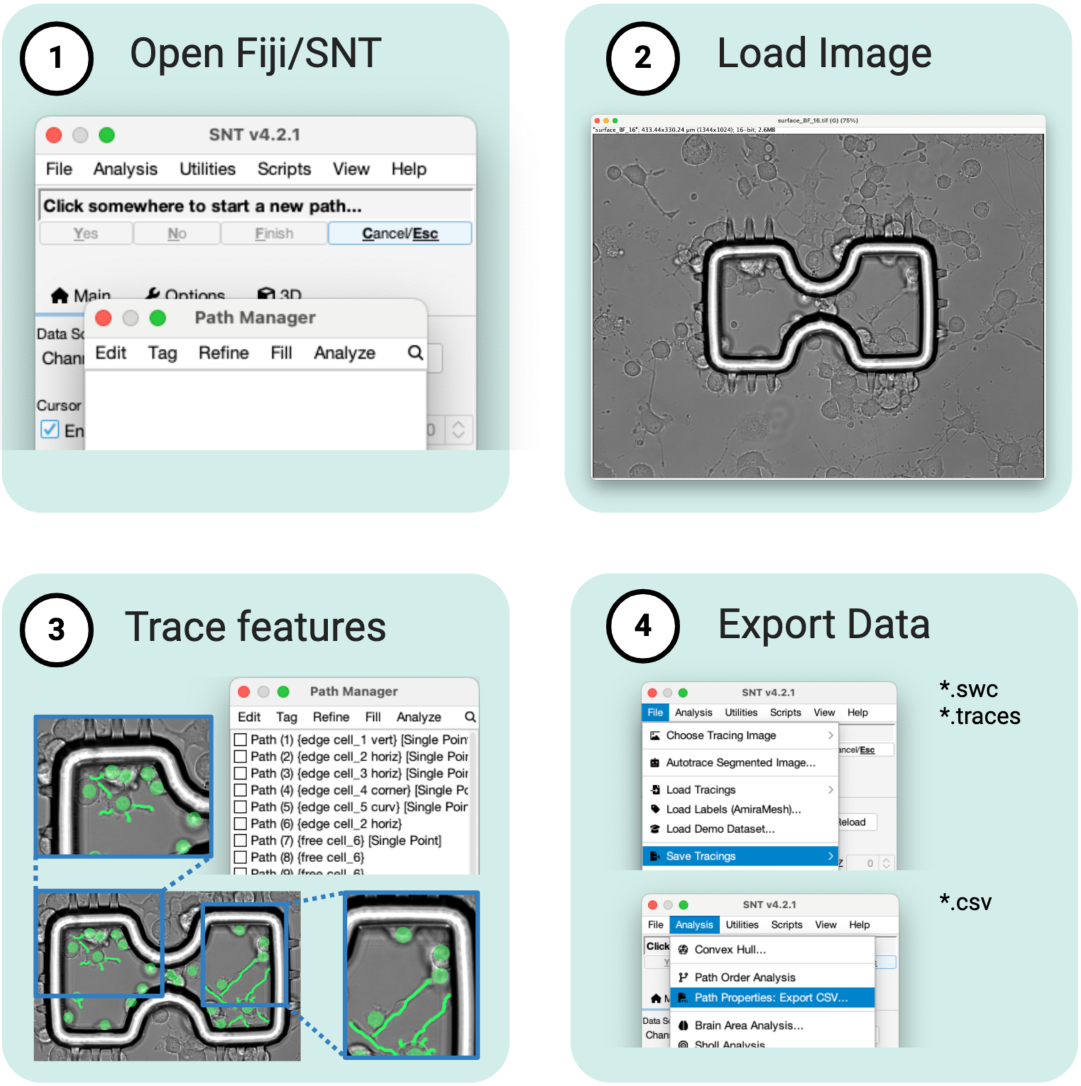

Figure 4.8.1: Workflow for manual tracing and data export using Fiji/`Neuroanatomy/Simple Neurite Tracer`[85] (SNT) plug-in. Images are uploaded to Fiji, adjusted for proper scaling, and then opened in the SNT plug-in. Cellular features are then annotated and compiled in the Path Manager window and raw data can then be saved. The process includes: 1) Open Fiji/SNT: Start by launching Fiji and, via `Neuroanatomy` in the `Plugins` drop-down menu, open `SNT` which will open the `SNT v4.2.1` and `Path Manager` windows, to enable feature tracing; 2) Load Image: Upload the desired image containing the features to be traced; 3) Trace Features: Trace specific cellular features which will be added to a list in the `Path Manager` window; any tracings are recorded both in `Path Manager` and on the image (see inset photos); 4) Export Data: Once tracing is completed, export the annotated data in `*.traces`, `*.swc`, and `*.csv` formats for further analysis. These file formats serve different roles in the data acquisition and analysis pipeline, as outlined in Table 4.2. A detailed explanation of the data acquisition workflow is provided in Appendix A.6, Raw Data Acquisition and Analysis. Created in https://BioRender.com.

File Type	Purpose
`*.traces`	A single file is saved per image; saves the state of the tracing session, allowing the user to reopen it later to modify or add paths if needed.
`*.swc`	A single file is saved per path listed in the Path Manager; plain text files that can be used for analysis; provide pixel-by-pixel locations of the respective cellular features.
`*.csv`	A single file is saved per image. Descriptions of stored data are found in appendix table A.6.2 in appendix section A.6

Table 4.2: The types of raw data files generated during the tracing process in Fiji/Neuroanatomy/Simple Neurite Tracer (SNT), along with their respective purposes. These file formats are essential for documenting and analyzing traced cellular features, and these data formats support flexible workflows and ensure reproducibility in the data analysis pipeline.

4.9 Ensuring Accuracy in Raw Data Gathering

Three examples of the same structure and its respective tracings on days 1, 3, and 5 demonstrate the difficulty associated with gathering accurate raw data (Fig. 4.9.1). While it is rather facile to determine cell membrane contact and respective associated neurites on day 1 (Fig. 4.9.1, i-a, ii-a, iii-a), by day 3 (Fig. 4.9.1, i-b, ii-b, iii-b) and day 5 (Fig. 4.9.1, i-c, ii-c, iii-c), the task becomes more difficult. As shown on days 3 and 5, the confinement structure becomes more crowded with cellular features and it is therefore more challenging to visually determine 1) cell membrane contact, 2) differences between cells, and 3) the correct relationship between a given neurite and its originating cell. In spite of this, the quantitative data provided in the following sections suggest predictable trends when collected in aggregate. These trends, if consistent, would lend support to any conclusions about cellular behavior in confinement, as discussed in subsequent sections.

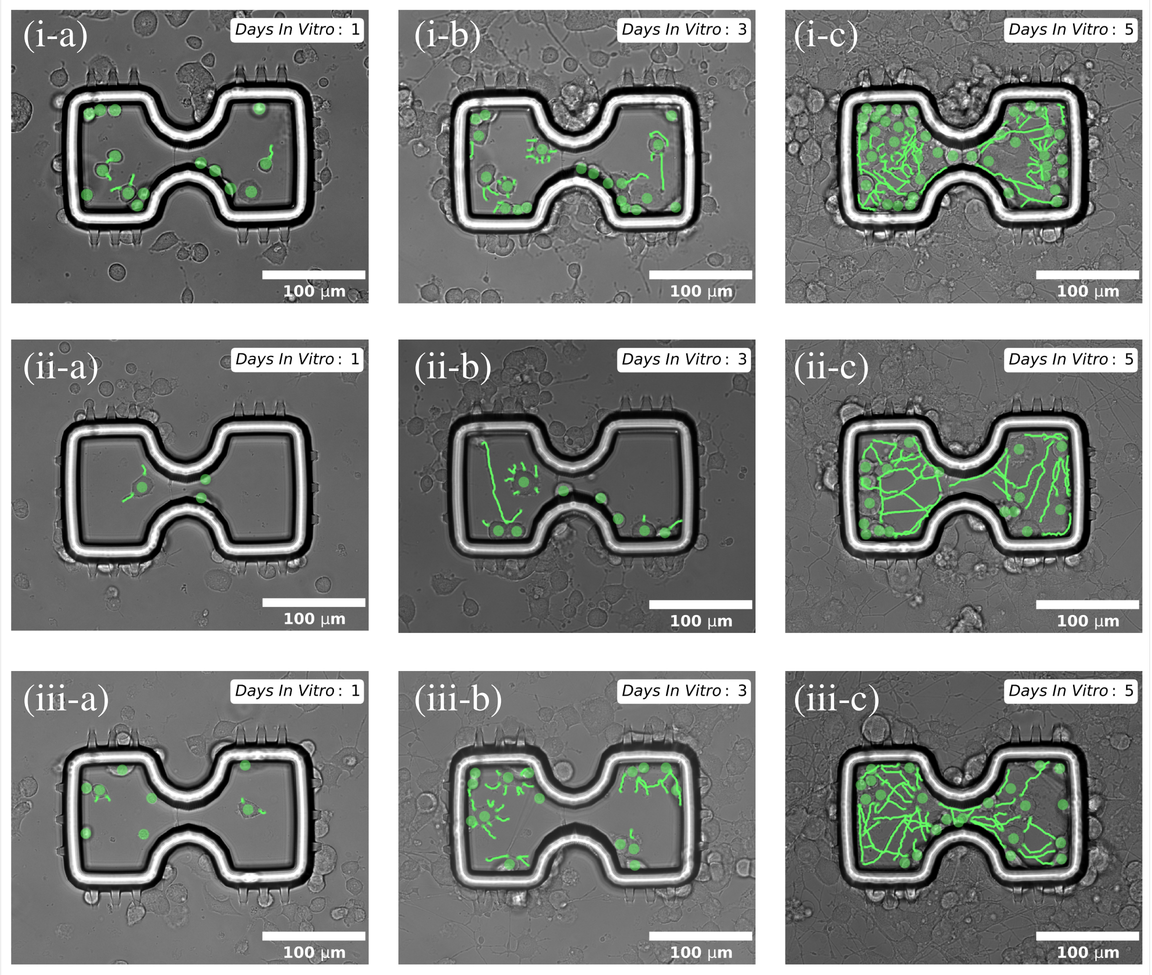

Figure 4.9.1: Ensuring Accuracy in Raw Data Gathering (representative images); first row: a confinement structure containing cells and displaying manually determined PC12 tracings on days 1 (i-a), 3 (i-b), and 5 (i-c); second row: a second confinement structure containing cells and manual tracings on days 1 (ii-a), 3 (ii-b), and 5 (ii-c); third row: a third confinement structure containing cells and manual tracings on days 1 (iii-a), 3 (iii-b), and 5 (iii-c). Green dots indicate cell bodies and green lines indicate cell neurites.

4.10 Experimental Reliability

Three technical repeats where cells confined in a total of 52 structures were compared to determine median cell counts of edge, isolated, and clustered cells (as defined in section 4.7, Labeling Cells and Classifying Population Type) in each structure (Fig. 4.10.1, (i), (ii), (iii), respectively, each accompanied by representative images). Statistical comparisons of each technical repeat to the aggregated median values of all technical repeats are also shown, with "ns" indicating non-significant differences in cell counts in all cases. A 95% confidence interval is also presented in all cases. Further details about cell seeding parameters used for this analysis can be found in Cell Seeding (sec. A.4.3). To the right of each plot in Fig. 4.10.1, a representative image of the cell and its respective cell label is provided.

The edge cells (Fig. 4.10.1, i) show a clear increase in median cell counts over time, rising from ~5 cells per structure on day 1 to ~15 cells per structure by day 5. This consistent increase suggests that the edges of the 3D confinement structure provide a favorable environment for cell adhesion and proliferation. In addition, the results of the Mann-Whitney U test in each case indicate there is no statistically significant difference between each repeat and the aggregated median on each day ("ns"). The absence of statistically significant differences between technical repeats and their aggregated medians suggests a high degree of predictability in cell behavior. This predictability supports the use of individual repeats for further experimental analyses.

Isolated cells (Fig. 4.10.1, ii) show minimal variation across experiments, with median cell counts decreasing and remaining close to zero from day 1 to day 5. At least two inferences can be drawn: 1) over time, as the confinement structures each get more crowded, there is less space available where a cell will not contact other cells, reducing the amount of isolated cells, and 2) the low starting count of isolated cells also suggests that, under confinement, cells might not prefer open space. Clustered cells (Fig. 4.10.1, iii) demonstrate contrasting behavior as all repeats show an increase in median cell count through day 5. As the structures become more crowded over time, it is increasingly likely that cells will interact with each other, leading to an increase in the number of clustered cells. Further, both isolated and clustered cells demonstrate no meaningful statistical differences between each repeat and their respective aggregated median ("ns"), reinforcing the conclusion that each repeat can contribute to further conclusions about cell behavior under confinement.

Each of the three types of labeled cells (edge, clustered, isolated) have unique relationships with their neighbors and the structure. The data indicate that cell attachment and proliferation within the confinement structure primarily occur along the edges, with few cells occupying open space. The absence of statistically significant differences between each repeat and their respective aggregated medians ("ns") suggests a consistent relationship between cells and the structures that confine them, which implies that a structure of this shape can play a role in supporting PC12 growth and behavior. The confinement structure influences positioning because the edges serve as a preferred site for cellular interaction. In addition, increasing amounts of edge cells suggest that as cells approach or interact with the structure, they are not leaving confinement. Therefore, the dimensions of the confinement structure, especially its $\sim 46\ \mu m$ height (as obtained in 3D Printed Confinement Microstructures, sec. 4.4) and its sufficient adhesion to the glass substrate at least demonstrate the confined cells are unable to interact with cells outside the confined area. Such a finding could inform future designs of microenvironments for neural tissue engineering.

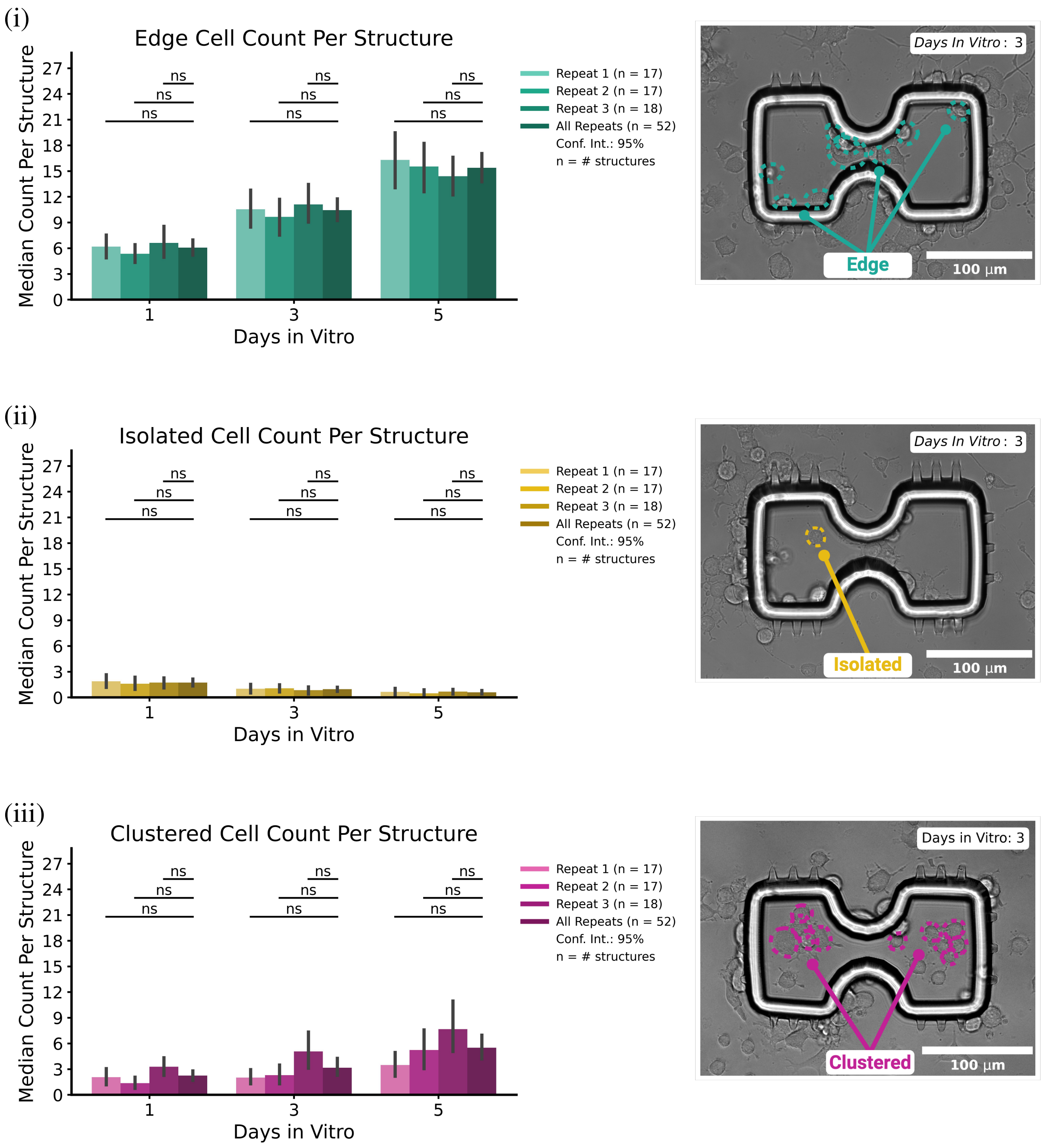

Figure 4.10.1: Comparison of median PC12 cell counts in confinement across three experimental repeats and representative images for edge (i), isolated (ii), and clustered (iii) cells (as defined in section 4.7) at 1, 3, and 5 days in vitro (n = # of structures analyzed, statistical comparisons were made using the Mann-Whitney U test). For edge cells, cell counts increase steadily over time, with no significant differences ("ns") between each repeat and the aggregated median ("all repeats"), indicating a consistent growth pattern along the edges of the confinement structure. Isolated cells show minimal variation, with consistently low counts across all time points and repeats and no significant differences between each repeat and the aggregated median ("all repeats"), suggesting that, under confinement, cells rarely remain isolated. Clustered cells display a slight increase in cell counts through day 5, with no significant differences ("ns") between each repeat and the aggregated median ("all repeats"), indicating a trend toward cell clustering over time in a confined environment.

4.11 Proliferation and Cell Density

Cell proliferation via normalized median cell count over 5 days for sparse, intermediate, and dense population types (as defined in section 4.7) for both confined and unconfined ((-) control) cells was examined (Fig. 4.11.1, i - iii). Representative images of confined cells (Fig. 4.11.1, iv, upper) and unconfined cells ((-) control, Fig. 4.11.1, iv, lower) are provided. Maximum confinement is based on a maximum cell count of 26 soma in a 15,352.1 μm^2 confined area and a corresponding cell count of 423 soma in an unconfined area of 250,000 μm^2 ((-) control). The unconfined data comprise 9 technical repeats, where a total of 46 unconfined populations were tracked. The confined data comprise 6 technical repeats where a total of 98 structures were tracked. The data are fitted with exponential regression curves, showing a consistent increase in cell number across all conditions, particularly by day 5. Each plot compares the proliferation of confined populations with their respective (-) controls for the different population types, from which inferences can be drawn about how confinement influences cell growth at a given cell density. Further details about samples and controls used for this analysis can be found in Cell Seeding (sec. A.4.3).

For the sparse population type (Fig. 4.11.1, i), confined cells appear to proliferate more rapidly than the (-) control group, reaching a higher normalized median cell count by day 5. This suggests confinement may provide a supportive microenvironment for enhanced cell proliferation, given a low initial cell count. Further, given the amount of open space within the confined area for sparse populations, this may reveal another factor that can help uncover optimal conditions for cell proliferation. The increasing difference between the confined and unconfined growth rates through day 5 suggests that confinement effects become more pronounced as the culture period extends. This difference has at least two possible, if competing, explanations: 1) there is an increased likelihood of interaction between individual confined cells over time and 2) through day 5, the amount of available space is optimal for cell proliferation.

For the intermediate population type (Fig. 4.11.1, ii), cell proliferation again exceeds that of the (-) control group, with the most substantial divergence occurring on day 5. This indicates that for intermediate populations, confinement may offer similar conditions to sparse populations – there is an optimal balance between cell-cell interactions and available space within the structure, and these conditions promote proliferation. The proliferation rates for both the confined cells and the (-) control also suggest that an increased likelihood of cell-cell interaction is sufficient to reduce the rate of cell proliferation.

In contrast, the dense population type (Fig. 4.11.1, iii) shows the most modest increase in cell proliferation compared to its sparse and intermediate counterparts. In addition, proliferation for the (-) control group is similar to proliferation for confined cells. The outcomes observed among both dense population types (confined and (-) control) at least suggests that when cells are in very close proximity with little open space, confinement neither promotes nor inhibits proliferation.

Cell density impacts proliferation of PC12 cells under confinement, with sparse confinement yielding the highest proliferation rates over time. As cell density under confinement increases, proliferation rates reduce, suggesting that cell count under confinement is related to proliferation rate. This at least indicates there is an optimal cell density for confined cells that will enhance cell proliferation. Attiah et al. also plotted an exponential growth regression ($y = 665809e^{0.9259x}$) against unnormalized proliferation data for PC12 cells seeded mainly at 1.9×10^4 cells/cm^2 on mouse laminin (assumed to be the same as - or sufficiently similar to - laminin used herein)[18]. In another investigation, cerebellar granule neuron cultures of different densities (2.2 × 10^4 and 4.4 × 10^4 cells/cm^2) demonstrated different survivability rates and different cell morphologies[24]. Further, it was demonstrated in P19 neurons that culture density impacts neuronal polarity, neurite outgrowth, and other cellular processes[26]. These findings underscore the complex relationship between cell density and proliferation under confinement, highlighting that while increased cell count may suppress growth, there is an optimal cell density even under confinement which can enhance proliferation beyond that observed in unconfined conditions.

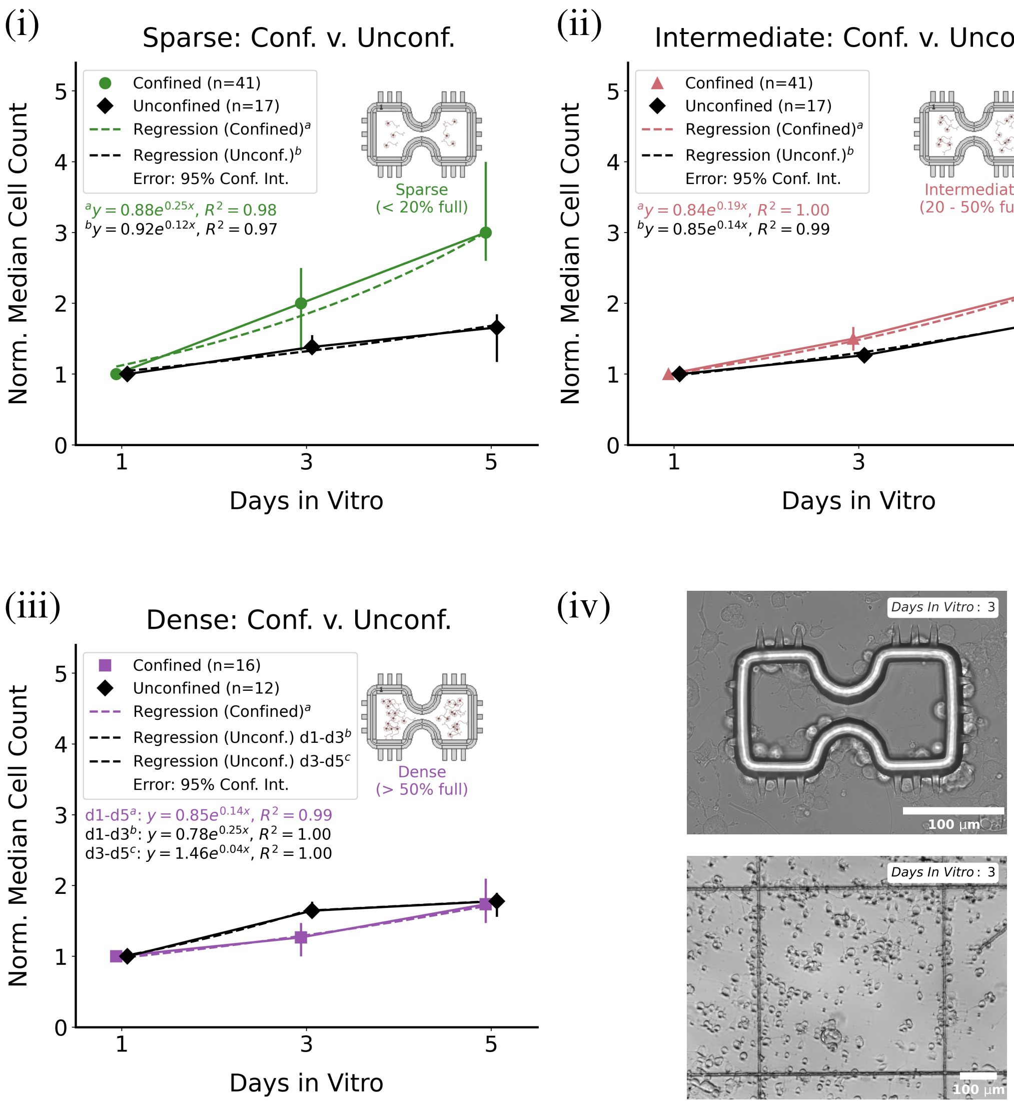

Figure 4.11.1: Comparison of confined and unconfined ((-) control) proliferation across sparse (i), intermediate (ii), and dense (iii) population types (as defined in section 4.7) based on a maximum cell count of 26 soma in a 15,352.1 μm^2 confined area and a corresponding cell count of 423 soma in an unconfined area of 250,000 μm^2; Two representative images (iv): (upper) PC12 cells inside a confinement structure after 3 days in vitro; (lower) PC12 cells proliferate inside a 500 μm x 500 μm grid, absent confinement structures, after 3 days in vitro ((-) control). Sparse, Confined vs Unconfined: confined cells show higher proliferation compared to the unconfined group, with normalized cell counts increasing significantly by day 5. The large difference between quadratic regression lines suggests cell density in the sparse population type under confinement enhances cell proliferation when compared to the unconfined group; Intermediate, Confined vs Unconfined: confined cells also proliferate faster than their unconfined counterparts. Notably, there is a smaller difference between confined and unconfined proliferation when compared to the sparse population type, suggesting that in the intermediate population type, a greater likelihood of cell-cell interaction slows proliferation; Dense, Confined vs Unconfined: unconfined cells appear to proliferate faster than confined cells between day 1 and day 3, however confined cells appear to proliferate faster between day 3 and day 5.

4.12 Path Lengths, All and Longest

In this section and the following section (sec. 4.13, Effect of Confined Cell Count on Neurite Length) the length of neurites is considered and six technical repeats where a total of 34 unconfined populations and 104 confined populations (cells growing within confinement structures) were tracked over 5 days. As it relates to both sections, for descriptions of cell and neurite labeling (edge, isolated, clustered) as well as population type (sparse, intermediate, dense), please refer to Labeling Cells and Classifying Population Type, sec. 4.7. Further details about samples and controls used for this analysis can be found in Cell Seeding (sec. A.4.3).

The median of all neurite lengths and the median of the longest neurite lengths per cell (Fig. 4.12.1) were analyzed over days 1, 3, and 5 in culture for the following 5 conditions: isolated confined, isolated unconfined, clustered confined, clustered unconfined and edge confined. Isolated unconfined and clustered unconfined conditions are negative controls. The following pairs of conditions were compared using the Mann-Whitney U test: isolated confined-isolated unconfined, clustered confined-clustered unconfined, edge confined-isolated unconfined, and edge confined-clustered unconfined, and statistical differences are indicated using the following notations: (*) $p < 0.05$, (**) $p < 0.01$, (***) $p < 0.001$, (****) $p < 0.0001$, and (ns) not significant. For the data provided in this section, unconfined cells cultured in a separate sample, absent any confinement structures, were analyzed. An example of an unconfined sample (negative control) is provided in fig. 4.11.1, (iv, lower image). It should also be noted that in appendix B, Confined vs. External Neurite Lengths, plots comparing neurite lengths between cell labels confined within the 3D-printed structures and neurite lengths of those cells directly external to the structures have been analyzed, highlighting that confinement, and not the presence of the printed structure, results in shorter neurite lengths with statistically significant differences across isolated, clustered, and edge labeled (exception: edge, d3, "ns") neurites over multiple days in vitro.

On day 1, among all neurites (Fig. 4.12.1, i), the clustered unconfined condition shows the highest median neurite length (~13 μm), followed closely by the isolated unconfined condition (~11 μm), then by the edge confined condition (~7 μm), clustered confined (~7 μm) and isolated confined (~5 μm). Among the four statistical comparisons, all are statistically significant ($p < 0.001$ denoted as ***). The longest neurites (Fig. 4.12.1, ii, iso. conf.: ~7, iso. unconf.: ~14, clus. conf.: ~8, clus. unconf.: ~14, edge conf.: ~9 μm) show a similar growth pattern and statistical significance ($p < 0.001$ denoted as ***) across all comparisons. Confinement appears to significantly impede day 1 neurite outgrowth for all neurites and the longest neurite per cell.

By day 3 (Fig. 4.12.1, iii), among all neurites, the isolated unconfined, clustered unconfined and edge confined conditions exhibit noticeable increases in neurite length (~15, ~19, ~15 μm, respectively), with isolated confined (~7 μm) and clustered confined (~7 μm) showing statistically significant differences from values in their respective confined counterparts ($p < 0.001$ denoted as *** in both cases). Edge confined neurites are now statistically similar to isolated unconfined neurites ("ns") while differences between edge confined neurites and clustered unconfined neurites are statistically significant ($p < 0.001$ denoted as ***). Among the longest neurites per cell (Fig. 4.12.1, iv), isolated unconfined and clustered unconfined differences from their respective confined counterparts are statistically significant (isolated confined v. unconfined: ~11 v. ~19 μm; clustered confined v. unconfined: ~11 v. ~23 μm; $p < 0.001$ denoted as *** in both cases). However, there are no statistical differences between the edge confined condition (~24 μm) and both unconfined conditions ("ns"). The median neurite length values on day 3 demonstrate that confinement continues to impact neurite extension, yet growth now also appears to hinge on whether a confined cell is in direct contact with its confinement structure. The differences among the confined neurites (edge, isolated, clustered) demonstrate that an originating cell's relationship to the structure and other cells determines neurite length. Further, the effect of cell-structure contact stimulates the longest edge confined neurites to grow in a way that resembles the longest isolated unconfined and clustered unconfined neurites. This outcome also suggests that by day 3 all confined and unconfined cells have determined their cell fate, which follows from an understanding of the discrete events that occur during neuronal differentiation of rat hippocampal neurons as first described by Dotti (Fig. 1.2.1)[17] and later by Micholt[42] using rat and mouse hippocampal neurons.

By day 5, among all neurites (Fig. 4.12.1, v), the same growth patterns and relationships are further reinforced. Isolated unconfined, clustered unconfined and edge confined neurites continue to grow longest (~33, ~38, ~29 μm, respectively) while isolated confined and clustered confined neurite lengths are still suppressed (~8, ~12 μm, respectively), and there are statistically significant differences across all comparison pairs ($p < 0.001$ denoted as *** in all cases). Among the longest neurites per cell on day 5 (Fig. 4.12.1, vi), the isolated unconfined and clustered unconfined neurites have grown much longer than their confined counterparts (~48 v. ~13 μm, ~44 v. ~19 μm, respectively), with both unconfined groups outgrowing the edge confined neurites (~39 μm). There are statistically significant differences across all comparison pairs ($p < 0.001$ denoted as *** in all cases). The patterns demonstrated on day 5 reinforce what is observed on day 3. Unconfined neurites grow much longer than their confined counterparts; however now unconfined neurites even begin to grow longer than edge confined neurites. This outcome suggests that even under confinement direct contact with the structure will stimulate neurite growth, yet neurite growth is meaningfully suppressed across all confined cells through 5 days. This outcome also implies that neurite outgrowth is meaningfully suppressed by confinement, irrespective of their contact with other cells or the structure.

The experimental results presented here (Fig. 4.12.1) suggest confinement plays a role in neurite outgrowth, particularly when cells have no direct contact with structural boundaries. The unconfined conditions consistently showed more rapid and longer neurite extension than their confined counterparts across all time points, supporting the idea that confinement suppresses PC12 outgrowth. Notably, the edge confined neurites, which had direct contact with the structure, exhibited a growth pattern that in some cases resembled the unconfined conditions, suggesting that structural interaction plays a key role in enhancing neurite extension despite confinement. In contrast, studies from other researchers demonstrated that different experimental setups can yield variable results. In experiments using PC12 cells in 3D collagen matrices of varying concentrations (0.4-1 mg/ml), mean neurite lengths often exceeded 70 μm by day 4. While PC12 neurite extension in 1 mg/ml collagen gels infused by varying concentrations of laminin (1-100μg/ml) showed mean neurite extension up to 80 μm by day 4[86]. In a separate study, researchers found that the mean lengths of the longest neurites per cell grown by neural stem cells on soft PDMS substrates reached ~50-80 μm, depending on substrate stiffness, after 7 days[87]. These investigations had some notable differences from the results presented here. For example, the shorter neurite lengths presented here could be attributed to a number of factors including: 1) lower concentrations of adhesion proteins, 2) the complexity in deciphering any connection between 3D behavior and 2D behavior, 3) the behavior of different cell types in response to substrate stiffness, and 4) the result of taking the median value instead of the mean; median calculations attempt to remove any possible bias introduced by outliers. These variations at least demonstrate that different experimental parameters can have a meaningful impact on neurite length in vitro.

Neurons seeded on surfaces with microfabricated topological modifications have shown some acceleration in neurite growth, when compared to those seeded on flat surfaces. In an investigation by Micholt et al. utilizing primary rat hippocampal neurons on 2D PLL modified substrates, it was found that neurites on flat surfaces grew to around 15 μm after 25 hours, but on modified surfaces with micron-scale pillar structures, average (likely the mean) neurite lengths extended to $22-27$ μm after 25 hours[42]. These outcomes were influenced by pillar size and spacing: smaller, closer pillars promoted longer neurites. Another potential factor which could yield different outcomes could be cell density. Micholt et al. plated rat hippocampal neurons at a higher density (500 cells/mm^2) compared to this study (150-250 cells/mm^2)[42]. These variations in experimental parameters, including differences in cell-cell, cell-substrate interactions, and the use of different cell lines, likely contributed to observed differences in neurite outgrowth. Such variations emphasize the impact of substrate architecture, surface features, and experimental conditions on neurite development, underscoring the importance of accounting for these factors when interpreting in vitro models.

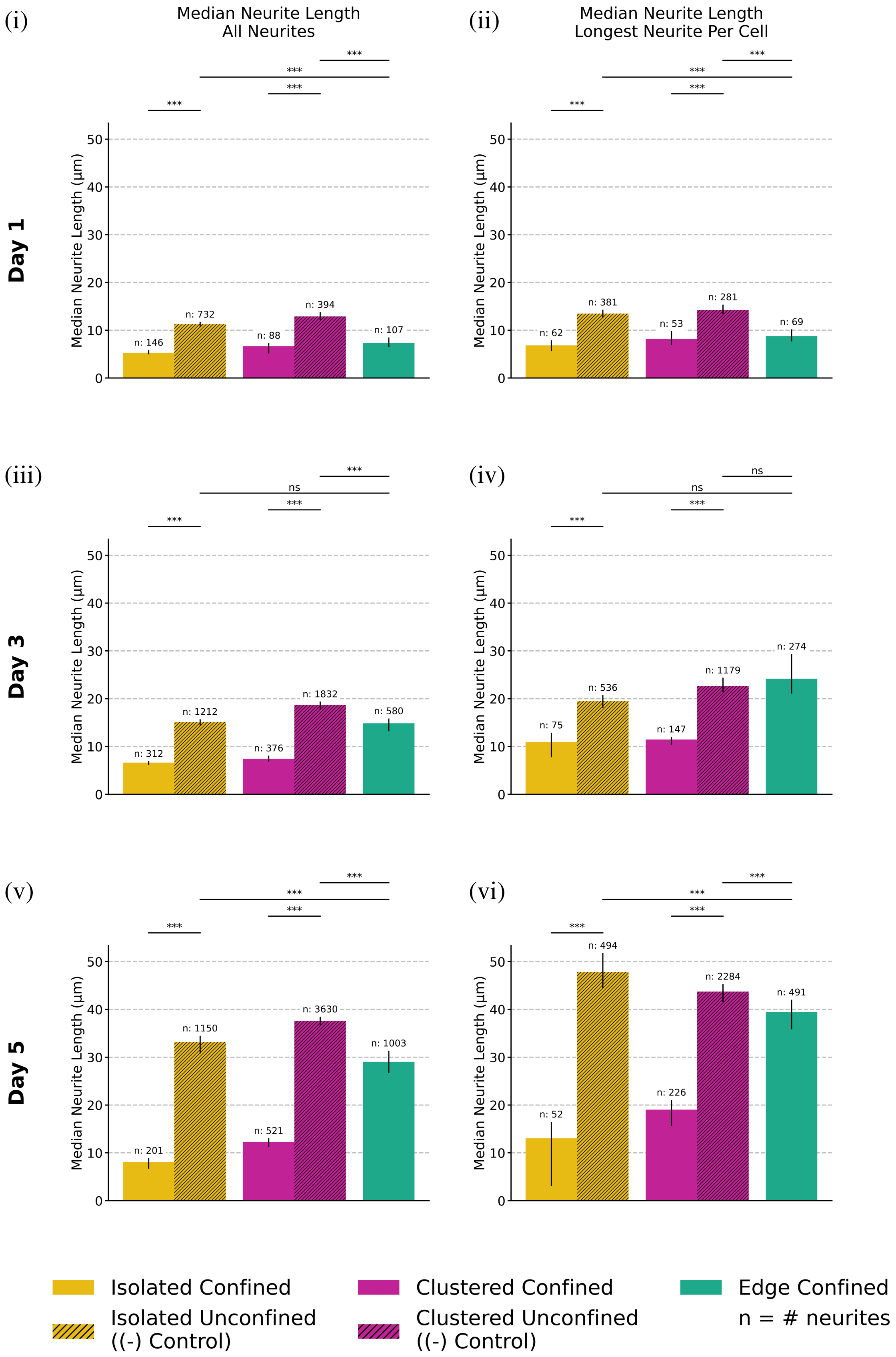

Figure 4.12.1: (caption on next page)

Figure 4.12.1: (Continued from previous page) Comparison of PC12 median neurite path lengths after 1, 3, and 5 days in vitro for edge, isolated, and clustered cells (^{a}as defined in Labeling Cells and Classifying Population Type, sec. 4.7). (i), (iii), (v) show median path lengths of all neurites (isolated-confined, isolated-unconfined, clustered-confined, clustered-unconfined, edge-confined) for days 1, 3, and 5 in vitro, respectively (d1: ~5, ~11, ~7, ~13, ~7 μm; d3: ~7, ~15, ~7, ~19, ~15 μm; d5: ~8, ~33, ~12, ~38, ~29 μm). (ii), (iv), (vi) show median path lengths of the longest neurites of each cell (isolated-confined, isolated-unconfined, clustered-confined, clustered-unconfined, edge-confined) for days 1, 3 and 5 in vitro, respectively (d1: ~7, ~14, ~8, ~14, ~9 μm; d3: ~11, ~19, ~11, ~23, ~24 μm; d5: ~13, ~48, ~19, ~44, ~39 μm). Error bars represent a 95% confidence interval. The following pairs of conditions were compared using the Mann-Whitney U test: isolated confined-isolated unconfined, clustered confined-clustered unconfined, edge confined-isolated unconfined, and edge confined-clustered unconfined, using the following notations: (*) $p < 0.05$, (**) $p < 0.01$, (***) $p < 0.001$, (****) $p < 0.0001$, "ns" not significant. Neuron graphic created in https://BioRender.com.

4.13 Effect of Confined Cell Count on Neurite Length

4.13.1 Neurite Length of Confined Cells on Same Day in Culture in Different Population Types

Comparisons of median neurite lengths by cell label at each time point for different population types were analyzed (Fig. 4.13.1). For a given population type (sparse, intermediate, dense), each plot directly compares the neurite lengths at each time point, for the different neurite labels (isolated, cultured, edge). The following pairs of conditions were compared using the Mann-Whitney U test: isolated-clustered, isolated-edge, clustered-edge, and statistical differences are indicated using the following notations: (*) $p < 0.05$, (**) $p < 0.01$, (***) $p < 0.001$, (****) $p < 0.0001$, and (ns) not significant. Therefore, each plot measures the impact of cell density on neurite extension, comparing differences in neurite length for each neurite label, on each day in culture. Each plot reveals how cell density could be influencing neurite outgrowth, with statistical comparisons of each neurite label on each day, providing insight into relationships across cell labels.

In the sparse population type (Fig. 4.13.1, i), there are no significant statistical differences across comparison pairs on day 1 (isolated/clustered/edge: ~7, ~6, ~7 μm, respectively). By day 3, edge cells begin to grow the longest neurites (isolated/clustered/edge: ~9, ~5, ~18 μm, respectively) with statistically significant differences across comparison pairs (isolated-clustered/clustered-edge/isolated-edge: $p < 0.01$ denoted as **, $p < 0.0001$ denoted as ****, and $p < 0.0001$ denoted as ****, respectively). By day 5, edge cell neurites are again the longest (isolated/clustered/edge: ~9, ~7, ~44 μm, respectively) with statistically significant differences across isolated-edge and clustered-edge comparison pairs (isolated-clustered/isolated-edge/clustered-edge: ns, $p < 0.0001$ denoted as ****, and $p < 0.0001$ denoted as **** respectively). It should be noted that for the sparse population type, the sample sizes for clustered cells on days 1 (n=9) and 5 (n=10) are too small to draw meaningful conclusions. Otherwise, these outcomes suggest that cells which directly contact the confinement structure experience optimal conditions for neurite extension in low cell densities, likely due to cues from the structure itself. Neurite lengths in isolated and clustered cells remain significantly shorter, especially on days 3 and 5, indicating that cells not in contact with the structure's edges experience topological and intercellular cues differently. By day 5, edge neurites have reached a median length of nearly 50 μm, significantly outpacing the other groups. These outcomes suggest that neurites originating from cells in contact with the structure take advantage of the available space within the confined area to grow. In contrast, the isolated and clustered cells demonstrate the opposite response. These outcomes appear to show that low cell density, and the concomitant high availability of open space, does not stimulate neurite growth as much as contact with the structure.

In the intermediate population type (Fig. 4.13.1, ii), a similar pattern emerges, with edge cells (d1,3,5: ~7, ~15, ~29 μm) showing longer neurites than isolated (d1,3,5: ~5, ~7, ~7 μm) and clustered groups (d1,3,5: ~6, ~7, ~11 μm) on days 3 and 5. Isolated-clustered, clustered-edge and isolated-edge statistical comparison pairs on day 1 are $p < 0.01$ denoted as **, ns, and $p < 0.001$ denoted as ***, respectively. By day 3, isolated-clustered, clustered-edge and isolated-edge statistical comparison pairs are ns, $p < 0.0001$ denoted as ****, and $p < 0.0001$ denoted as ****, respectively. By day 5, isolated-clustered, clustered-edge and isolated-edge statistical comparison pairs are $p < 0.001$ denoted as ***, $p < 0.0001$ denoted as ****, and $p < 0.0001$ denoted as ****, respectively. This suggests that the intermediate population type does not suppress any effect contact with the structure has on enhancing neurite growth. It also suggests that direct cell-cell contact could play a part in enhancing neurite growth in the intermediate population type and that as cells spend time under confinement, neurite growth is influenced primarily by cell-structure contact, although cell-cell contact has some impact.

In the dense population type (Fig. 4.13.1, iii), edge cells again show the longest neurite lengths at all time points (d1,3,5: ~9, ~14, ~29 μm). However, on day 1 and day 5, clustered cells (d1,3,5: ~8, ~8, ~12 μm) are growing longer neurites than isolated cells (d1,3,5: ~5, ~7, ~9 μm). On day 1, isolated-clustered, clustered-edge and isolated-edge statistical comparison pairs are $p < 0.05$ denoted as *, ns, and $p < 0.01$ denoted as **, respectively. On day 3, isolated-clustered, clustered-edge and isolated-edge statistical comparison pairs are $p < 0.01$ denoted as **, $p < 0.0001$ denoted as ****, and $p < 0.0001$ denoted as ****, respectively. On day 5, isolated-clustered, clustered-edge and isolated-edge statistical comparison pairs are $p < 0.01$ denoted as **, $p < 0.0001$ denoted as ****, and $p < 0.0001$ denoted as ****, respectively. Neurite lengths in the dense population type suggest cell-cell contact may play a slightly greater role in promoting neurite outgrowth, than cell-cell contact in lower density populations. With statistically significant differences, isolated cells extend shorter neurites than edge cells at all time points (d1: $p < 0.01$ denoted as **, d3,5: $p < 0.0001$ denoted as ****), indicating that in dense populations, lack of cell-cell and cell-structure contact meaningfully suppresses neurite growth.

Neurite outgrowth is enhanced for cells in direct contact with the edges of the confinement structure, for all population types. The effect direct cell-structure contact has on neurite growth therefore overcomes the impact of the diminishing amount of open space and concomitant increasing cell count. As cell density increases, the advantage of edge contact diminishes somewhat, but cell-structure interactions still enhance neurite extension. These outcomes underscore the nuanced contributions made to neurite outgrowth by 1) the amount of other cells under confinement and 2) cell-structure interaction. The presence of other cells and interactions between cells and the microenvironment should therefore be considered when interrogating cellular phenomena in vitro.

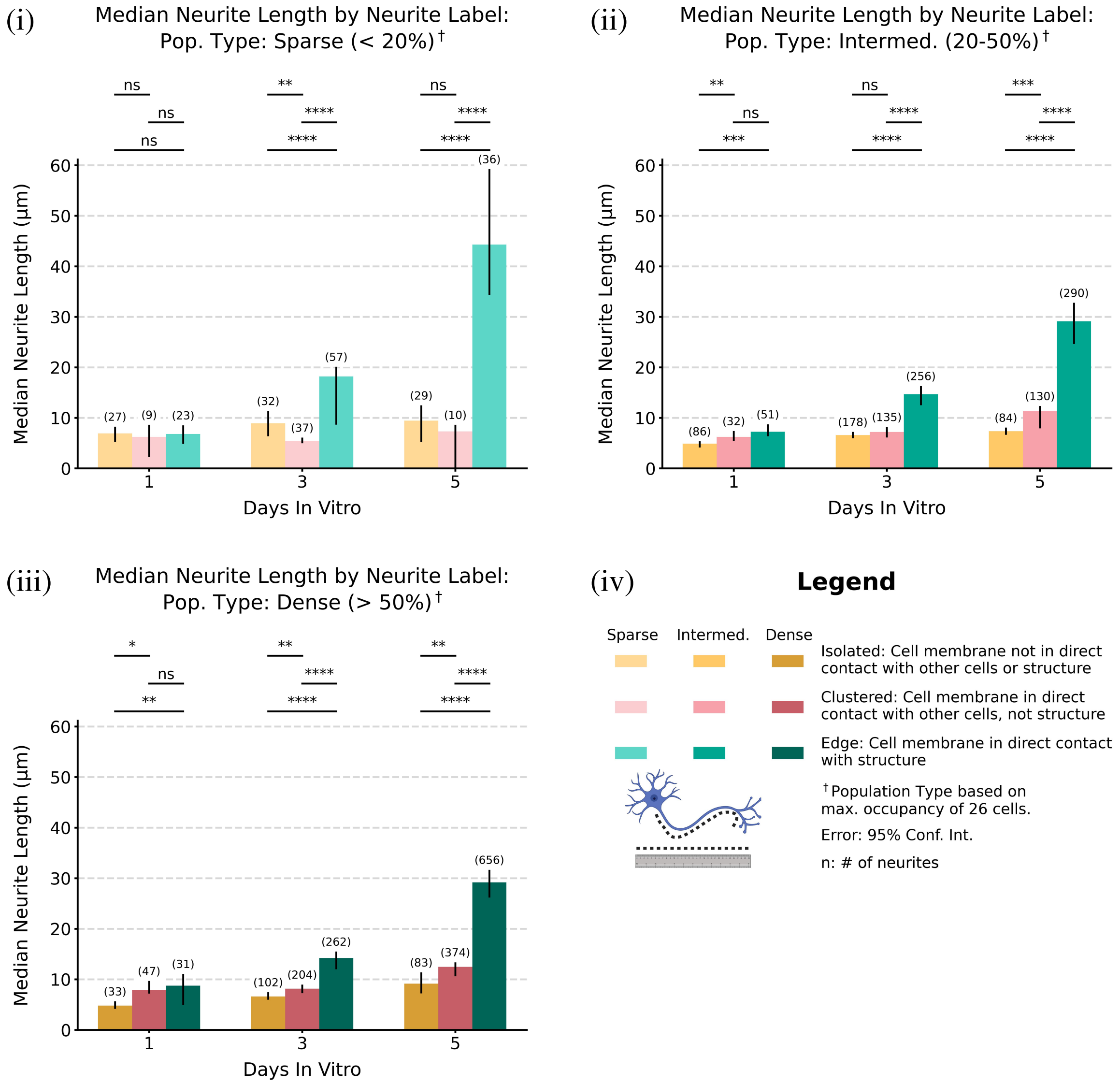

Figure 4.13.1: Median neurite length comparison across three population types: sparse (i), intermediate (ii), dense (iii), including legend (iv). The following pairs of conditions were compared using the Mann-Whitney U test: isolated-clustered, clustered-edge, isolated-edge. In the sparse population type, edge cells show the longest neurites (d1,3,5: ~7, ~18, ~44 μm) by days 3 and 5, with statistically significant differences (d3,5: $p < 0.0001$ denoted as ****) compared to isolated (d1,3,5: ~7, ~9, ~9 μm) and clustered groups (d1,3,5: ~6, ~5, ~7 μm). There are no statistically significant differences between any comparison pair on day 1 ("ns"). There is a statistically significant difference between isolated and clustered groups on day 3 ($p < 0.01$, denoted as **) but no statistically significant difference ("ns") between these groups on day 5. In the intermediate population type, edge cell neurites (d1,3,5: ~7, ~15, ~29 μm) grow longer neurites than isolated cells (d1,3,5: ~5, ~7, ~7 μm) and clustered cells (d1,3,5: ~6, ~7, ~11 μm) starting on day 3. Statistical comparison pairs are $p < 0.01$, denoted as ** (isolated-clustered), "ns" (clustered-edge) and $p < 0.001$ denoted as *** (isolated-edge) on day 1, ns (isolated-clustered) and $p < 0.0001$ denoted as **** (isolated-edge, clustered-edge) on day 3, and $p < 0.001$ denoted as *** (isolated-clustered) and $p < 0.0001$ denoted as **** (isolated-edge, clustered-edge) on day 5. The growth of edge neurites on days 3 and 5 indicates the intermediate population type has a similar effect on edge cells as the sparse population type. Neurite behavior in the dense population type shows a similar pattern, where edge cell neurites grow longest (d1,3,5: ~9, ~14, ~29 μm); there are also statistically significant differences between isolated (d1,3,5: ~5, ~7, ~ 9 μm) and clustered cell neurite lengths (d1,3,5: ~8, ~8, ~12 μm) with isolated-clustered statistical comparison pairs demonstrating statistically significant differences at all time points (d1: $p < 0.05$ denoted as *, d3, d5: $p < 0.01$ denoted as **). Remaining statistical comparisons also suggest that by days 3 and 5, the dense population type impacts neurite growth for (continued on next page)

Figure 4.13.1: (continued from previous page) clustered and edge cells (isolated-edge, clustered-edge d1: $p < 0.01$ denoted as **, "ns", d3: $p < 0.0001$ denoted as ****, both, d5: $p < 0.0001$ denoted as ****, both). High cell density likely causes this outcome, suggesting the increased presence of other cells enhances neurite growth for clustered cells as well, but only at high culture densities. Across all population types, edge cells consistently extend their neurites, but as the number of cells in confinement increases, cell number plays a greater role in promoting neurite growth for clustered cells. Neuron graphic created in https://BioRender.com.

4.13.2 Neurite Lengths of Different Neurite Labels in Different Population Types

Neurite lengths by population type at each day were compared for each neurite label (Fig. 4.13.2). For a given neurite label (edge, isolated, clustered), each plot directly compares the median neurite lengths at each time point for different population types (sparse, Fig. 4.13.2, i; intermediate, Fig. 4.13.2, ii; dense, Fig. 4.13.2, iii). Therefore, each plot measures the impact of cell density on neurite extension, comparing differences in neurite length at each day in culture, for each neurite label. Each plot reveals how cell density could be influencing neurite outgrowth, with statistical comparisons for neurites of each neurite label under different population types at each time point. The following pairs of conditions were compared using the Mann-Whitney U test: sparse-intermediate, sparse-dense, intermediate-dense.

In a comparison of edge neurites across population types for each time point, there are no statistical differences for any comparison pair on day 1 and day 3 (Fig. 4.13.2, i). Neurite lengths on d1 are ~7-9 μm, on d3 ~18-14 μm, and on d5 ~44-29 μm. By day 5, there is a statistically significant difference between edge cell neurites (sparse-intermediate, sparse-dense both $p < 0.01$ denoted as **), but no statistically significant difference between intermediate and dense categories ("ns"). This at least suggests that when there is direct contact between the cell body and the confinement structure, the amount of cells under confinement may enhance neurite growth only well after cells have differentiated. In a comparison of isolated neurites across population types for each time point (Fig. 4.13.2, ii), neurite behavior is slightly different. On day 1, isolated neurites growing in the sparse type (~7 μm) are statistically different from isolated neurites growing in intermediate (~5 μm) and dense (~5 μm) types (sparse-intermediate: $p < 0.05$, denoted as *, sparse-dense: $p < 0.01$, denoted as **). However, on day 1, there is no statistically significant difference ("ns") between isolated neurites growing in the intermediate type and isolated neurites growing in the dense type. By day 3 (~9-7 μm) and day 5 (~9, ~7, ~9 μm respectively), there are no statistically significant differences among any of the remaining comparison pairs. This suggests that, as isolated cells extend their neurites through days 3 and 5, the presence or absence of neighboring cells has no impact on neurite extension.

In a comparison of clustered cell median neurite lengths across population types for each time point (Fig. 4.13.2, iii), neurites in the sparse population type (~6 μm) on day 1 demonstrate no statistically significant difference ("ns") with either neurites in the intermediate (~6 μm) or the dense type (~8 μm) while neurites in the intermediate population type demonstrate some statistical difference with neurites in the dense population type ($p < 0.05$ denoted as *). On day 3, neurites in the sparse population type (~ 5 μm) demonstrate with statistical significance, differences with neurites in the intermediate and dense population types (~ 7, ~ 8 μm respectively; sparse-intermediate: $p < 0.001$ denoted as ***, sparse-dense: $p < 0.0001$ denoted as ****) while intermediate and dense population types show no statistically significant differences ("ns"). On day 5, clustered neurites demonstrate no statistically significant differences ("ns") across all comparison pairs (~7, ~11, ~12 μm, sparse, intermediate and dense, respectively). The statistical relationship between comparison pairs on days 1, 3 and 5 suggests the effect of cell count under confinement on clustered cell neurite lengths is complex. In addition, the sample sizes (d1, sparse, n=9 and d5, sparse, n = 10) are too small to draw meaningful conclusions. Otherwise, one possible conclusion is that there is some intermediate cell count that bears a difference to the dense population type on day 1 and the sparse population type on day 3, but no difference with the dense population type on day 5; in addition, there are meaningful statistical differences between the sparse and dense population types on day 3 that somehow work counterintuitively: the sparse population type suppresses neurite outgrowth whereas the dense population type promotes it. Nevertheless, as demonstrated, there could be some amount of cells (intermediate population type) under confinement which induces the same effect as the dense population type on days 3 and 5; this effect, then, could induce a behavior only in cells which directly contact other cells and are not in contact with the structure.

These outcomes imply that the structure and other cells play a nuanced and specific role, with respect to the cells within its confinement. When cells are able to directly contact the structure (edge), the presence of other cells under confinement appears to play a role in neurite extension on day 5. When cells are under confinement, but do not directly interact with the structure or other cells (isolated), the presence of other cells in confinement appears to play a role on day 1, and have no impact on neurite outgrowth as the cells grow over time. Finally, when cells are able to contact other cells directly, but not the structure (clustered), there could be an intermediate cell count value that may affect neurite outgrowth on day 1 and day 3.

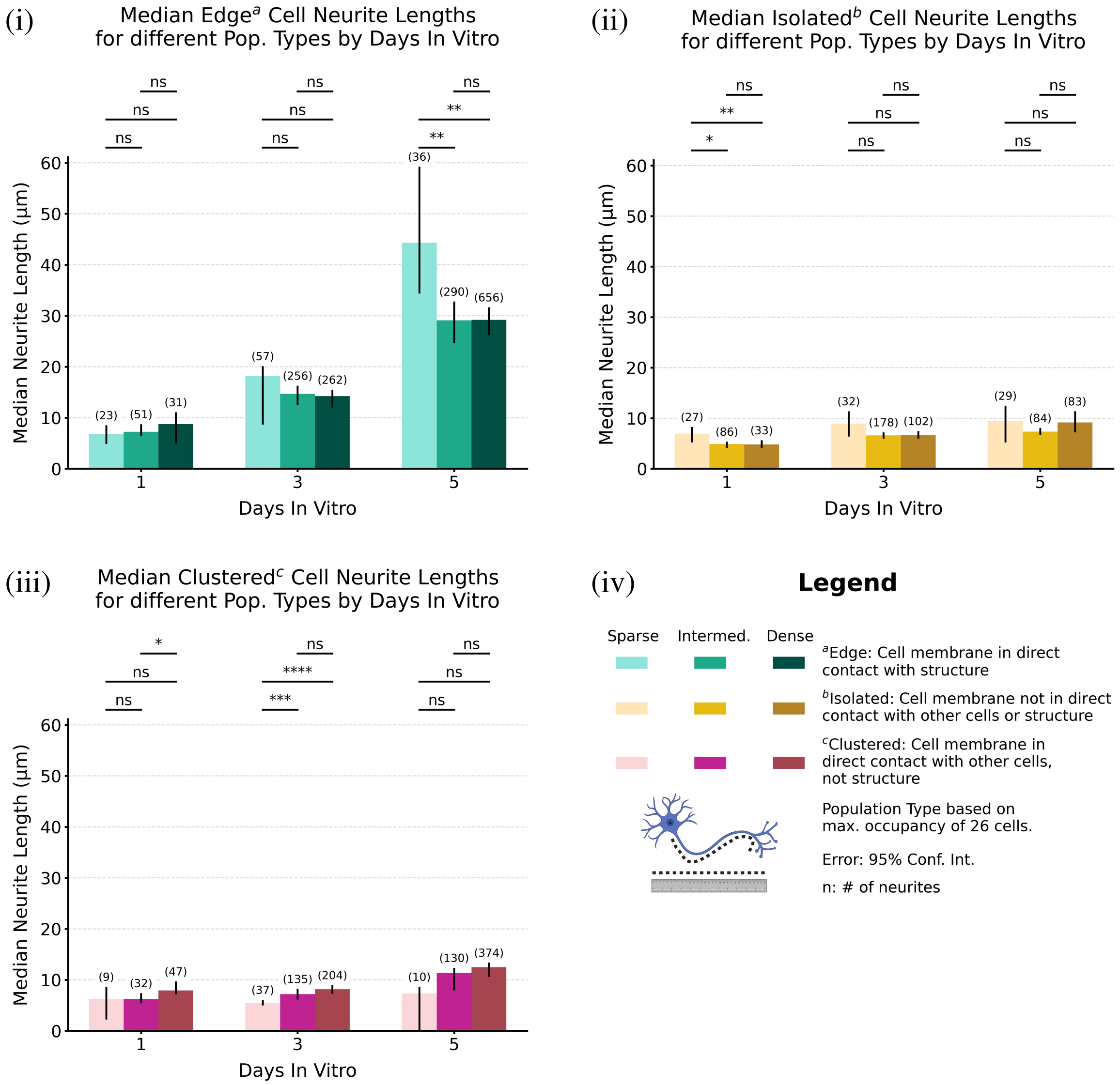

Figure 4.13.2: Median neurite length comparison by cell label (edge (i), isolated (ii), clustered (iii)) for each population type (sparse, intermediate, dense), including legend (iv). The following pairs of conditions were compared using the Mann-Whitney U test: sparse-intermediate, sparse-dense, intermediate-dense. Edge cells show no significant differences ("ns") in median neurite length across occupancies at d 1 and 3 (d1: ~7-9 μm; d3: ~18-14 μm; d5: ~44-29 μm) however, on day 5 there is a statistically significant difference between sparse-intermediate and sparse-dense (both $p < 0.01$ denoted as **). Isolated cells in the sparse population type show some statistically significant differences on d1 (~7, ~5, ~5 μm, respectively; sparse-intermediate: $p < 0.05$ denoted as *, sparse-dense: $p < 0.01$ denoted as **, intermediate-dense: "ns"); by d3 (~9-7 μm) and d5 (~9, ~7, ~9 μm, respectively), there are no statistically significant differences in median neurite length ("ns"). Clustered cells show a statistically significant difference between intermediate and dense population type median neurite lengths on d1 (~6, ~6, ~8 μm, respectively; sparse-intermediate, sparse-dense both "ns", intermediate-dense: $p < 0.05$ denoted as *); on d3 there is a statistically significant difference between sparse and intermediate population types (d3: ~5 v. ~7 μm, $p < 0.001$ denoted as ***) and between sparse and dense population types (d3: ~5 v. ~8 μm, $p < 0.0001$ denoted as ****), but no statistically significant difference between intermediate and dense ("ns") population types. Clustered cell neurites on day 5 demonstrate no significant difference ("ns") across comparison pairs (sparse, intermediate, dense: ~7, ~11, ~12 μm, respectively). It should be noted that for clustered neurites, sample sizes for the sparse population type at days 1 (n=9) and 5 (n=10) are too small to draw meaningful conclusions. These outcomes suggest cell-cell contact plays a critical, yet complex role in promoting neurite outgrowth, especially in clustered cell populations where cells are in direct contact with other cells, but not the confinement structure. Neuron graphic created in https://BioRender.com.

4.13.3 Neurite Length by Population Type and Neurite Label

Median neurite lengths of a given neurite label (isolated, clustered, edge) were compared over days 1, 3 and 5 for given population types (sparse, intermediate, dense) (Fig. 4.13.3). The following pairs of conditions were compared using the Mann-Whitney U test: day 1 - day 3, day 1 - day 5, day 3 - day 5. Therefore, each plot measures how median neurite length changes for each neurite label category over time, comparing differences in neurite length for each population type. Each plot reveals how population type could be temporally influencing the neurite outgrowth of a specific neurite label, with statistical comparisons between each time point, for neurites extending from each neurite label. Further details about samples and controls used for this analysis can be found in Cell Seeding (sec. A.4.3).

As indicated in fig. 4.13.3 (i), which shows temporal changes in median neurite length for cells in the sparse population type, neurite outgrowth is limited for isolated and clustered cells. For isolated neurites, from d1 to d5, median neurite length changes from ~7-9 μm, with statistical significance only across the d1-d5 comparison pair ($p < 0.05$ denoted as *). For clustered neurites, from d1 to d5, median neurite length changes from ~6-7 μm, with a statistically significant difference across the d3-d5 comparison pair ($p < 0.01$ denoted as **). It should be noted for clustered neurites in the sparse population type, sample sizes at days 1 (n=9) and 5 (n=10) are too small to draw meaningful conclusions. For edge neurites, from d1 to d5, median neurite length changes from ~7-44 μm, with a statistically significant difference between d1 and d3 and between d1 and d5 ($p < 0.0001$ denoted as **** in both cases) as well as a statistically significant difference between d3 and d5 ($p < 0.001$ denoted as ***). This suggests that the sparse population type may at least suppress neurite outgrowth when cells are in contact with no other cells or the structure (isolated condition) and when cells are only in contact with each other (clustered condition). Further, this effect does not appear to translate to edge neurites, which implies that direct contact with the structure could be the sole determining factor in neurite outgrowth even in low population densities.

Temporal changes in neurite outgrowth are shown for each neurite label in the intermediate population type (Fig. 4.13.3, ii). Neurites originating from isolated cells grow from ~5-7 μm from d1 to d5 with statistically significant differences across comparison pairs (d1/3: $p < 0.001$ denoted as ***, d1/5: $p < 0.0001$ denoted as ****, d3/5: $p < 0.01$ denoted as **). Neurites originating from clustered cells grow from ~6-11 μm from d1 to d5, with statistically significant differences between comparison pairs (d1/3: $p < 0.05$ denoted as *, d1/5: $p < 0.001$ denoted as ***, d3/5: $p < 0.01$ denoted as **). Neurites originating from edge cells grow from ~7-29 μm from d1 to d5 with statistically significant differences across all comparison pairs ($p < 0.0001$ denoted as **** in all cases). These outcomes suggest that for intermediate population types, neurite outgrowth is stimulated over time in all cases. Cell count for the intermediate population type could therefore be more effective in overcoming any effect of direct structural contact, when compared with the sparse population type. This further implies that for intermediate population types there is an interplay between cell count and whether cells directly contact other cells or the structure.

Temporal changes in neurite outgrowth are shown for each neurite label in the dense population type (Fig. 4.13.3, iii). Neurites originating from isolated cells grow from ~5-9 μm from d1 to d5 with significant statistical differences across comparison pairs (d1/3: $p < 0.01$ denoted as **, d1/5: $p < 0.0001$ denoted as ***, d3/5: $p < 0.05$ denoted as *). Neurites originating from clustered cells grow from ~8-12 μm from d1 to d5, with varying statistical differences between comparison pairs (d1/3: ns, d1/d5, d3/d5: < 0.0001, denoted as ***). Neurites originating from edge cells grow from ~9-29 μm from d1 to d5 with significant statistical differences across all comparison pairs (d1/d3: $p < 0.01$ denoted as **, d1/d5, d3/d5: $p < 0.0001$ denoted as ***). These outcomes demonstrate that for the dense population type, neurite outgrowth is stimulated over time in almost all cases (exception: d1/d3, clustered). This suggests that, similar to the intermediate population type, the effect of the dense population type is enough to stimulate neurite growth in cells that do not contact the structure directly. Further, similar to the intermediate population type, it implies that for the dense population type, there is an interplay between cell count and whether cells directly contact other cells or the structure.

These results suggest cell count affects neurite outgrowth for cells under confinement. Edge cells consistently show neurite extension, suggesting that physical contact with the 3D structure stimulates neurite growth. Further, there appears to be some minimum threshold for cell density that enhances neurite outgrowth for cells not in direct contact with the confinement structure. In addition, for the intermediate and dense population types, neurites are stimulated to extend within the confined environment, despite the decreasing availability of open space. One other conclusion that might be drawn is that the sparse population type does not provide sufficient environmental cues to promote neurite extension when cells are not in direct contact with the structure. The results underscore the importance of accounting for cellular spatial arrangements in 3D-printed structures when considering applications that utilize in vitro neuronal cell culture.

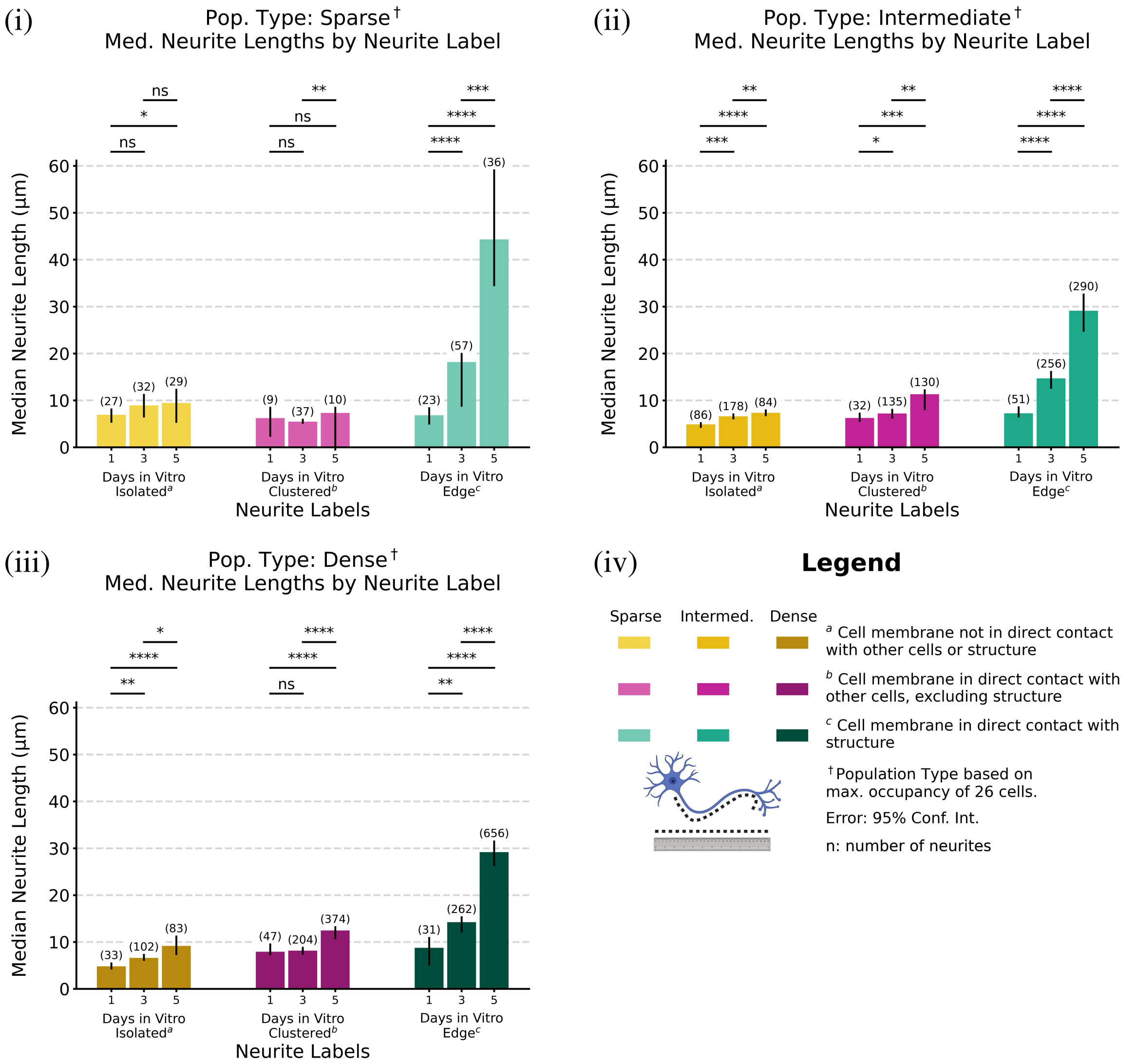

Figure 4.13.3: Median neurite length comparisons across three population types: sparse (i), intermediate (ii), and dense (iii), including a legend (iv). The following pairs of conditions were compared using the Mann-Whitney U test: day 1 - day 3, day 1 - day 5, day 3 - day 5. In the sparse population type (i), neurite outgrowth remains limited for isolated (~7-9 μm) and clustered cells (~6-7 μm) with statistically significant differences (isolated: d1/5: $p < 0.05$ denoted as *; clustered: d 3/5: $p < 0.01$ denoted as **). It should be noted that for clustered cells, sample sizes at days 1 (n=9) and 5 (n=10) are too small to draw meaningful conclusions. There were statistically significant increases observed for edge cells (d1 - d5: ~7-44 μm) from d1-d3 and d1-d5 ($p < 0.0001$, denoted as ****) as well as between d3 and d5 ($p < 0.001$ denoted as ***). For the intermediate population type (ii) median neurite lengths for isolated cells (~5-7 μm from d1 to d5) show statistically significant differences across all comparison pairs (d1/3: $p < 0.001$, d1/5: $p < 0.0001$ denoted as ****, d3/5: $p < 0.01$ denoted as **); clustered cell neurites grow from ~6-11 μm from d1 to d5, with statistically significant differences between comparison pairs (d1/3: $p < 0.05$ denoted as *, d1/d5: $p < 0.001$ denoted as ***, d3/d5: $p < 0.01$ denoted as **); edge cell neurites grow from ~7-29 μm from d1 to d5 with statistically significant differences across all comparison pairs ($p < 0.0001$ denoted as ****). For the dense population type (iii) median neurite lengths for isolated cells grow from ~5-9 μm from d1 to d5 with statistically significant differences across comparison pairs (d1/3: $p < 0.01$ denoted as **, d1/5: $p < 0.0001$ denoted as ****, d3/5: $p < 0.05$ denoted as *); clustered cell neurites grow from ~8-12 μm from d1 to d5, with varying statistical differences between comparison pairs (d1/3: ns, d1/d5, d3/d5: < 0.0001 denoted as ****); edge cell neurites grow from ~9-29 μm from d1 to d5 with statistically significant differences across all comparison pairs (d1/d3: $p < 0.01$ denoted as **, d1/d5, d3/d5: $p < 0.0001$ denoted as ****). (continued on next page)

Figure 4.13.3: (continued from previous page) Edge cells consistently show neurite extension across population types, suggesting direct contact with the structure overcomes any impact induced by population type. Only in the higher population types (intermediate, dense) are neurites from isolated and clustered cells showing meaningful growth, implying that greater amounts of cells under confinement induce neurite extension when cells do not directly contact the structure. Neuron graphic created in https://BioRender.com.

4.13.4 Comparison of Results and Literature

Population type, representing cell count under confinement, appears to play a role in neurite growth. While the specific role played by neighboring cells under confinement may remain elusive, the outcomes presented here suggest that neighboring cells at least induce behavior changes within the confinement structure. The growth of neurites is at least somewhat influenced by both neighboring cells and the physical environment, as demonstrated by multiple studies, and the results presented here. In the sparse population type, PC12 edge neurites extend significantly longer than isolated and clustered neurites, with median lengths reaching a maximum of ~44 μm by day 5 (edge, sparse, d 5). This outcome aligns with Drubin et al. who reported PC12 average (likely mean) neurite lengths of ~50 μm after 5 days in culture. While substrates in both studies differed (10 μg/ml laminin used herein v. 100 μg/ml PLL), they also did not categorize cells according to intercellular contact or investigate cells under confinement[88]. Additionally, results presented here were conducted at higher cell concentrations (culture density from Drubin et al.[88]: ~1.5×10^4 cells/cm^2; v. sparse: ~3.3×10^4 cells/cm^2, intermediate: ~6.5×10^4, dense: ~12.4×10^4). In an investigation using PC12 cells by Attiah et al., mean neurite lengths of ~20 μm were reported after five days in culture[18], with cells cultured at 1.9×10^4 cells/cm^2 (cf. sparse, day 5, isolated, clustered herein, ~9, 7 μm respectively) seeded on laminin. These differences suggest that neighboring cells can impact neurite outgrowth.

In the intermediate population type, neurite growth was also significant, with edge cells showing lengths of up to ~29 μm by day 5. The dense population type also appeared to induce neurite growth differentially, according to neurite label (Fig. 4.13.3, iii). While neurite growth across densities appeared to be impacted by neighboring cells, comparisons by neurite type, where different population types were compared on the same day (Fig. 4.13.2), showed that in over half of the comparison pairs, neurite length was independent of population type. This suggests that while different cell label categories under confinement extend neurites of different lengths, the impact of neighboring cells is induced on isolated and clustered cells on days 1 and 3, and on edge cells on day 5.

Direct contact with artificial structures could be a meaningful strategy to guide and thereby control neurite growth. Yao et al. demonstrated that microgroove topography on laminin-coated PLGA directed neurite outgrowth in PC12 cells, with narrower grooves (5 μm spacing) stimulating longer neurite extension compared to wider grooves (10 μm)[43]. In the results reported herein, also using PC12 cells, the confinement area offered a different type of physical environment, but edge cells (whose membranes directly touched the structure) consistently exhibited the longest neurites. This suggests that direct interaction with structural elements, whether grooves or confinement edges, plays a role in stimulating neurite growth. Results reported herein and those obtained by Yao et al. also support the slightly broader idea that environmental physical cues, such as surface topography or confinement structures, can enhance neurite outgrowth. Together, these studies highlight how neurons respond dynamically to physical confinement, where structural guidance, alongside cell density, influences neurite extension.

4.14 Neurites Per Cell

In this section, the median count of neurites per cell is considered across population types, neurite labels and days in culture (when confidence interval bar not shown: upper confidence interval bound = lower confidence interval bound = median neurite count). Six technical repeats where a total of 34 unconfined populations and 104 confined populations (cells growing within confinement structures) were tracked over 5 days. Definitions of neurite label (edge, isolated, clustered) and population type (sparse, intermediate, dense) are found in section 4.7, Labeling Cells and Classifying Population Type. Further details about samples and controls used for this analysis can be found in Cell Seeding (sec. A.4.3). Only cells with a minimum of 1 neurite were used for the median neurite count calculations, and all cellular processes with path lengths greater than 0 μm were considered neurites. An explanation for these decisions is offered in Comparison of Results and Literature (sec. 4.14.5).

4.14.1 Neurite Count Comparison, Over Time, Across Population Types

Median neurite counts per cell of a given cell label (edge, isolated, clustered) were compared over time for given population types (sparse, intermediate, dense) (Fig. 4.14.1). The following pairs of conditions were compared using the Mann-Whitney U test: day 1 - day 3, day 1 - day 5, day 3 - day 5, and statistical differences are indicated using the following notations: (*) $p < 0.05$, (**) $p < 0.01$, (***) $p < 0.001$, (****) $p < 0.0001$, and (ns) not significant. Therefore, each plot measures how neurite count changes for each cell label over time, comparing temporal differences in neurite count for each population type. Each plot reveals how population type could be influencing the neurite count of a specific cell label, with statistical comparisons between each time point, for each cell label.

Fig. 4.14.1 (i) shows temporal changes in median neurite count per cell in the sparse population type. Edge cells (d1: 1, d3: 1, d5: 1) demonstrate no statistically significant difference ("ns") across all comparison pairs. Isolated cells (d1: 2, d3: 5, d5: 5.5) also demonstrate no statistically significant difference ("ns") across all comparison pairs. Clustered cells (d1: 1, d3: 4, d5: 1) demonstrate a statistically significant difference between day 1 and day 3 ($p < 0.01$ denoted as **) and day 3 and day 5 ($p < 0.05$ denoted as *), and no statistically significant difference ("ns") between day 1 and day 5. This suggests that the sparse population type does not impact neurite outgrowth when cells are in contact with the structure (edge) and when cells are in contact with no other cells (isolated). It may also indicate that cell-cell contact may stimulate neurite outgrowth, but only temporarily. The low sample sizes, however, for the isolated (d 1,3,5) and clustered labels (d 1,3,5), make it difficult to make a meaningful claim about neurite outgrowth in the sparse population type.

Fig. 4.14.1 (ii) shows temporal changes in median neurite count per cell in the intermediate population type. Edge cells (d1: 1, d3: 1, d5: 2) demonstrate no statistically significant difference ("ns") across d1/d3 and d3/d5 comparison pairs and a statistically significant difference between d1/d5 ($p < 0.05$ denoted as *). Isolated cells (d1: 2, d3: 4, d5: 3) demonstrate a highly statistically significant difference between d1/d3 ($p < 0.05$ denoted as *) and no statistically significant difference ("ns") across remaining comparison pairs. Clustered cells (d1: 1, d3: 3, d5: 3) demonstrate a statistically significant difference between d1/d3 ($p < 0.01$ denoted as **) and d1/d5 ($p < 0.001$ denoted as ***), and no statistically significant difference between d3/d5 ("ns"). Small sample sizes in the intermediate population type (isolated, d5, $n = 7$; clustered, d5, $n = 8$) make it difficult to make a meaningful claim about neurite outgrowth at these time points in the intermediate population type. This suggests the intermediate population type might affect d1-d5 neurite outgrowth when cells are in contact with either the structure or other cells, and only temporarily (d1 - d3) affect neurite outgrowth for cells in contact with no other cells.

Fig. 4.14.1 (iii) shows temporal changes in median neurite count per cell in the dense population type. Edge cells (d1: 2, d3: 1, d5: 1) demonstrate no statistically significant difference ("ns") across all comparison pairs. Isolated cells (d1: 2, d3: 3, d5: 4) demonstrate a statistically significant difference between d1/d3 ($p < 0.05$ denoted as *) and d1/d5 ($p < 0.01$ denoted as **) and no statistically significant difference ("ns") between d3/d5. Clustered cells (d1: 2, d3: 2, d5: 2) demonstrate no statistically significant difference ("ns") across all comparison pairs. These outcomes suggest the dense population type may affect neurite outgrowth only when cells are not in contact with the structure or other cells. These outcomes also imply that the dense population type has no impact on neurite outgrowth for edge or clustered cells.

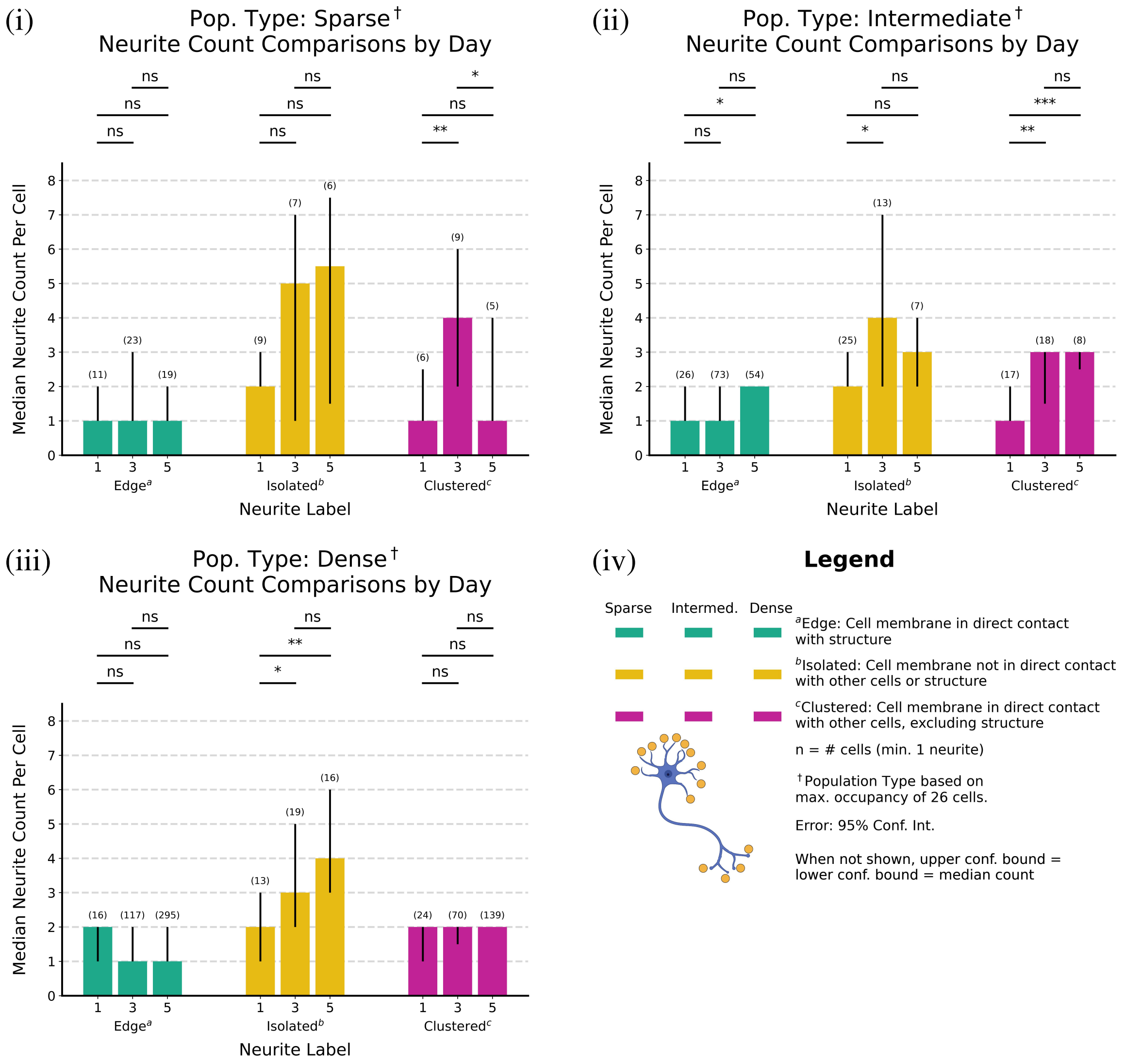

Figure 4.14.1: Comparison of median neurite counts for each cell type over d1 - d 5 for sparse (i), intermediate (ii), and dense (iii) population types, including a legend (iv); when confidence interval bar not shown: upper confidence interval bound = lower confidence interval bound = median neurite count. The following pairs of conditions were compared using the Mann-Whitney U test: day 1 - day 3, day 1 - day 5, day 3 - day 5. In the sparse population type, edge cells (d1: 1, d3: 1, d5: 1) demonstrate no statistically significant difference ("ns") across all comparison pairs; isolated cells (d1: 2, d3: 5, d5: 5.5) also demonstrate no statistically significant difference ("ns") across all comparison pairs; clustered cells (d1: 1, d3: 4, d5: 1) demonstrate a statistically significant difference between day 1 and day 3 ($p < 0.01$ denoted as **) and day 3 and day 5 ($p < 0.05$ denoted as *), and no statistically significant difference ("ns") between day 1 and day 5. Small sample sizes (isolated, clustered; d 1,3,5) make it difficult to make any meaningful claim about neurite outgrowth in this population type. In the intermediate population type, edge cells (d1: 1, d3: 1, d5: 2) demonstrate no statistically significant difference ("ns") across d1/d3 and d3/d5 comparison pairs and a statistically significant difference between d1/d5 ($p < 0.05$ denoted as *); isolated cells (d1: 2, d3: 4, d5: 3) demonstrate a statistically significant difference between d1/d3 ($p < 0.05$ denoted as *) and no statistically significant difference ("ns") across remaining comparison pairs; clustered cells (d1: 1, d3: 3, d5: 3) demonstrate a statistically significant difference between d1/d3 ($p < 0.01$ denoted as **) and d1/d5 ($p < 0.001$), and no statistically significant difference between d3/d5 ("ns"). Small sample sizes in the intermediate population type (iso. d5; clu. d5) make it difficult to make any meaningful claim about neurite outgrowth in this population type. In the dense population type, edge cells (d1: 2, d3: 1, d5: 1) demonstrate no statistically significant difference ("ns") across all comparison pairs; isolated cells (d1: 2, d3: 3, d5: 4) demonstrate a statistically significant difference between d1/d3 ($p < 0.05$ denoted as *) and d1/d5 ($p < 0.01$ denoted as **) and no statistically significant difference ("ns") between d3/d5; clustered cells (d1: 2, d3: 2, d5: 2) demonstrate no statistically significant difference ("ns") across all comparison pairs. Neuron graphic created in https://BioRender.com.

4.14.2 Neurite Count Comparison by Days In Vitro, for Different Population Types

Median neurite counts of a given cell label (edge, isolated, clustered) under confinement were compared over different population types (sparse, intermediate, dense) (Fig. 4.14.2). The following pairs of conditions were compared using the Mann-Whitney U test: edge-isolated, edge-clustered, isolated-clustered, and statistical differences are indicated using the following notations: (*) $p < 0.05$, (**) $p < 0.01$, (***) $p < 0.001$, (****) $p < 0.0001$, and (ns) not significant. Therefore, each plot measures how neurite count changes for each cell label grouping on each day in culture, comparing differences in neurite count for each label grouping. Each plot reveals how population type could be influencing the neurite count of a specific cell label grouping, with statistical comparisons between each cell label.

Fig. 4.14.2 (i) shows changes in median neurite count per cell for each cell label on a given day, for cells in the sparse population type. Cells on day 1 (edge: 1, iso.: 2, clu.: 1) demonstrate a statistically significant difference between edge and isolated cells ($p < 0.05$ denoted as *), and no statistically significant difference ("ns") across remaining comparison pairs. Cells on day 3 (edge: 1, iso.: 5, clu.: 4) demonstrate a statistically significant difference ($p < 0.01$ denoted as **) between edge and clustered groups, and no statistically significant difference ("ns") across remaining comparison pairs. Cells on day 5 (edge: 1, iso.: 5.5, clu.: 1) demonstrate a statistically significant difference ($p < 0.05$ denoted as *) between edge and isolated groups, and no statistically significant difference ("ns") across remaining comparison pairs. This suggests that the effect of the sparse population type on neurite count may be negligible or rather complex. For example, there is no statistically significant difference between isolated and clustered groups at all time points. The edge group demonstrates a difference with the isolated group on days 1 and 5, and a difference with the clustered group on day 3. This at least indicates that edge cells uniquely respond to the sparse population type, and that there are possible distinctions in the responses of isolated and clustered cells, from day 1 to day 5. In the cases of isolated and clustered cells on days 1, 3 and 5, small sample sizes make it difficult to make any claims about relative behavior.

Fig. 4.14.2 (ii) shows changes in median neurite count per cell for each cell label on a given day, for cells in the intermediate population type. Cells on day 1 (edge: 1, iso.: 2, clu.: 1) demonstrate a statistically significant difference between edge and isolated cells ($p < 0.05$ denoted as *), and isolated and clustered cells ($p < 0.01$ denoted as **), and no statistically significant difference ("ns") between edge and clustered groups. Cells on day 3 (edge: 1, iso.: 4, clu.: 3) demonstrate a statistically significant difference ($p < 0.01$ denoted as **) between edge and isolated groups, and between edge and clustered groups ($p < 0.05$ denoted as *), and no statistically significant difference ("ns") between isolated and clustered groups. Cells on day 5 (edge: 2, iso.: 3, clu.: 3) demonstrate a statistically significant difference ($p < 0.05$ denoted as *) between edge and clustered groups, and no statistically significant difference ("ns") across remaining comparison pairs. Smaller sample sizes in the intermediate population type at day 5 for clustered and isolated neurites make it difficult to make any meaningful claim about neurite outgrowth at these time points within this population type. These outcomes also suggest that the effect of the intermediate population type on neurite count may be negligible or rather complex. For example, on days 1 and 3, there are some demonstrated distinctions in median neurite count between edge and isolated cells, but this disappears by day 5; on days 3 and 5, there are distinctions between edge and clustered cells, that were not present on day 1; lastly, there is a distinction between isolated and clustered median neurite counts on day 1 which disappears on days 3 and 5. This could at least suggest that the intermediate population type induces a different outcome on different cell label grouping at different times.

Fig. 4.14.2 (iii) shows changes in median neurite count per cell for each cell label grouping on a given day, for cells in the dense population type. Cells on day 1 (edge: 2, iso.: 2, clu.: 2) demonstrate no statistically significant difference ("ns") across all comparison pairs. Cells on day 3 (edge: 1, iso.: 3, clu.: 2) demonstrate a statistically significant difference ($p < 0.0001$ denoted as ****) between edge and isolated groups, between edge and clustered groups ($p < 0.05$), and between isolated and clustered groups ($p < 0.01$ denoted as **). Cells on day 5 (edge: 1, iso.: 4, clu.: 2) demonstrate a statistically significant difference ($p < 0.0001$ denoted as ****) between edge and isolated groups and between isolated and clustered groups and a statistically significant difference between edge and clustered groups ($p < 0.05$ denoted as *). While there are no differences across comparison pairs on day 1, there are demonstrated differences between all comparison pairs on days 3 and 5. This implies that the dense population type influences neurite outgrowth differently, depending on whether cells are in contact with the structure or other cells. For example on days 3 and 5, neurite outgrowth is highest for isolated cells, suggesting cells that do not contact other cells or the structure may prioritize neurite outgrowth over their counterparts. These outcomes also imply that, under the dense population type, cells which directly contact the structure or other cells may not extend additional neurites, because they already experience direct interaction with another feature within the microenvironment.

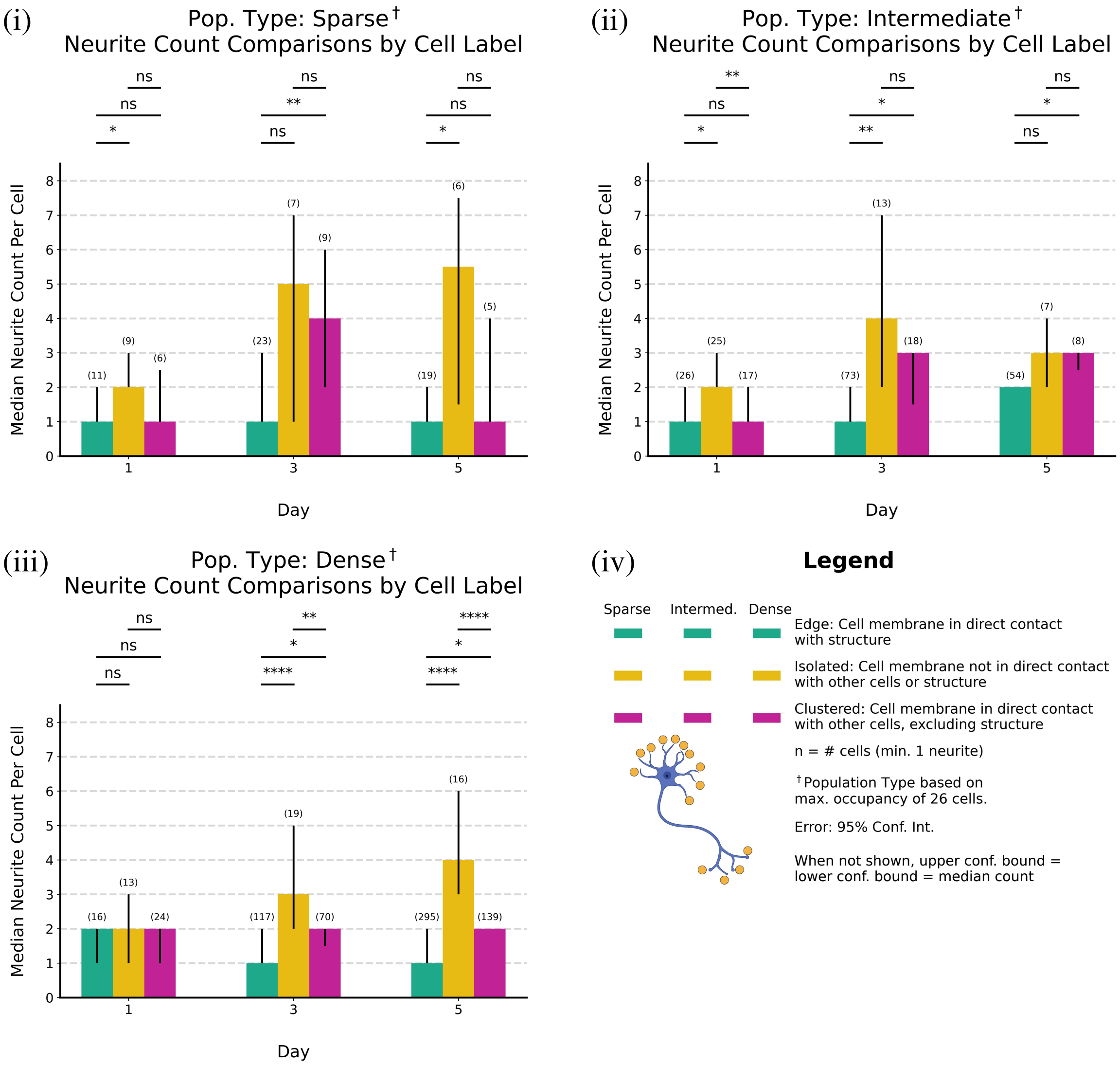

Figure 4.14.2: Comparison of median neurite counts for each cell label on a given day in culture for sparse (i), intermediate (ii), and dense (iii) population types, including a legend (iv); when confidence interval bar not shown: upper confidence interval bound = lower confidence interval bound = median neurite count. The following pairs of conditions were compared using the Mann-Whitney U test: edge-isolated, edge-clustered, isolated-clustered. In the sparse population type, cells on day 1 (edge: 1, iso.: 2, clu.: 1) demonstrate a statistically significant difference between edge and isolated cells ($p < 0.05$ denoted as *), and no statistically significant difference ("ns") across remaining comparison pairs. Cells on day 3 (edge: 1, iso.: 5, clu.: 4) demonstrate a statistically significant difference ($p < 0.01$ denoted as **) between edge and clustered groups, and no statistically significant difference ("ns") across remaining comparison pairs. Cells on day 5 (edge: 1, iso.: 5.5, clu.: 1) demonstrate a statistically significant difference ($p < 0.05$ denoted as *) between edge and isolated groups, and no statistically significant difference ("ns") across remaining comparison pairs. Small sample sizes (isolated, clustered; d 1,3,5) make it difficult to make any meaningful claim about neurite outgrowth in this population type. In the intermediate population type, cells on day 1 (edge: 1, iso.: 2, clu.: 1) demonstrate a statistically significant difference between edge and isolated cells ($p < 0.05$ denoted as *), and isolated and clustered cells ($p < 0.01$ denoted as **), and no statistically significant difference ("ns") between edge and clustered groups. Cells on day 3 (edge: 1, iso.: 4, clu.: 3) demonstrate a statistically significant difference ($p < 0.01$ denoted as **) between edge and isolated groups, and between edge and clustered groups ($p < 0.05$ denoted as *), and no statistically significant difference ("ns") between isolated and clustered groups. Cells on day 5 (edge: 2, iso.: 3, clu.: 3) demonstrate a statistically significant difference ($p < 0.05$ denoted as *) between edge and clustered groups, and no statistically significant difference ("ns") across remaining comparison pairs. (continued on next page)

Figure 4.14.2: (continued from previous page) Small sample sizes (iso., clu.; d 5) make it difficult to make any meaningful claim about neurite outgrowth in this population type. In the dense population type, cells on day 1 (edge: 2, iso.: 2, clu.: 2) demonstrate no statistically significant difference ("ns") across all comparison pairs. Cells on day 3 (edge: 1, iso.: 3, clu.: 2) demonstrate a statistically significant difference ($p < 0.0001$ denoted as ****) between edge and isolated groups, between edge and clustered groups ($p < 0.05$ denoted as *), and between isolated and clustered groups ($p < 0.01$ denoted as **). Cells on day 5 (edge: 1, iso.: 4, clu.: 2) demonstrate a statistically significant difference ($p < 0.0001$ denoted as ****) between edge and isolated groups, isolated and clustered groups, and edge and clustered groups ($p < 0.05$ denoted as *). Neuron graphic created in https://BioRender.com.

4.14.3 Neurite Count Under Different Population Type, by Cell Label

Neurite counts of a given cell label (edge, isolated, clustered) for cells under confinement were compared on the same day in culture over different population types (sparse, intermediate, dense) Fig. 4.14.3). The following pairs of conditions were compared using the Mann-Whitney U test: sparse-intermediate, sparse-dense, intermediate-dense, and statistical differences are indicated using the following notations: (*) $p < 0.05$, (**) $p < 0.01$, (***) $p < 0.001$, (****) $p < 0.0001$, and (ns) not significant. Therefore, each plot measures how neurite count changes for each cell label grouping in different population types. Each plot reveals how population type could be influencing the neurite count of a specific cell type, with statistical comparisons between each population type, for neurites extending from a given cell label.

Fig. 4.14.3 (i) shows changes in median neurite count per edge cell for different population types on the same day in culture. Edge cells on day 1 (sparse: 1, int.: 1, dense: 2) demonstrate no statistically significant differences ("ns") across comparison pairs. Edge cells on day 3 (sparse: 1, int.: 1, dense: 1) demonstrate no statistically significant differences ("ns") across comparison pairs. Edge cells on day 5 (sparse: 1, int.: 2, dense: 1) demonstrate no statistically significant differences ("ns") between sparse-intermediate and sparse-dense comparison pairs and a statistically significant difference ($p < 0.05$, denoted as *) between intermediate and dense population types. This suggests that population type mostly does not affect neurite outgrowth when cells are in contact with the structure, with the sole exception that on day 5, there may be some distinct impact on cells in intermediate and dense population types. This also at least implies that cell-structure contact could be influencing neurite outgrowth, independent of the number of cells under confinement.

Fig. 4.14.3 (ii) shows changes in median neurite count per isolated cell for different population types on the same day in culture. Isolated cells on day 1 (sparse: 2, int.: 2, dense: 2) demonstrate no statistically significant differences ("ns") across comparison pairs. Isolated cells on day 3 (sparse: 5, int.: 4, dense: 3) demonstrate no statistically significant differences ("ns") across comparison pairs. Isolated cells on day 5 (sparse: 5.5, int.: 3, dense: 4) also demonstrate no statistically significant differences ("ns") across comparison pairs. These outcomes suggest population type does not affect neurite outgrowth when cells are not in direct contact with other cells or the structure. This at least implies that an absence of direct contact with other cells or the structure drives neurite outgrowth independent of the presence of other confined cells. Small sample sizes of isolated cells in sparse (d 1, 3, 5) and intermediate (d 5) population types make it difficult to make any meaningful claim about neurite count in these population types.

Fig. 4.14.3 (iii) shows changes in median neurite count per clustered cell for different population types on the same day in culture. Clustered cells on day 1 (sparse: 1, int.: 1, dense: 2) demonstrate no statistically significant differences ("ns") across comparison pairs. Clustered cells on day 3 (sparse: 4, int.: 3, dense: 2) demonstrate statistically significant differences ("ns") between sparse-isolated ($p < 0.05$) and sparse-dense ($p < 0.01$ denoted as **) comparison pairs and no statistically significant difference ("ns") between intermediate and dense groups. Clustered cells on day 5 (sparse: 1, int.: 3, dense: 2) demonstrate no statistically significant differences ("ns") between sparse-intermediate and sparse-dense comparison pairs and a statistically significant difference ($p < 0.05$ denoted as *) between intermediate and dense population types. These outcomes suggest that when cells are contacting other cells, and not the structure, there are no differences in median neurite count on day 1, some differences between population types on day 3, and one difference on day 5. These outcomes also suggest there is a complex relationship between population type and neurite outgrowth starting on day 3. On day 3, differences between the sparse population type and the other two population types appear, then disappear on day 5. On day 5, a new difference emerges between intermediate and dense population types, while the differences between sparse population type and the other two population types have been suppressed. This at least implies that neurite outgrowth among clustered cells is somewhat driven by the presence of other cells under confinement at later timepoints (d 3, 5), and that there are no distinctions in neurite outgrowth among clustered cells in population types on day 1. The low number of clustered cells in the sparse population type at days 1, 3 and 5, and the intermediate population type at day 5, however, make it difficult to draw any conclusions about these cell types in this population type at these time points.

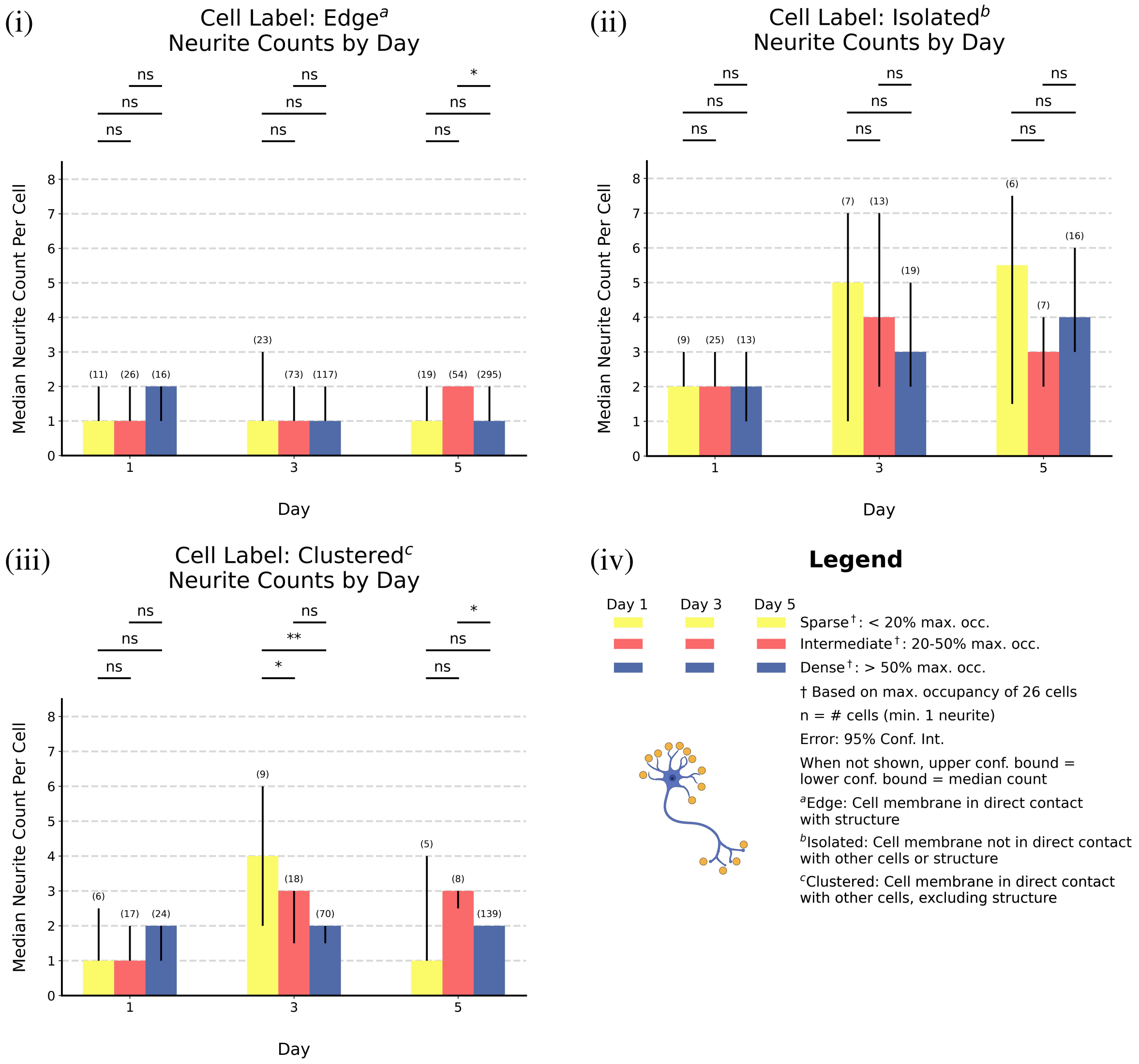

Figure 4.14.3: Comparison of median neurite counts for (i) edge, (ii) isolated, and (iii) clustered cell label groupings across sparse, intermediate, and dense population types over different days in culture, including a legend (iv); when confidence interval bar not shown: upper confidence interval bound = lower confidence interval bound = median neurite count. The following pairs of conditions were compared using the Mann-Whitney U test: sparse-intermediate, sparse-dense, intermediate-dense. Edge cells on day 1 (sparse: 1, int.: 1, dense: 2) demonstrate no statistically significant differences ("ns") across comparison pairs. Edge cells on day 3 (sparse: 1, int.: 1, dense: 1) demonstrate no statistically significant differences ("ns") across comparison pairs. Edge cells on day 5 (sparse: 1, int.: 2, dense: 1) demonstrate no statistically significant differences ("ns") between sparse-intermediate and sparse-dense comparison pairs and a statistically significant difference ($p < 0.05$ denoted as *) between intermediate and dense groups. Isolated cells on day 1 (sparse: 2, int.: 2, dense: 2) demonstrate no statistically significant differences ("ns") across comparison pairs. Isolated cells on day 3 (sparse: 5, int.: 4, dense: 3) demonstrate no statistically significant differences ("ns") across comparison pairs. Isolated cells on day 5 (sparse: 5.5, int.: 3, dense: 4) demonstrate no statistically significant differences ("ns") across comparison pairs. Small sample sizes for sparse (d 1, 3, 5) and intermediate (d 5) population types make it difficult to make a meaningful claim about isolated cells at these population types and time points. Clustered cells on day 1 (sparse: 1, int.: 1, dense: 2) demonstrate no statistically significant differences ("ns") across comparison pairs. Clustered cells on day 3 (sparse: 4, int.: 3, dense: 2) demonstrate statistically significant differences between sparse-isolated ($p < 0.05$ denoted as *) and sparse-dense ($p < 0.01$) comparison pairs and no statistically significant difference ("ns") between intermediate and dense population types. (continued on next page)

Figure 4.14.3: (continued from previous page) Clustered cells on day 5 (sparse: 1, int.: 3, dense: 2) demonstrate no statistically significant differences ("ns") between sparse-intermediate and sparse-dense comparison pairs and a statistically significant difference ($p < 0.05$ denoted as *) between intermediate and dense population types. Small sample sizes in the sparse population type on d 1, 3, 5 and intermediate population type on d 5 make it difficult to make a meaningful claim about clustered cells in this population type at these time points. Neuron graphic created in https://BioRender.com.

4.14.4 Neurite Count, Confined vs. Unconfined, Over Time

Median neurite counts were compared for each confined cell label (isolated, clustered, edge) and unconfined cell label (isolated, clustered) at each day in culture (Fig. 4.14.4). The following pairs of conditions were compared using the Mann-Whitney U test: isolated confined -isolated unconfined, clustered confined - clustered unconfined, edge confined - isolated unconfined, edge confined - clustered unconfined, and statistical differences are indicated using the following notations: (*) $p < 0.05$, (**) $p < 0.01$, (***) $p < 0.001$, (****) $p < 0.0001$, and (ns) not significant. Therefore, the plot measures how confinement could be influencing the neurite count of a specific cell label.

The day 1 values shown in Fig. 4.14.4 (iso. conf.: 2, iso. unconf.: 1, clu. conf.: 1, clu. unconf.: 1, edge conf: 1) show statistically significant differences between isolated confined and isolated unconfined ($p < 0.001$ denoted as ***), clustered confined and clustered unconfined ($p < 0.01$ denoted as **), and clustered unconfined and edge confined ($p < 0.05$ denoted as *) groups, while demonstrating no statistically significant difference ("ns") between isolated unconfined and edge confined cell labels. These day 1 outcomes suggest that 1) confinement enhances neurite count for isolated and clustered cells, 2) the effect of direct contact with the structure edge has a similar impact on neurite count as isolated cells absent confinement, and 3) because the confidence interval is higher for the edge group, contact with the structure edge has an effect on neurite count different from cell-cell contact absent confinement (edge conf. v. clu. unconf.). These outcomes suggest that confinement enhances neurite count and that contact with the structure edge might be similar to unconfined isolated cells and might increase neurite count more than contact with other cells.

The day 3 values shown in Fig. 4.14.4 (iso. conf.: 3, iso. unconf.: 2, clu. conf.: 2, clu. unconf.: 1, edge conf.: 1) show statistically significant differences between isolated confined and isolated unconfined, clustered confined and clustered unconfined ($p < 0.0001$ denoted as ****), and clustered unconfined and edge confined ($p < 0.001$ denoted as ***) cells, while demonstrating no statistically significant difference ("ns") between isolated unconfined and edge confined cells. These day 3 outcomes reinforce those observed on day 1: 1) confinement enhances neurite count for isolated and clustered cells, 2) the effect of direct contact with the structure edge has a similar impact on neurite count as isolated cells under no confinement, and 3) because the confidence interval is higher for edge cells, contact with the structure edge has an effect on neurite count different from cell-cell contact absent confinement (edge conf. v. clu. unconf.). These outcomes also suggest that, as time elapses from day 1 to day 3, the enhanced effect on neurite count of confinement at least remains constant.

The day 5 values shown in Fig. 4.14.4 (iso. conf.: 4, iso. unconf.: 2, clu. conf.: 2, clu. unconf.: 1, edge conf.: 2) show highly significant statistical differences between isolated confined and isolated unconfined, clustered confined and clustered unconfined and clustered confined and edge confined cells ($p < 0.0001$ denoted as **** in all cases), as well as a statistically significant difference between isolated unconfined and edge confined cells ($p < 0.01$ denoted as **). These day 5 outcomes are slightly different from those observed on days 1 and 3: 1) confinement continues enhancing neurite count for isolated and clustered cells, 2) contact with the structure edge continues to affect neurite count different from cell-cell contact absent confinement, and 3) because the confidence interval is now entirely below the median for edge cells, contact with the structure edge still stimulates neurite count more than cell-cell contact absent confinement (edge conf. v. clu. unconf.) and also suppresses it relative to isolated unconfined cells. These outcomes suggest that, as time elapses from day 1 to day 3, the stimulative effect on neurite count of confinement mostly remains constant and the difference between isolated unconfined and edge confined groups implies that by day 5, the effect of the absence of confinement on isolated cells stimulates neurite count to a greater extent than contact with the structure.

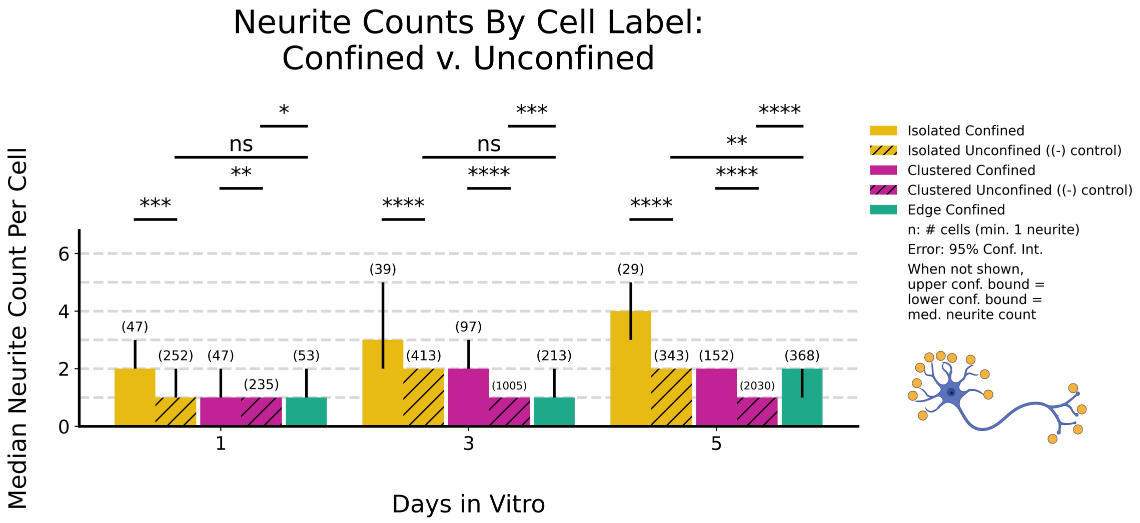

Figure 4.14.4: Comparison of median neurite counts between confined cell labels isolated, clustered, and edge and unconfined cell labels isolated and clustered unconfined ((-) control) across days 1, 3, and 5; when confidence interval bar not shown: upper confidence interval bound = lower confidence interval bound = median neurite count. The following pairs of conditions were compared using the Mann-Whitney U test: isolated confined - isolated unconfined, clustered confined - clustered unconfined, edge confined - isolated unconfined, edge confined - clustered unconfined. Day 1 values shown in Fig. 4.14.4 (iso. conf.: 2, iso. unconf.: 1, clu. conf.: 1, clu. unconf.: 1, edge conf.: 1) show statistically significant differences between isolated confined and isolated unconfined ($p < 0.001$ denoted as ***), clustered confined and clustered unconfined ($p < 0.01$ denoted as **), and clustered unconfined and edge confined ($p < 0.05$ denoted as *) cell labels, while demonstrating no statistically significant difference ("ns") between isolated unconfined and edge confined cell labels. Day 3 values shown in Fig. 4.14.4 (iso. conf.: 3, iso. unconf.: 2, clu. conf.: 2, clu. unconf.: 1, edge conf.: 1) show statistically significant differences between isolated confined and isolated unconfined, clustered confined and clustered unconfined ($p < 0.0001$ denoted as ****), and clustered unconfined and edge confined ($p < 0.001$ denoted as ***) cell labels, while demonstrating no statistically significant difference ("ns") between isolated unconfined and edge confined cell labels. Day 5 values shown in Fig. 4.14.4 (iso. conf.: 4, iso. unconf.: 2, clu. conf.: 2, clu. unconf.: 1, edge conf.: 2) show statistically significant differences between isolated confined and isolated unconfined, clustered confined and clustered unconfined, and clustered unconfined and edge confined ($p < 0.0001$ denoted as ****) cell labels, and between isolated unconfined and edge confined cell labels ($p < 0.01$ denoted as **). Neuron graphic created in https://BioRender.com.

4.14.5 Comparison of Results and Literature

Neurite outgrowth is a fundamental process in neuronal development and regeneration, influenced by various factors such as cell density, substrate properties, cell-cell, and cell-structure interactions. Therefore, it might be useful to understand how confinement, direct physical contact with other cells or the confinement structure, and the amount of neighboring cells affect the number of neurites extended by a soma. By categorizing cells into edge, clustered or isolated cell labels, grouping confined environments by cell number into sparse, intermediate, or dense population types and calculating neurite counts for unconfined cells, the influence of cell interactions, neighboring cells, and confinement on neurite count can be determined.

For this investigation, only cells with a minimum of 1 neurite were chosen to calculate the median. Cells with no identifiable neurites were not part of any results presented here. In addition, while differentiating neurons project lamellipodia and filopodia into their environment, and these are not typically considered neurites, any neuronal process with a length greater than 0 μm was considered a neurite for this investigation. While this contrasts with other approaches and the morphology of non-neurite cellular outgrowths are typically less than a few microns long, the quantifiable threshold differentiating lamellipodia and filopodia from neurites is difficult to ascertain. This strategy is guided by Dotti et al.'s investigation into differentiating hippocampal neurons (Fig. 1.2.1)[17]: around 0.5 d in culture, differentiating neurons have begun to extend minor processes into the environment and by approximately 1.5 d in culture, differentiating neurons have begun to grow an axon. Therefore our approach of including any observed cellular process after 1 d, at least suggests the morphological features observed are very likely neurites.

Results presented here indicate that using 1) population type to account for the number of cells under confinement, 2) the presence or absence of cell-cell or cell-structure contact, and 3) the presence or absence of confinement, suggests these factors could play a role in the number of neurites extended by a PC12 cell. First, the sparse population type seems to have no influence on neurite count for edge and isolated confined cells from d 1 to d 5 (Fig. 4.14.1, i). In addition, the dense population type appears to have no influence on neurite count for edge and clustered confined cells from d 1 to d 5 (Fig. 4.14.1, iii). The former outcome could suggest that the sparse population type drives neurite count only for clustered confined cells, while the latter outcome suggests the dense population type drives neurite formation only for isolated confined cells. In addition, 1) confinement seems to consistently enhance neurite count for isolated and clustered cells over time, when compared to their respective unconfined counterparts (Fig. 4.14.4) and 2) edge confined cells tend to extend more neurites than unconfined clustered cells, indicating that cell-structure contact may stimulate neurite outgrowth more effectively than cell-cell contact (Fig. 4.14.4).

When comparing findings presented here with existing literature, there are distinctions that should be accounted for, especially in light of different outcomes. Song et al. demonstrated that dissociated dorsal root ganglia neurons cultured on 100 μg/ml laminin-coated micropatterns of various widths (10-40 μm) showed no meaningful statististical difference among neurite counts (compiled after 24 h), across different pattern widths[20]. A sound comparison might exist between the edge cells presented herein and the confined neurons measured by Song et al. Outcomes ranged from ~3.4 - 4.5 neurites/cell across pattern widths[20] (cf. <2 herein, after 24 h, Fig. 4.14.4); so Song et al. counted many more neurites after 24 h than were counted herein. This could be the result of an increased laminin concentration (100 μg/ml v. 10 herein), a difference originating from the different cell lines used, or the result of differing micropatterning dimensions (10-40, v. ~$100-200$ μm herein). While their focus was on neurite orientation and length on patterned substrates, results presented herein focus on the role played by population type and cell interactions with the microenvironment, complicating any direct analysis.

In another investigation, Xu et al. observed that primary embryonic rat hippocampal neurons exhibited normal polarized morphology and neurite outgrowth both in 3D collagen matrices and on 2D collagen-coated substrates. Researchers measured the number of neurites originating from the soma over time finding that on 2D collagen coated substrates (0.1 mg/ml), ~3 neurites/cell grew after 3 days in culture for cells cultured at a density of ~1×10^4 cells/cm^2 (cf. sparse population type: ~3.3×10^4 cells/cm^2) compared with results presented herein (d3, sparse, isolated confined: 5, clustered confined: 4 neurites/cell, Fig. 4.14.2, (i))[21]. Since the sparse population type was plated at a greater density than the results presented by Xu et al., this may account for the higher neurite counts/cell obtained herein. In addition, comparisons across cell lines inherently weaken any sound argument around differences in experimental outcomes. The difference in neurite counts also highlights the complexity of neuronal development in vitro and suggests that variations in culture conditions can significantly impact neurite formation.

A related investigation by Béduer et al. only counted neurites longer than 10 μm in adult human progenitor cells cultured on PDMS substrates (coated with 100 μg/ml polylysine followed by 40 μg/ml laminin) with varying groove dimensions (from ~5-60 μm)[19]. They cultured cells at 7.5×10^4 cells/cm^2 (cf. intermediate: ~6.5×10^4, dense: ~12.4×10^4). Primarily, across widening substrates, they found that there were ~1-2 neurites/cell after 7 days in culture (cf. results herein: dense d5 isolated, clustered: 4, 2 neurites/cell respectively, Fig. 4.14.1, iii). The promise of both investigations mainly lies in how neurons and neuron-like PC12 cells interact with synthetic topographical modifications; however Beduer et al. mainly focused on differentiation rates and neurite length while the focus of the results presented herein is on how PC12 cells grouped by label (edge, isolated, clustered) respond to confinement and how the presence of neighboring cells under confinement might impact neurite count.

In a study by Attiah et al. using PC12 cells cultured on laminin and collagen type 1 modified substrates over 8 days, a rapid increase in total neurite count was observed for cells on collagen type 1, while those on laminin showed a much slower rate of increase[18]. Similarly, results presented here (PC12 on laminin) demonstrate slow increases in neurite count across certain cell labels and population types (e.g., edge and clustered cells, Fig 4.14.1). However, this analysis focused on neurite counts per cell at a higher culture density (sparse: $\sim 3.3 \times 10^4$, cells/cm^2), whereas Attiah's study used a lower density (1.9×10^4, cells/cm^2) and summed neurites across randomly chosen cells. Although the differences in data collection and analysis (Attiah's total neurite count versus our per-cell neurite analysis calculation) complicate direct quantitative comparisons, the slow increases observed in both studies on laminin-coated substrates may still align qualitatively. It is also possible that the lower cell density in Attiah's study may have suppressed overall neurite counts. While direct comparison is difficult due to methodological differences, the shared experimental conditions (PC12 cells on laminin) could partly explain the similar trends of slow neurite growth over time.

The results presented here contribute to the growing body of knowledge on how physical and environmental factors influence neurite outgrowth. While existing literature emphasizes the role of substrate composition and patterning on neurite extension, our findings highlight the impact of population type and confinement structures. The observation that confinement enhances neurite outgrowth in isolated and clustered PC12 cells adds a novel perspective to the understanding of neuron-environment interactions. Moreover, the differential effects of population type on edge, clustered, and isolated cells underscore the complexity of neurite outgrowth regulation. Our results, in conjunction with previous studies, suggest that both biochemical cues from substrate coatings and physical cues from the cellular environment synergistically influence neuronal development. This integrated understanding could inform future strategies in neural tissue engineering and regenerative medicine, where controlling neurite outgrowth is critical.

4.15 Real Time Cell Behavior

Live imaging was conducted on PC12 cells in confinement structures over 60 h starting at $t_0 = 33\,\text{h}$ after seeding (Fig. 4.15.1). The data analyzed in this section comes from one technical repeat where cells in 9 confinement structures were analyzed. Cells are labeled as edge, isolated, or clustered. The data reveals temporal changes in cell status (i.e. cell label) relative to the structure and other cells. "Cell Status Over Time," (Fig. 4.15.1, (i)) tracks the total cell counts for each label, while "Status Changes of All Cells Over Time," (Fig. 4.15.1, (ii)) shows transitions between these statuses, and accumulates the percentage of time cells within the confined population spend in each of the three labeled categories. Further details about samples used for this analysis can be found in Cell Seeding (sec. A.4.3).

Fig. 4.15.1, (i) demonstrates cells have a clear preference for cell-structure contact (edge). The number of edge cells increases over time, peaking around 60 cells by ~85 h, while the isolated and clustered cells exhibit a decline in cell count through 93 h. Isolated cells consistently remain the minority group, with counts dropping to almost zero through 93 h. While there is a decrease of available space over time, the persistently low isolated cell count also suggests a preference for cells to contact either neighboring cells or the structure. Cells therefore likely prefer some form of contact rather than remain isolated. The decrease in clustered cells over time also implies that contact with the structure is preferred. The behavior of isolated and clustered populations suggests that neither available space nor cell-cell contact are as preferable as contact with the confinement structure.

Fig. 4.15.1, (ii) supports the findings mentioned above by tracking changes in cell label over time. Red circles are cells present at the beginning of the analysis and blue squares are cells that appear during the imaging period, as a result of proliferation. The percentage of total time spent by the cell population as edge cells is 77%; cells within the population spend less time in the clustered condition (21% of total time) and an even smaller amount of time in the isolated condition (2% of total time). Cell-structure contact remains a preferred modus operandi for cells within this population, followed by cell-cell contact. These outcomes suggest that under confinement, in the presence of open space, cells still prefer to remain in direct contact with features in the microenvironment. Therefore, it is possible that there is an interplay between cell migration, cell-cell contact and structural elements that should be accounted for when designing microenvironments with potential applications for tissue engineering or neuronal network modeling.

Fig. 4.15.1, (a - d) shows a single confinement structure at 10 frame intervals (1 frame = 30 min.) starting at frame 10. Image *a* shows that there are 5 cells under confinement, and that all cells touch the edge (3a, 5a, 5a, 4c, 5c); image *b* shows 5 cells under confinement (3a - edge, 5a - edge, 5a - other, 5c - edge, 4c - isolated); image *c* shows 5 cells under confinement (3a - edge, 5a - edge, 6a - edge, 5c - edge, 4c - edge); image *d* shows 7 cells under confinement (3a - edge, 4a - edge, 5a - edge, 5b - clustered (2 cells), 6b - edge, 4c - edge). This series of images represents how cells behave inside confinement structures: most cells prefer the structure edge or contact with other cells, most of the time. In addition, while the confined cells prefer some mode of contact, many also continue to extend neurites, change their morphology, and interrogate their environment (*a* 5c, *b* 5c, *c* 5c, *d* 6b are the same cell; *a* 4c, *b* 4c, *c* 4c, *d* 4c are the same cell).

Results presented here demonstrate that PC12 cells under confinement primarily prefer contact with the structure's edge. The increasing number of edge cells, peaking at 60 by ~85 h, suggests that cell-structure contact is favored over cell-cell contact (clustered) and isolation (isolated). To gain some insight into possible explanations for this phenomenon, the 3D printed structure and its substrate were coated with fluorescently labeled laminin. Fluorescent microscopic images of the structure and substrate revealed no distinct accumulation of laminin around or close to the edge of the structure (results presented in appendix C, Laminin Coating Heterogeneity). Nevertheless, the strong preference of PC12 cells for structure contact emphasizes the importance of the physical environment in guiding cell behavior within confined spaces. In a related investigation, Gunay et al. demonstrated that PC12 cell morphology and neurite extension were influenced by the physical topography of their environment, with 3D peptide ampiphile hydrogels enhancing cell adhesion and growth[89]. Their findings, and the findings presented herein, highlight the role the physical microenvironment plays in cell behavior.

Cells show a preference for contact, either with neighboring cells or the structure, rather than remaining isolated in open 2D space. This suggests that PC12 cells are healthier when in contact, leading them to actively seek interactions and avoid isolation. Koroleva et al. similarly observed that neural stem cells in a 3D-printed honeycomb scaffold demonstrated enhanced cell-cell contacts and adaptation, with scaffolds facilitating increased cellular communication[52]. Isolation appears to be less advantageous, especially in engineered environments, and cells are possibly most likely to form contacts with structural features when they are available.

Over time, the number of clustered cells decreases, reinforcing the idea that cells strongly prefer contact with the structure. This implies that cell-cell interactions are secondary to contact with structural elements in the microenvironment. Janzen et al. also noted that seeding mouse cortical neurons in 3D scaffolds promoted more extensive dendritic growth and synapse formation than when cells were seeded on 2D substrates[90]. The results presented here as well as those obtained by Janzen suggest that contact with the structure, rather than 2D clustering, could enhance healthy cell and cell network development. The interconnectedness of neurons, and the outgrowth of neurites could be stimulated by the presence of a supportive scaffold. 3D modifications can therefore be a useful tool when developing in vitro neural tissue models.

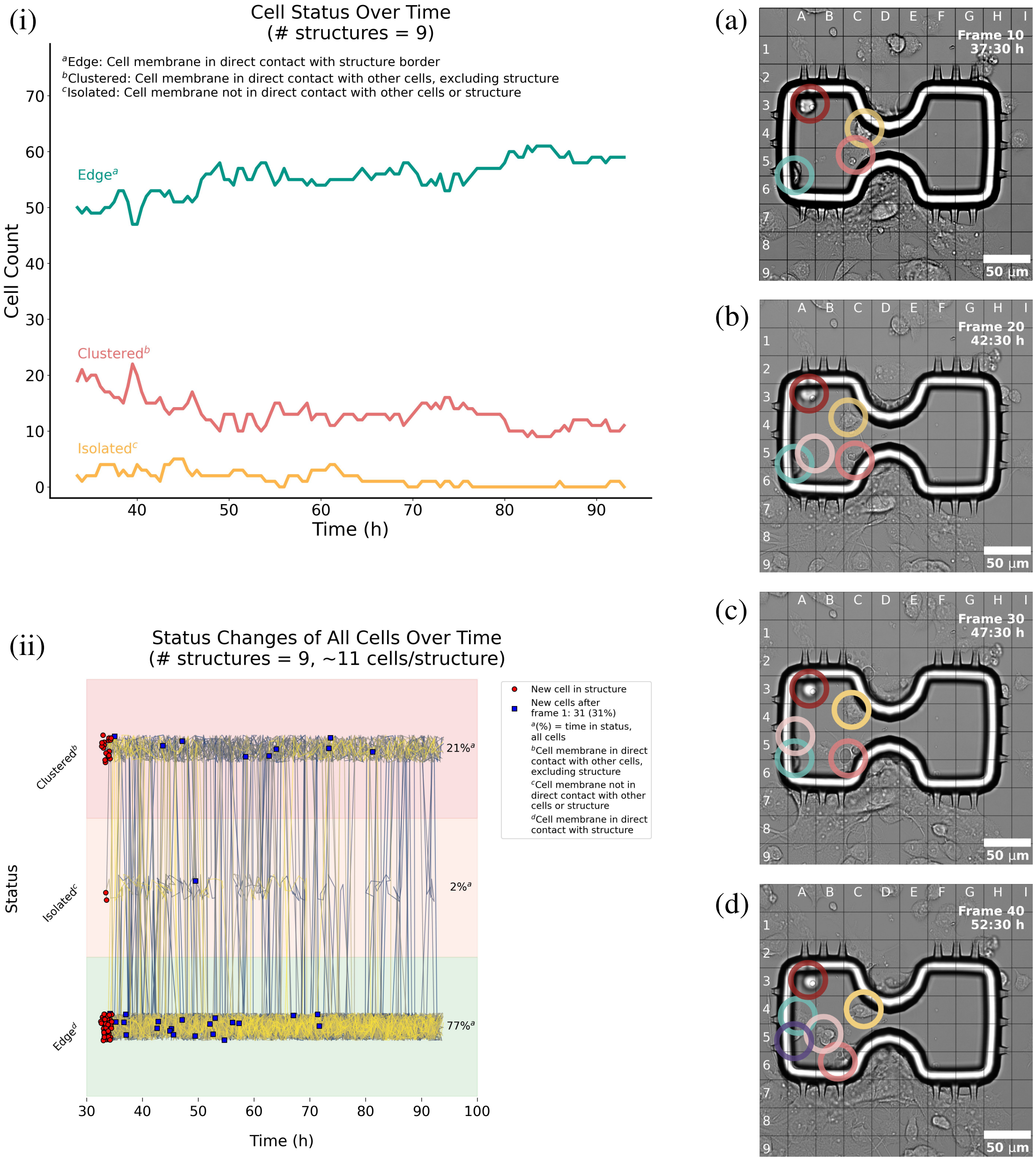

Figure 4.15.1: Count of total number of cells with each cell label (edge, isolated, clustered) over 60 h (t_0 = 33 h). Edge cells increase up to 60 while clustered cells and isolated cells decrease over the same duration (i). Time spent by cells with one of the three labels for 60 h, from t_0 = 33 h to 93 h (ii). Isolated cells remain the minority throughout the experiment, with less than 2% of total time spent in the isolated status; a greater number of cells spend time in the clustered status (21%); the edge label is the most prominent within the population, with the confined cell population spending 77% of total time in contact with the structure. (a)-(d) shows a single confinement structure at 10 frame intervals (1 frame = 30 min.) starting at frame 10; *a* shows 5 cells under confinement, and that all cells touch the edge (3a, 5a, 5a, 4c, 5c); *b* shows 5 cells under confinement (3a - edge, 5a - edge, 5a - other, 5c - edge, 4c - isolated); *c* shows 5 cells under confinement (3a - edge, 5a - edge, 6a - edge, 5c - edge, 4c - edge); *d* shows 7 cells under confinement (3a - edge, 4a - edge, 5a - edge, 5b - clustered (2 cells), 6b - edge, 4c - edge).

4.16 Discussion

By simultaneously examining how spatial relationships and physical constraints influence PC12 morphology and migration, potentially novel behaviors have been uncovered that could inform the design of in vitro neuronal tissue models and networks. Our characterization of PC12 cells reinforced their reliability as a neuronal model system, demonstrating they could be utilized in conditions designed to interrogate in vitro neuronal behavior. Laminin was used as the sole adhesion protein because it is an ECM component and its interaction with PC12 cells is well understood. The implementation of 3D-printed confinement microstructures enabled us to investigate PC12 behavior in a controlled microscale environment. The precise design and fabrication of these structures facilitated cell survival and growth comparable to traditional two-dimensional culture and highlighted the influence of physical constraints on PC12 differentiation, neurite extension, and migration. The experimental setup combined advanced 2PP 3D printing technology with the biocompatibility of PDMS and polymerized IP-Visio resin, proving to be robust and reliable. The classification system using three cell labels and three population types allowed for systematic analysis of how spatial arrangement and cell count affect PC12 behavior. Despite challenges in data acquisition due to increased PC12 density over time, consistent trends were observed, reinforcing the validity of conclusions.

Key findings revealed that confinement can enhance cell proliferation and neurite outgrowth, particularly for the sparse population type. The edge of the confinement structures emerged as a favorable site for cell adhesion, neurite extensions, and a preferred destination during migration, emphasizing the role played by the physical microenvironment. The interplay between cell-cell interactions and cell-structure contacts also influenced PC12 development. Cells given the edge label, in direct contact with the confinement structure, consistently exhibited enhanced neurite extension, suggesting that particular physical cues from the environment may stimulate neurite growth more effectively than cell-cell interactions alone. In contrast, confined cells that do not directly contact the structure or other cells have suppressed neurite lengths when compared to their unconfined counterparts.

While numerous studies have explored neuronal behavior in vitro, and have arrived at meaningful conclusions, migration and cellular interactions in the presence of controlled open environments appears to hold some potential for further exploration. This knowledge gap likely reflects both the rapid advancements in technology and the possible need for a range of investigations to bridge it. In particular, migration, neurite growth, and intercellular interactions within structured microenvironments are areas that warrant closer examination. The results demonstrated here at least partially provide conclusions that aim to fill this gap by rigorously analyzing neuronal behavior in a well characterized, well understood, and replicable in vitro environment.

Such approaches are also relevant in the context of regenerative medicine investigations that exploit synthetic environments to guide neural growth. As previously mentioned, Janzen et al. demonstrated that rat cortical neurons cultured in 3D matrices—with stiffness parameters designed to mimic brain tissue—exhibit increased viability, network maturation, and more extensive dendritic arborization compared to traditional 2D conditions[90]. Additionally, Buchmann et al. used 3D-printed structures for co-culturing mesencephalic neurons and astrocytes with improved spatial definition, mitigating certain drawbacks of purely 3D culture systems[47]. By applying the same types of confinement and analytical strategies described herein, similar investigations could be devised to examine how network formation, cellular interactions, and tissue-like organization unfold under engineered constraints. This emphasis on precise structural control and confinement thus complements existing findings in neural tissue engineering, with the potential to inform new strategies in regenerative medicine.

The results presented here underscore the importance of considering both biological and synthetic factors when interpreting neuronal behavior. The novel behaviors observed in PC12 cells under confinement could pave the way for studies aimed at optimizing in vitro neuronal models and developing effective strategies for guiding neuronal behavior. The outcomes presented, therefore, provide at least some insight into how to understand the impact of a number of environmental factors on neuronal behavior. By demonstrating the relative impact of a number of phenomena which occur in synthetic environments on neuronal behavior, the outcomes presented here could be relevant to investigations focused on neural tissue and regenerative medicine.

5 Conclusions and Outlook

The investigation presented above sought to determine how spatial relationships and physical constraints influence PC12 morphology and migration, revealing potentially novel behaviors that can inform the design of in vitro neuronal tissue models and networks. By employing PC12 cells within 3D-printed confinement microstructures, we demonstrated that confinement can enhance cell proliferation and neurite outgrowth, particularly for cells in the sparse population type. The edge of the confinement structures emerged as a feature of the microenvironment that favored cell adhesion, neurite extensions, and directed migration, highlighting the role of physical cues in neuronal development.

Findings presented herein underscore the interplay between cell-cell interactions and cell-structure contacts, with edge cells exhibiting enhanced neurite extension compared to confined cells not in contact with the structures. This suggests that specific structural cues from the cellular environment at the micrometer scale may stimulate neurite growth more effectively than cell-cell interactions alone. These observations contribute to filling the knowledge gap in understanding neuronal behavior in the presence of confined open spaces, a topic that has been infrequently investigated.

While the study provides valuable insights, it also opens avenues for further research. Future work could involve a detailed cell cycle analysis to understand the proliferation dynamics within confined environments. Exploring different microstructure shapes and sizes could reveal how geometric variations influence neuronal behavior. Implementing a Euclidean analysis (i.e. a nearest neighbor analysis) could offer a quantitative assessment of spatial relationships and migration patterns. Performing a nearest neighbor analysis might also shed light on the influence of cell proximity on neurite extension and network formation. Detaching and reattaching differentiated PC12 cells could provide insights into the plasticity and adaptability of neuronal networks under physical constraints. Future research could build on the findings presented here, potentially using our approach as a foundation to model neuronal networks and understand their responsiveness to physical confinement.

An understanding of the complex neural circuits formed within in vitro models could be enhanced by integrating advanced neuroimaging and connectomics approaches, such as those available through platforms like `https://flywire.ai/`. Such methods align with recent advancements in neurobiology and neurocomputation, where the intersection of neuroscience and computing has enabled strides in mimicking brain functions within artificial systems. This intersection presents the potential for biological neural networks to inform neuromorphic system development, which could, in turn, provide valuable insights into neuronal behavior in structured environments. Addressing challenges like the credit assignment problem in hierarchical networks, for instance, has led to innovative learning algorithms that reflect biological processes. One study involving pyramidal neurons introduced a novel learning rule, in which high-frequency bursts guided synaptic plasticity via top-down feedback, allowing for precise credit assignment across multiple synaptic layers—a feature echoed in machine learning advancements[91]. Integrating hardware innovations such as memristors, which emulate synaptic behavior, could further enhance brain-computer interfaces and neural prosthetics. Memristors have recently facilitated the connection between biological and artificial neurons, mimicking natural synaptic function through adjustable signal strengths based on neuron activity[92,93].

Electrostimulation of neurons represents another frontier in this line of research, with electrode material choices playing an important role in the efficacy of neural stimulation and recording. For instance, nanostructured IrOx-graphene electrodes, known for their high charge storage capacity, have demonstrated superior results in promoting mouse cortical neurite regeneration compared to platinum[94]. Similarly, ruthenium oxide (RuOx) electrodes offer significantly lower impedance and a higher signal-to-noise ratio than conventional materials, like indium tin oxide (ITO), enhancing the accuracy of neural recording in mouse cortical neurons[95]. Looking forward, the development of three-dimensional high-density microelectrode arrays (MEAs) with integrated optical stimulation and drug delivery capabilities holds promise for offering precise, localized control over neural networks within 3D cultures. Such systems can capture synaptic latencies in the range of 2 to 8 ms in iPSC-derived neurons, closely mirroring biological transmission times and providing realistic mappings of functional connectivity in 3D environments[96]. Together, these advancements highlight a path toward more sophisticated models that mirror biological systems and support deeper explorations of neuronal dynamics within controlled environments, building upon the foundational insights from in vitro models like those explored in this study.

Among the most important considerations when developing synthetic devices meant to stimulate neurons are biocompatibility, electrical characteristics of the material, and how the interaction impacts meaningful neuronal behaviors. While biocompatibility is typically widely considered, as discussed above, parameters like charge storage capacity and signal-to-noise ratio also warrant focus. Additionally, when attempting to gain insight into network connectivity and behavior upon stimulation, it is important to consider that network properties may change over time[96]. An in-depth understanding of neuronal tissue stimulation, neural repair, and neuronal network behavior should therefore rely both on the biological outcomes evidenced during these investigations and the electrical and material properties used to activate and study the network.

The outcomes of this research contribute to the fundamental understanding of neuronal behavior under physical constraints and have broader implications for regenerative medicine, neuroengineering, and neurocomputational modeling. Questions remain regarding the mechanisms by which cells sense and interpret physical cues—what do the cells feel that causes this behavior, when do they feel it, and how do they interpret it? Addressing these questions will require interdisciplinary approaches, combining biology, engineering, and computational sciences. The continued exploration of these themes at the basic research level at least promises to advance our ability to design sophisticated neural models and interfaces, enhancing our understanding of the nervous system and its application to technology and medicine.

List of Figures

List of Tables

References

(1) Ingber, D. E. Human Organs-on-Chips for Disease Modelling, Drug Development and Personalized Medicine. *Nat. Rev. Genet.* **2022**, *23*, 467–491.

(2) Tischler, A. S.; Greene, L. A. Nerve Growth Factor-Induced Process Formation by Cultured Rat Pheochromocytoma Cells. *Nature* **1975**, *258*, 341–342.

(3) Fujii, D. K.; Massoglia, S. L.; Savion, N.; Gospodarowicz, D. Neurite Outgrowth and Protein Synthesis by PC12 Cells as a Function of Substratum and Nerve Growth Factor. *J. Neurosci.* **1982**, *2*, 1157–1175.

(4) Westerink, R. H. S.; Ewing, A. G. The PC12 Cell as Model for Neurosecretion. *Acta Physiol.* **2008**, *192*, 273–285.

(5) Kandel, E. R., *Principles of Neural Science*, 5th ed; McGraw-Hill: New York, 2013.

(6) Bentivoglio, M.; Cotrufo, T.; Ferrari, S.; Tesoriero, C.; Mariotto, S.; Bertini, G.; Berzero, A.; Mazzarello, P. The Original Histological Slides of Camillo Golgi and His Discoveries on Neuronal Structure. *Front. Neuroanat.* **2019**, *13*.

(7) de Castro, F. Cajal and the Spanish Neurological School: Neuroscience Would Have Been a Different Story Without Them. *Front. Cell. Neurosci.* **2019**, *13*.

(8) Vaudry, D.; Stork, P. J. S.; Lazarovici, P.; Eiden, L. E. Signaling Pathways for PC12 Cell Differentiation: Making the Right Connections. *Science* **2002**, *296*, 1648–1649.

(9) Kimmelman, A. C.; Rodriguez, N. N.; Chan, A. M.-L. R-Ras3/M-Ras Induces Neuronal Differentiation of PC12 Cells through Cell-Type-Specific Activation of the Mitogen-Activated Protein Kinase Cascade. *Mol. Cell. Biol.* **2002**, *22*, 5946–5961.

(10) Sierra-Fonseca, J. A.; Najera, O.; Martinez-Jurado, J.; Walker, E. M.; Varela-Ramirez, A.; Khan, A. M.; Miranda, M.; Lamango, N. S.; Roychowdhury, S. Nerve Growth Factor Induces Neurite Outgrowth of PC12 Cells by Promoting Gβγ-microtubule Interaction. *BMC Neurosci.* **2014**, *15*, 132.

(11) Cabrera, J. R.; Lucas, J. J. MAP2 Splicing Is Altered in Huntington's Disease. *Brain Pathol.* **2017**, *27*, 181–189.

(12) Chua, P.; Lim, W. K. Optimisation of a PC12 Cell-Based in Vitro Stroke Model for Screening Neuroprotective Agents. *Sci. Rep.* **2021**, *11*, 8096.

(13) Howard, J.; Hyman, A. A. Growth, Fluctuation and Switching at Microtubule plus Ends. *Nat. Rev. Mol. Cell Biol.* **2009**, *10*, 569–574.

(14) Akhmanova, A.; Steinmetz, M. O. Tracking the Ends: A Dynamic Protein Network Controls the Fate of Microtubule Tips. *Nat. Rev. Mol. Cell Biol.* **2008**, *9*, 309–322.

(15) Flynn, K. C.; Hellal, F.; Neukirchen, D.; Jacob, S.; Tahirovic, S.; Dupraz, S.; Stern, S.; Garvalov, B. K.; Gurniak, C.; Shaw, A. E.; Meyn, L.; Wedlich-Söldner, R.; Bamburg, J. R.; Small, J. V.; Witke, W.; Bradke, F. ADF/Cofilin-Mediated Actin Retrograde Flow Directs Neurite Formation in the Developing Brain. *Neuron* **2012**, *76*, 1091–1107.

(16) Arimura, N.; Kaibuchi, K. Neuronal Polarity: From Extracellular Signals to Intracellular Mechanisms. *Nat. Rev. Neurosci.* **2007**, *8*, 194–205.

(17) Dotti, C.; Sullivan, C.; Banker, G. The Establishment of Polarity by Hippocampal Neurons in Culture. *J. Neurosci.* **1988**, *8*, 1454–1468.

(18) Attiah, D. G.; Kopher, R. A.; Desai, T. A. Characterization of PC12 Cell Proliferation and Differentiation-Stimulated by ECM Adhesion Proteins and Neurotrophic Factors. *J. Mater. Sci. Mater. Med.* **2003**, *14*, 1005–1009.

(19) Béduer, A.; Vieu, C.; Arnauduc, F.; Sol, J.-C.; Loubinoux, I.; Vaysse, L. Engineering of Adult Human Neural Stem Cells Differentiation through Surface Micropatterning. *Biomaterials* **2012**, *33*, 504–514.

(20) Song, M.; Uhrich, K. E. Optimal Micropattern Dimensions Enhance Neurite Outgrowth Rates, Lengths, and Orientations. *Ann. Biomed. Eng.* **2007**, *35*, 1812–1820.

(21) Xu, T.; Molnar, P.; Gregory, C.; Das, M.; Boland, T.; Hickman, J. J. Electrophysiological Characterization of Embryonic Hippocampal Neurons Cultured in a 3D Collagen Hydrogel. *Biomaterials* **2009**, *30*, 4377–4383.

(22) Johansson, F.; Carlberg, P.; Danielsen, N.; Montelius, L.; Kanje, M. Axonal Outgrowth on Nano-Imprinted Patterns. *Biomaterials* **2006**, *27*, 1251–1258.

(23) Yu, M.; Huang, Y.; Ballweg, J.; Shin, H.; Huang, M.; Savage, D. E.; Lagally, M. G.; Dent, E. W.; Blick, R. H.; Williams, J. C. Semiconductor Nanomembrane Tubes: Three-Dimensional Confinement for Controlled Neurite Outgrowth. *ACS Nano* **2011**, *5*, 2447–2457.

(24) Young, T.-H.; Huang, J.-H.; Hung, S.-H.; Hsu, J.-P. The Role of Cell Density in the Survival of Cultured Cerebellar Granule Neurons. *J. Biomed. Mater. Res.* **2000**, *52*, 748–753.

(25) Badoyannis, H. C.; Sharma, S. C.; Sabban, E. L. The Differential Effects of Cell Density and NGF on the Expression of Tyrosine Hydroxylase and Dopamine β-Hydroxylase in PC12 Cells. *Mol. Brain Res.* **1991**, *11*, 79–87.

(26) Parnas, D.; Linial, M. Acceleration of Neuronal Maturation of P19 Cells by Increasing Culture Density. *Dev. Brain Res.* **1997**, *101*, 115–124.

(27) Ivenshitz, M.; Segal, M. Neuronal Density Determines Network Connectivity and Spontaneous Activity in Cultured Hippocampus. *J. Neurophysiol.* **2010**, *104*, 1052–1060.

(28) Agrawal, L.; Saidani, M.; Guillaud, L.; Terenzio, M. Development of 3D Culture Scaffolds for Directional Neuronal Growth Using 2-Photon Lithography. *Mater. Sci. Eng. C* **2021**, *131*, 112502.

(29) Francisco, H.; Yellen, B. B.; Halverson, D. S.; Friedman, G.; Gallo, G. Regulation of Axon Guidance and Extension by Three-Dimensional Constraints. *Biomaterials* **2007**, *28*, 3398–3407.

(30) Marino, A.; Ciofani, G.; Filippeschi, C.; Pellegrino, M.; Pellegrini, M.; Orsini, P.; Pasqualetti, M.; Mattoli, V.; Mazzolai, B. Two-Photon Polymerization of Sub-micrometric Patterned Surfaces: Investigation of Cell-Substrate Interactions and Improved Differentiation of Neuron-like Cells. *ACS Appl. Mater. & Interfaces* **2013**, *5*, 13012–13021.

(31) Thomsen, M. S.; Routhe, L. J.; Moos, T. The Vascular Basement Membrane in the Healthy and Pathological Brain. *J. Cereb. Blood Flow & Metab.* **2017**, *37*, 3300–3317.

(32) Koh, H. S.; Yong, T.; Chan, C. K.; Ramakrishna, S. Enhancement of Neurite Outgrowth Using Nano-Structured Scaffolds Coupled with Laminin. *Biomaterials* **2008**, *29*, 3574–3582.

(33) Hardelauf, H.; Waide, S.; Sisnaiske, J.; Jacob, P.; Hausherr, V.; Schöbel, N.; Janasek, D.; van Thriel, C.; West, J. Micropatterning Neuronal Networks. *Analyst* **2014**, *139*, 3256–3264.

(34) Rossino, P.; Gavazzi, I.; Timpl, R.; Aumailley, M.; Abbadini, M.; Giancotti, F.; Silengo, L.; Marchisio, P. C.; Tarone, G. Nerve Growth Factor Induces Increased Expression of a Laminin-Binding Integrin in Rat Pheochromocytoma PC12 Cells. *Exp. Cell Res.* **1990**, *189*, 100–108.

(35) Tomaselli, K. J.; Hall, D. E.; Flier, A.; Cehlsen, K. R.; Turner, D. C.; Carbonettqll, S.; Reichardt, F. A Neuronal Cell Line (PC12) Expresses Two Beta 1-Class Integrins—Alpha 1 Beta 1 and Alpha 3 Beta 1—That Recognize Different Neurite Outgrowth-Promoting Domains in Laminin. *Neuron* **1990**, *5*, 651–662.

(36) Sonnenberg, A.; Linders, C. J.; Modderman, P. W.; Damsky, C. H.; Aumailley, M.; Timpl, R. Integrin Recognition of Different Cell-binding Fragments of Laminin (P1, E3, E8) and Evidence That Alpha 6 Beta 1 but Not Alpha 6 Beta 4 Functions as a Major Receptor for Fragment E8. *J. Cell Biol.* **1990**, *110*, 2145–2155.

(37) Tashiro, K.; Monji, A.; Yoshida, I.; Hayashi, Y.; Matsuda, K.; Tashiro, N.; Mitsuyama, Y. An IKLLI-containing Peptide Derived from the Laminin α 1 Chain Mediating Heparin-binding, Cell Adhesion, Neurite Outgrowth, and Proliferation Represents a Binding Site for Integrin Alpha3beta1 and Heparan Sulphate Proteoglycan. *Biochem. J.* **1999**, *340*, 119–126.

(38) Ichikawa, N.; Iwabuchi, K.; Kurihara, H.; Ishii, K.; Kobayashi, T.; Sasaki, T.; Hattori, N.; Mizuno, Y.; Hozumi, K.; Yamada, Y.; Arikawa-Hirasawa, E. Binding of Laminin-1 to Monosialoganglioside GM1 in Lipid Rafts Is Crucial for Neurite Outgrowth. *J. Cell Sci.* **2009**, *122*, 289–299.

(39) Hanics, J.; Szodorai, E.; Tortoriello, G.; Malenczyk, K.; Keimpema, E.; Lubec, G.; Hevesi, Z.; Lutz, M. I.; Kozsurek, M.; Puskár, Z.; Tóth, Z. E.; Wagner, L.; Kovács, G. G.; Hökfelt, T. G. M.; Harkany, T.; Alpár, A. Secretagogin-Dependent Matrix Metalloprotease-2 Release from Neurons Regulates Neuroblast Migration. *Proc. Natl. Acad. Sci.* **2017**, *114*, E2006–E2015.

(40) Baldwin, S. P.; Krewson, C. E.; Saltzman, W. M. PC12 Cell Aggregation and Neurite Growth in Gels of Collagen, Laminin and Fibronectin. *Int. J. Dev. Neurosci.* **1996**, *14*, 351–364.

(41) Xiao, M.; Ulloa Severino, F. P.; Iseppon, F.; Cheng, G.; Torre, V.; Tang, M. 3D Free-Standing Ordered Graphene Network Geometrically Regulates Neuronal Growth and Network Formation. *Nano Lett.* **2020**, *20*, 7043–7051.

(42) Micholt, L.; Gärtner, A.; Prodanov, D.; Braeken, D.; Dotti, C. G.; Bartic, C. Substrate Topography Determines Neuronal Polarization and Growth In Vitro. *PLoS ONE* **2013**, *8*, e66170.

(43) Yao, L.; Wang, S.; Cui, W.; Sherlock, R.; O'Connell, C.; Damodaran, G.; Gorman, A.; Windebank, A.; Pandit, A. Effect of Functionalized Micropatterned PLGA on Guided Neurite Growth. *Acta Biomater.* **2009**, *5*, 580–588.

(44) Tonazzini, I.; Meucci, S.; Faraci, P.; Beltram, F.; Cecchini, M. Neuronal Differentiation on Anisotropic Substrates and the Influence of Nanotopographical Noise on Neurite Contact Guidance. *Biomaterials* **2013**, *34*, 6027–6036.

(45) Xie, J.; Liu, W.; MacEwan, M. R.; Bridgman, P. C.; Xia, Y. Neurite Outgrowth on Electrospun Nanofibers with Uniaxial Alignment: The Effects of Fiber Density, Surface Coating, and Supporting Substrate. *ACS Nano* **2014**, *8*, 1878–1885.

(46) Chen, J.; Huang, D.; Wang, L.; Hou, J.; Zhang, H.; Li, Y.; Zhong, S.; Wang, Y.; Wu, Y.; Huang, W. 3D Bioprinted Multiscale Composite Scaffolds Based on Gelatin Methacryloyl (GelMA)/Chitosan Microspheres as a Modular Bioink for Enhancing 3D Neurite Outgrowth and Elongation. *J. Colloid Interface Sci.* **2020**, *574*, 162–173.

(47) Buchmann, S.; Enrico, A.; Holzreuter, M. A.; Reid, M.; Zeglio, E.; Niklaus, F.; Stemme, G.; Herland, A. Probabilistic Cell Seeding and Non-Autofluorescent 3D-printed Structures as Scalable Approach for Multi-Level Co-Culture Modeling. *Mater. Today Bio* **2023**, *21*, 100706.

(48) Turunen, S.; Käpylä, E.; Lähteenmäki, M.; Ylä-Outinen, L.; Narkilahti, S.; Kellomäki, M. Direct Laser Writing of Microstructures for the Growth Guidance of Human Pluripotent Stem Cell Derived Neuronal Cells. *Opt. Lasers Eng.* **2014**, *55*, 197–204.

(49) Raimondi, M. T.; Eaton, S. M.; Nava, M. M.; Laganà, M.; Cerullo, G.; Osellame, R. Two-Photon Laser Polymerization: From Fundamentals to Biomedical Application in Tissue Engineering and Regenerative Medicine. *J. Appl. Biomater. & Funct. Mater.* **2012**, *10*, 56–66.

(50) Spratte, T. Tailoring Actuation Properties of Thermoresponsive Hydrogels and Implementation into Soft Robotic Applications. Ph.D. Thesis, Ruprecht-Karls-Universität Heidelberg, Heidelberg, Germany, 2023.

(51) LaFratta, C. N.; Fourkas, J. T.; Baldacchini, T.; Farrer, R. A. Multiphoton Fabrication. *Angew. Chem. Int. Ed.* **2007**, *46*, 6238–6258.

(52) Koroleva, A.; Deiwick, A.; El-Tamer, A.; Koch, L.; Shi, Y.; Estévez-Priego, E.; Ludl, A.-A.; Soriano, J.; Guseva, D.; Ponimaskin, E.; Chichkov, B. In Vitro Development of Human iPSC-Derived Functional Neuronal Networks on Laser-Fabricated 3D Scaffolds. *ACS Appl. Mater. & Interfaces* **2021**, *13*, 7839–7853.

(53) Kajtez, J.; Wesseler, M. F.; Birtele, M.; Khorasgani, F. R.; Rylander Ottosson, D.; Heiskanen, A.; Kamperman, T.; Leijten, J.; Martínez-Serrano, A.; Larsen, N. B.; Angelini, T. E.; Parmar, M.; Lind, J. U.; Emnéus, J. Embedded 3D Printing in Self-Healing Annealable Composites for Precise Patterning of Functionally Mature Human Neural Constructs. *Adv. Sci.* **2022**, *9*, 2201392.

(54) Li, J.; Reimers, A.; Dang, K. M.; Brunk, M. G. K.; Drewes, J.; Hirsch, U. M.; Willems, C.; Schmelzer, C. E. H.; Groth, T.; Nia, A. S.; Feng, X.; Adelung, R.; Sacher, W. D.; Schütt, F.; Poon, J. K. S. 3D Printed Neural Tissues with *in Situ* Optical Dopamine Sensors. *Biosens. Bioelectron.* **2023**, *222*, 114942.

(55) Fendler, C.; Harberts, J.; Rafeldt, L.; Loers, G.; Zierold, R.; Blick, R. H. Neurite Guidance and Neuro-Caging on Steps and Grooves in 2.5 Dimensions. *Nanoscale Adv.* **2020**, *2*, 5192–5200.

(56) Maruyama, H.; Fujiwara, K.; Kumeta, M.; Koyama, D. Ultrasonic Control of Neurite Outgrowth Direction. *Sci. Rep.* **2021**, *11*, 20099.

(57) Omidinia-Anarkoli, A.; Ephraim, J. W.; Rimal, R.; De Laporte, L. Hierarchical Fibrous Guiding Cues at Different Scales Influence Linear Neurite Extension. *Acta Biomater.* **2020**, *113*, 350–359.

(58) Yamamoto, H.; Moriya, S.; Ide, K.; Hayakawa, T.; Akima, H.; Sato, S.; Kubota, S.; Tanii, T.; Niwano, M.; Teller, S.; Soriano, J.; Hirano-Iwata, A. Impact of Modular Organization on Dynamical Richness in Cortical Networks. *Sci. Adv.* **2018**, *4*, eaau4914.

(59) Shirai, S.; Acharya, S. K.; Bose, S. K.; Mallinson, J. B.; Galli, E.; Pike, M. D.; Arnold, M. D.; Brown, S. A. Long-Range Temporal Correlations in Scale-Free Neuromorphic Networks. *Netw. Neurosci.* **2020**, *4*, 432–447.

(60) Sato, Y.; Yamamoto, H.; Kato, H.; Tanii, T.; Sato, S.; Hirano-Iwata, A. Microfluidic Cell Engineering on High-Density Microelectrode Arrays for Assessing Structure-Function Relationships in Living Neuronal Networks. *Front. Neurosci.* **2023**, *16*.

(61) Moon, H. C.; Choi, H.; Kikionis, S.; Seo, J.; Youn, W.; Ioannou, E.; Han, S. Y.; Cho, H.; Roussis, V.; Choi, I. S. Fabrication and Characterization of Neurocompatible Ulvan-Based Layer-by-Layer Films. *Langmuir* **2020**, *36*, 11610–11617.

(62) Kim, M.-H.; Park, J. H.; Joo, S.; Hong, D.; Park, M.; Choi, J. Y.; Moon, H. W.; Kim, Y.-G.; Kang, K.; Choi, I. S. Accelerated Development of Hippocampal Neurons and Limited Adhesion of Astrocytes on Negatively Charged Surfaces. *Langmuir* **2018**, *34*, 1767–1774.

(63) Yang, J.; Du, M.; Wang, L.; Li, S.; Wang, G.; Yang, X.; Zhang, L.; Fang, Y.; Zheng, W.; Yang, G.; Jiang, X. Bacterial Cellulose as a Supersoft Neural Interfacing Substrate. *ACS Appl. Mater. & Interfaces* **2018**, *10*, 33049–33059.

(64) Yang, M.; Chen, P.; Qu, X.; Zhang, F.; Ning, S.; Ma, L.; Yang, K.; Su, Y.; Zang, J.; Jiang, W.; Yu, T.; Dong, X.; Luo, Z. Robust Neural Interfaces with Photopatternable, Bioadhesive, and Highly Conductive Hydrogels for Stable Chronic Neuromodulation. *ACS Nano* **2023**, *17*, 885–895.

(65) Kleber, C.; Bruns, M.; Lienkamp, K.; Rühe, J.; Asplund, M. An Interpenetrating, Microstructurable and Covalently Attached Conducting Polymer Hydrogel for Neural Interfaces. *Acta Biomater.* **2017**, *58*, 365–375.

(66) Patil, A. C.; Bandla, A.; Liu, Y.-H.; Luo, B.; Thakor, N. V. Nontransient Silk Sandwich for Soft, Conformal Bionic Links. *Mater. Today* **2020**, *32*, 68–83.

(67) Aranda-Abreu, G. E.; Behar, L.; Chung, S.; Furneaux, H.; Ginzburg, I. Embryonic Lethal Abnormal Vision-Like RNA-Binding Proteins Regulate Neurite Outgrowth and Tau Expression in PC12 Cells. *J. Neurosci.* **1999**, *19*, 6907–6917.

(68) Fischer, I.; Richter-Landsberg, C.; Safaei, R. Regulation of Microtubule Associated Protein 2 (MAP2) Expression by Nerve Growth Factor in PC12 Cells. *Exp. Cell Res.* **1991**, *194*, 195–201.

(69) Greene, L. A.; Tischler, A. S. Establishment of a Noradrenergic Clonal Line of Rat Adrenal Pheochromocytoma Cells Which Respond to Nerve Growth Factor. *Proc. Natl. Acad. Sci. USA* **1976**, *73*, 2424–2428.

(70) Jeon, C.-Y.; Jin, J.-K.; Koh, Y.-H.; Chun, W.; Choi, I.-G.; Kown, H.-J.; Kim, Y.-S.; Park, J.-B. Neurites from PC12 Cells Are Connected to Each Other by Synapse-like Structures. *Synapse* **2010**, *64*, 765–772.

(71) Kanai, Y.; Hirokawa, N. Sorting Mechanisms of Tau and MAP2 in Neurons: Suppressed Axonal Transit of MAP2 and Locally Regulated Microtubule Binding. *Neuron* **1995**, *14*, 421–432.

(72) Dehmelt, L.; Halpain, S. The MAP2/Tau Family of Microtubule-Associated Proteins. *Genome Biol.* **2004**, *6*, 204.

(73) Akeson, R.; Warren, S. L. PC12 Adhesion and Neurite Formation on Selected Substrates Are Inhibited by Some Glycosaminoglycans and a Fibronectin-Derived Tetrapeptide. *Exp. Cell Res.* **1986**, *162*, 347–362.

(74) Das, K. P.; Freudenrich, T. M.; Mundy, W. R. Assessment of PC12 Cell Differentiation and Neurite Growth: A Comparison of Morphological and Neurochemical Measures. *Neurotoxicol. Teratol.* **2004**, *26*, 397–406.

(75) Brückner, D. B.; Fink, A.; Schreiber, C.; Röttgermann, P. J. F.; Rädler, J. O.; Broedersz, C. P. Stochastic Nonlinear Dynamics of Confined Cell Migration in Two-State Systems. *Nat. Phys.* **2019**, *15*, 595–601.

(76) *NanoGuide*, https://support.nanoscribe.com/hc/en-gb/articles/360011709499-IP-Visio, (accessed 01/27/2025).

(77) Schmid, M.; Ludescher, D.; Giessen, H. Optical Properties of Photoresists for Femtosecond 3D Printing: Refractive Index, Extinction, Luminescence-Dose Dependence, Aging, Heat Treatment and Comparison between 1-Photon and 2-Photon Exposure. *Opt. Mater. Express* **2019**, *9*, 4564–4577.

(78) Minnick, G.; Safa, B. T.; Rosenbohm, J.; Lavrik, N. V.; Brooks, J.; Esfahani, A. M.; Samaniego, A.; Meng, F.; Richter, B.; Gao, W.; Yang, R. Two-Photon Polymerized Shape Memory Microfibers: A New Mechanical Characterization Method in Liquid. *Adv. Funct. Mater.* **2023**, *33*, 2206739.

(79) Foley, J. D.; Grunwald, E. W.; Nealey, P. F.; Murphy, C. J. Cooperative Modulation of Neuritogenesis by PC12 Cells by Topography and Nerve Growth Factor. *Biomaterials* **2005**, *26*, 3639–3644.

(80) Namba, T.; Funahashi, Y.; Nakamuta, S.; Xu, C.; Takano, T.; Kaibuchi, K. Extracellular and Intracellular Signaling for Neuronal Polarity. *Physiol. Rev.* **2015**, *95*, 995–1024.

(81) Qiu, Y.; Wang, X.; Yu, H.; Zhang, Y.; Zheng, J.; Wang, J.; Gan, Q.; Liu, L.; Li, W. J. Engineering 3D Microenvironments with Femtosecond Laser-Fabricated Microtubes to Direct Neuronal Network Formation. *Addit. Manuf.* **2024**, *88*, 104249.

(82) McDonald, J. C.; Whitesides, G. M. Poly(Dimethylsiloxane) as a Material for Fabricating Microfluidic Devices. *Accounts Chem. Res.* **2002**, *35*, 491–499.

(83) Xu, K.; Liu, X.; Li, X.; Yin, J.; Wei, P.; Qian, J.; Sun, J. Effect of Electrical and Electromechanical Stimulation on PC12 Cell Proliferation and Axon Outgrowth. *Front. Bioeng. Biotechnol.* **2021**, *9*, DOI: `10.3389/fbioe.2021.757906`.

(84) Biffi, E.; Regalia, G.; Menegon, A.; Ferrigno, G.; Pedrocchi, A. The Influence of Neuronal Density and Maturation on Network Activity of Hippocampal Cell Cultures: A Methodological Study. *PLOS ONE* **2013**, *8*, e83899.

(85) Arshadi, C.; Günther, U.; Eddison, M.; Harrington, K. I. S.; Ferreira, T. A. SNT: A Unifying Toolbox for Quantification of Neuronal Anatomy. *Nat. Methods* **2021**, *18*, 374–377.

(86) Krewson, C. E.; Chung, S. W.; Dai, W.; Mark Saltzman, W. Cell Aggregation and Neurite Growth in Gels of Extracellular Matrix Molecules. *Biotechnol. Bioeng.* **1994**, *43*, 555–562.

(87) Teixeira, A. I.; Ilkhanizadeh, S.; Wigenius, J. A.; Duckworth, J. K.; Inganäs, O.; Hermanson, O. The Promotion of Neuronal Maturation on Soft Substrates. *Biomaterials* **2009**, *30*, 4567–4572.

(88) Drubin, D. G.; Feinstein, S. C.; Shooter, E. M.; Kirschner, M. W. Nerve Growth Factor-Induced Neurite Outgrowth in PC12 Cells Involves the Coordinate Induction of Microtubule Assembly and Assembly-Promoting Factors. *J. Cell Biol.* **1985**, *101*, 1799–1807.

(89) Gunay, G.; Sever, M.; Tekinay, A. B.; Guler, M. O. Three-Dimensional Laminin Mimetic Peptide Nanofiber Gels for In Vitro Neural Differentiation. *Biotechnol. J.* **2017**, *12*, 1700080.

(90) Janzen, D.; Bakirci, E.; Wieland, A.; Martin, C.; Dalton, P. D.; Villmann, C. Cortical Neurons Form a Functional Neuronal Network in a 3D Printed Reinforced Matrix. *Adv. Healthc. Mater.* **2020**, *9*, 1901630.

(91) Payeur, A.; Guerguiev, J.; Zenke, F.; Richards, B. A.; Naud, R. Burst-Dependent Synaptic Plasticity Can Coordinate Learning in Hierarchical Circuits. *Nat. Neurosci.* **2021**, *24*, 1010–1019.

(92) Tian, C.; Wei, L.; Li, Y.; Jiang, J. Recent Progress on Two-Dimensional Neuromorphic Devices and Artificial Neural Network. *Curr. Appl. Phys.* **2021**, *31*, 182–198.

(93) Serb, A.; Corna, A.; George, R.; Khiat, A.; Rocchi, F.; Reato, M.; Maschietto, M.; Mayr, C.; Indiveri, G.; Vassanelli, S.; Prodromakis, T. Memristive Synapses Connect Brain and Silicon Spiking Neurons. *Sci. Rep.* **2020**, *10*, 2590.

(94) Lichtenstein, M. P.; Pérez, E.; Ballesteros, L.; Suñol, C.; Casañ-Pastor, N. Short-Term Electrostimulation Enhancing Neural Repair *in Vitro* Using Large Charge Capacity Nanostructured Electrodes. *Appl. Mater. Today* **2017**, *6*, 29–43.

(95) Atmaramani, R.; Chakraborty, B.; Rihani, R. T.; Usoro, J.; Hammack, A.; Abbott, J.; Nnoromele, P.; Black, B. J.; Pancrazio, J. J.; Cogan, S. F. Ruthenium Oxide Based Microelectrode Arrays for *in Vitro* and *in Vivo* Neural Recording and Stimulation. *Acta Biomater.* **2020**, *101*, 565–574.

(96) Shin, H.; Jeong, S.; Lee, J.-H.; Sun, W.; Choi, N.; Cho, I.-J. 3D High-Density Microelectrode Array with Optical Stimulation and Drug Delivery for Investigating Neural Circuit Dynamics. *Nat. Commun.* **2021**, *12*, 492.

(97) Wiatrak, B.; Kubis-Kubiak, A.; Piwowar, A.; Barg, E. PC12 Cell Line: Cell Types, Coating of Culture Vessels, Differentiation and Other Culture Conditions. *Cells* **2020**, *9*, 958.

(98) Koizumi, S.; Bootman, M. D.; Bobanović, L. K.; Schell, M. J.; Berridge, M. J.; Lipp, P. Characterization of Elementary Ca2+ Release Signals in NGF-Differentiated PC12 Cells and Hippocampal Neurons. *Neuron* **1999**, *22*, 125–137.

(99) Kosik, S.; Finch, A. MAP2 and Tau Segregate into Dendritic and Axonal Domains After the Elaboration of Morphologically Distinct Neurites: An Lmmunocytochemical Study of Cultured Rat Cerebrum. *J. Neurosci.* **1987**, *7*, 3142–3153.

(100) Gauci, S. C.; Gernhardt, M.; Frisch, H.; Houck, H. A.; Blinco, J. P.; Blasco, E.; Tuten, B. T.; Barner-Kowollik, C. 3D Printed Microstructures Erasable by Darkness. *Adv. Funct. Mater.* **2022**, 2206303.

(101) Choi, G.; Cha, H. J. Recent Advances in the Development of Nature-Derived Photocrosslinkable Biomaterials for 3D Printing in Tissue Engineering. *Biomater. Res.* **2019**, *23*, 18.

Acknowledgments

"It [friendship] helps the young, too, to keep from error; it aids older people by ministering to their needs and supplementing the activities that are failing from weakness; those in the prime of life it stimulates to noble actions – "two going together" – for with friends men are more able both to think and act."

– Aristotle, Nichomachean Ethics, Book VIII, 1, Friendship

This experience has been incredible. There were, no doubt, ups and downs, moments of confusion and frustration. This, unfortunately, is usually one of the best sources of learning and development. But, there were also moments of pure fascination and excited surprise; the downs were the investment, the ups paid a dividend. My journey is more complete and more rewarding because of those who support me and those who have sometimes even carried me through the difficult episodes and chapters of life's story.

First, I am grateful to my parents, Rosemary and Stephen, who have seen the many highs and lows on my journey and provided me with gifts and guidance; they are reliable through and through, and certainly taught me persistence and effort. This outcome is also not possible with Matthew Storey, a dear friend and excellent mentor who helped me write my story; he is directly responsible for turning a confused, ambitious man into a focused and satisfied one.

My principal investigator, *meine Doktormutter*, Prof. Dr. Christine Selhuber-Unkel, gets a special thanks. Her efforts, guidance, questions, time, and curiosities helped me at the beginning, middle, and end of this PhD. Few people I've met juggle numerous, expanding, and sometimes disconnected responsibilities with unyielding effort, kindness, and professionalism the way she does.

The colleagues I've met since my arrival here have been essential to any success I can claim. They are the necessary ingredient in a recipe that produced lively scientific discussions, resolved my many confusions, and provided invaluable technical guidance exactly when I needed it. The distance covered by a single step on this journey is multiplied because of their thoughtful input, healthy skepticism, and supportive feedback.

Many from the different chapters of my life deserve my thanks. Here is a list of names, in no particular order, and a bit describing my specific gratitude. Some names may not be so familiar to every reader, but every one is essential to this outcome in some way.

(soon to be Dr.) Malin Schmidt	Thanks for being helpful, precise, organized and having an outstanding work attitude
Dr. Fereydoon Taheri	Thanks for being humble, insightful, intellectual and guiding my work in an innovative direction
(soon to be Dr.) Yasmin Antonelli	No doubt, much of my biology is better because you kindly answered even my most basic questions
Dr. Christine Arndt	Thanks for your supervisions during my master's thesis, it helped me also learn about the group
Dr. Didem Aycan	Thanks for being friendly and sharing your experience with me (and for the turkish coffee)
(soon to be Dr.) Chantal Barwig	Thanks for being so friendly and for sharing your technical knowledge
Dr. Federico Colombo	Thanks for your technical support, and answering my many questions about biology and cell culture
Dr. Nathalie Couturier	Thanks for your technical support, and answering my many questions about understanding and culturing neurons
(soon to be Dr.) Gaurav Dave	Thanks Gaurav for your 3D printing knowledge and friendliness
(soon to be Dr.) Angeles De la Cruz	I'm so grateful for our conversations, and your persistence is really inspiring
(soon to be Dr.) Miguel Estrada	Thanks for being so friendly, and having a good sense of humor
Kevin Fitzpatrick	May you rest in eternal peace, you'll always be remembered for helping me when I needed it most
Tanisha Gebert	Thanks for always being helpful and friendly, I'm glad for your guidance and support
(soon to be Dr.) Sophie Geiger	I'm so impressed by your knowledge and skill, thanks for always being friendly and supportive
(soon to be Dr.) Mona Haemmerle	Thanks for being supportive of - and complimenting - my work
Dr. John Hines	May you rest in eternal peace, I am grateful for our sincere discussions about science, getting a PhD, and biology
Dr. Sarah Hoerner	I am grateful for your patience and guidance as I began to learn about working with neurons
(soon to be Dr.) Kathi Kaiser	Thanks for being a great office mate and having a good sense of humor
Dr. Trevor Kalkus	I'm grateful for your help through the PhD, I'm so glad you joined the group
(soon to be Dr.) Mishal Khan	Thanks for helping me through the thesis writing especially and for being a great office mate
Trudy Lampert	Your timely guidance and assistance was crucial to my future success (and improving my writing)
Dr. Aldo Leal-Egana	Thanks for your wisdom, help, and inspiring presentations
Frau Steffi Maerksch	Thanks Steffi for your help through the entire process, and your many kindnesses
Dr. Mehran Mehrabanian	I'm grateful for your advice and for keeping these labs running
(*very* soon to be Dr.) Ankit Mishra	Thanks for your sense of humor and for sharing your knowledge since the beginning
Dr. Sadaf Pashapour	Thanks for your support through my many scientific struggles
Dr. Sunil Rajput	Thanks Sunny for your advice and support early on in this process
(soon to be Dr.) Krishna Ramesh	I'm grateful for our scientific talks, and your friendly personality
Dr. Maria Regato Herbella	Thanks for your friendly support during the writing process
Beni Scherke	Thanks for being so friendly and supportive, and keeping my work moving in the right direction
Dr. Barbara Schamberger	I'm grateful for your advice and guidance - I'm a better biologist because of your help
Florine Sessler	I'm grateful you shared your talents - my work looks a lot better because of your kindness
(soon to be Dr.) Annabelle Sonn	Thanks for being so friendly and helpful, keeping the labs organized and professional
Prof. Dr. Joachim Spatz	Thank you for guiding the outstanding PhD program, Matter to Life
Dr. Tobias Spratte	Thanks for your great conversations and helpful hand through my master's thesis and the early part of my PhD
Dr. Mohammedreza Taale	Your support, insight and perspective continue to help me make good scientific decisions
(soon to be Dr.) Zeynab Tavasolyzadeh	Thanks for being friendly and a great colleague
Tamara Unterreiner	Thanks for your diligence and patience with silanization. This was a critical part of obtaining reliable experimental results.
Dr. Maria Villiou	Thanks for sharing your knowledge and experiences, this helped me grow a lot
Dr. Zhe Wang	Thanks for sharing your deep experience and always asking good questions
Sebastian Weber	Thanks for your SEM skills, and for keeping the biolab running!

Appendix

A Materials and Methods

A.1 Cell Culture

A.1.1 Cell Passaging

As taken from[97]. 45 ml of growth medium is prepared by mixing 38.25 ml of RPMI 1640 Medium (Thermo, A1049101), 4500 μml of Horse Serum (Sigma-Aldrich, H1138-100ML or H1270-100ML), and 2250 μl of Fetal Bovine Serum (FBS Premium, South American origin, Pan Biotech, P30-3302). This mixture is sterile filtered using a 0.22 um filter (Merck, SLGV033RS), then warmed at 37°C for 30 minutes.

PC12 cells (Sigma-Aldrich, 88022401-1VL) are centrifuged at 180g for 12 minutes at room temperature. Cells are then resuspended in 5 ml of the pre-warmed growth medium and cell clusters are broken up by aspirating the solution 4-5 times using a syringe with a 22g needle tip. The desired amount of cells and the remainder of the pre-warmed media is then applied to a new culture flask, and placed in an incubator (37°C, 5% CO_2) with the flask standing upright.

A.1.2 Cell Differentiation

As guided by[68,97,98]. Differentiation medium is prepared as follows: RPMI 1640 Medium (Thermo, A104901), donor horse serum (Sigma-Aldrich, H1138-100ML) to a 1% concentration, L-glutamine (Glutamax Supplement, Thermo, #35050061) to a 2 mM concentration, gentamicin (Thermo, # 15710064) to a 25 µg/mLlconcentration, amphotericin B (Thermo, # 15290018) to a 2.5 µg/ml concentration and recombinant β-NGF of human origin (Sigma-Aldrich, cat. no. SRP3015) to a 100 ng/ml concentration. The differentiation medium is sterilized using a 0.22 µm filter then warmed at 37°C for 30 minutes. Cells are resuspended in differentiation medium then applied to a pre-treated surface for experimentation.

A.2 Cell Characterization, Immunostaining

As guided by[67,68,99]. PC12 cells (Sigma-Aldrich, 88022401-1VL) are cultured in differentiation medium, as described previously (Sec. A.1.2). 1/2 the medium is changed every 48 h for 12 days. On day 12, cells were fixed using 4% paraformaldehyde (PFA, Thermo, A11313.22, made into a 4% w/v solution in PBS) for 10 minutes, followed by washing with PBS and then with 0.1% Tween 20 (Sigma-Aldrich, P7949-500ml) in PBS ("PBST") three times for 5 minutes each. Cell membranes were permeabilized using 0.1% Triton X-100 (Sigma-Aldrich, T9284-500ml) in PBS for 10 minutes at room temperature. Blocking was performed using 1% BSA (Sigma-Aldrich, A7906-50G) in PBST (0.08g BSA in 8 ml PBST) for 30 minutes. Cells were then incubated overnight at 4°C with diluted MAP2 primary antibody (1:1000 in PBST, Synaptic Systems 188 011, mouse) and Tau primary antibody (1:1000 in PBST, Synaptic Systems 314 004, guinea pig). After washing three times with PBST for 5 minutes each, cells were incubated for 2 hours at room temperature with diluted MAP2 secondary antibody (1:1000 in PBST, Goat anti-Mouse IgG Alexa Fluor 594, Thermo, A11005) and Tau secondary antibody (1:1000 in PBST, Goat anti-guinea pig Alexa Fluor 488, Thermo, A11073), along with DAPI staining solution (1:2000 diluted in PBS, Thermo, H1399). Following another three washes with PBST for 5 minutes each, the cells were left in PBST after the final wash. Cells at passage 5 were used for this analysis. Images were obtained via fluorescence microscopy (Olympus IX81) and annotated via Python.

A.3 ECM coatings assay

The following coating solutions were prepared: 1) Collagen Type I (10 μg/ml in sterile water) from 5 mg/ml, Collagen Type I, Rat Tail, Ibidi, item no. 50202, 2) Laminin (Sigma, L2020, diluted in PBS to 10 μg/ml), 3) Poly-L-Lysine (1 mg/ml) in sodium borate buffer; sodium borate buffer was prepared from boric acid (cat. no. B7660 Sigma, ~2 g), sodium tetraborate (cat. no. 221732, Sigma, ~3 g), Nanopure water (~500 ml) and PLL (MW 70,000 - 150,000, Sigma, cat. no. P1274, ~1 g). 150 μl of each coating solution was applied to each of 3 wells in a 48 well plate, and the well plate was incubated overnight at 4°C. Following this, wells were washed with sterile PBS 3x for 5 min each. Then 500 ul of 200,000 cells/ml solution in differentiation medium were seeded in triplicate in each of the pre-treated wells and 3 (-) control (uncoated) wells. ½ medium was changed every 48h. Cells were imaged, via phase contrast on d4 after seeding. Cells at passage 2 were used for this assay.

A.4 Microenviroments

A.4.1 Silanization

Based on[100]. Prior to 3D printing, glass coverslips (30 mm diameter, #1.5, 0.16-0.19 mm thickness, Epredia) were first silanized: coverslips were cleaned with isopropanol (CAS No. 67-63-0) using Kimtech wipes, followed by a cleaning with acetone (Honeywell, Cat. #32201-1L) and drying with a nitrogen or argon stream. Any residual film was removed with a Kimtech wipe, and dust fibers were cleared using a nitrogen or argon stream. Cleaned coverslips were then placed in a glass petri dish or metal holder and subjected to air plasma cleaning (O_2 gas, 200W, 30 min, ~0.5 mbar). Each coverslip was placed in its own chamber and individually submerged in anhydrous toluene (Sigma-Aldrich, Cat. No. 179418-2.5L), to which 4 mM 3-(trimethoxysilyl)propyl acrylate ("3-TMS", Sigma-Aldrich, Cat. No. 475149-25ML, CAS No. 4369-14-6) at 1:1000 v:v was added. The coverslips were then left on a shaker overnight at 240 rpm; the upward facing side was henceforward considered the silanized side. After silanization, the coverslips were placed in a Teflon holder. Coverslips were then dipped in each of two beakers of regular toluene and one beaker of acetone. Coverslips were then dried with a nitrogen or argon stream. If any residue remained on the coverslip, it was dipped in 99% ethanol and dried with gas again. Finally the silanized coverslips were baked at 80°C for 2 hours and stored under dry and dark conditions. Silanized coverslips were used within 2 weeks.

A.4.2 Microenvironment Preparation

The bottom of an Ibidi 35 mm petri dish (Ibidi #80806 or #81156) was removed. To the bottom/outside of the dish two component biocompatible glue (Picodent Eco-sil, #1300 6100) was applied and the 30 mm diameter coverslip (Epredia, #1.5) containing the structures was placed. A small reservoir was created by surrounding the structures with a PDMS (Sylgard 184, Dow Chemical) block where an 8 mm hole had been created with a biopsy punch. Biocompatible glue was used to adhere the PDMS to the glass. The petri dish, PDMS, and 3D printed microstructures were sterilized by spraying with 70% ethanol/water solution, then applying pen-strep (Pan Biotech, #P-6-07050) to the entire petri dish for 10 minutes. The pen-strep was removed by washing with PBS (remove 1/2 volume in each step), twice for 2 min each. A laminin solution (Sigma-Aldrich, #L2020, diluted in PBS to 10 μg/ml) was applied to the reservoir containing the structures and the petri dish was incubated overnight at 4°C. The following day, unbound laminin was removed with 2 PBS washing steps for 3 min each. Following this, a PC12 cell solution in differentiation medium was applied to the reservoir containing the structures. Additional RPMI 1640 was applied outside the reservoir to minimize evaporation.

A.4.3 Cell Seeding

Sterilized microenvironments were seeded with cells as follows: PC12 cells were suspended in differentiation medium as described above (Sec. A.1.2). 150-200 μl of the desired concentration of cells was applied to the PDMS-enclosed reservoir, filling the reservoir. ½ the volume of the culture medium was changed every 48 h. For specific cell seeding parameters used to obtain results presented in Proliferation and Cell Density (sec 4.11), Proliferation and Cell Density (sec 4.11), Path Lengths, All and Longest (sec 4.12), Effect of Confined Cell Count on Neurite Length (sec 4.13), Neurites Per Cell (sec 4.14), Real Time Cell Behavior (sec 4.15), please see table A.4.1. The number of technical repeats (with the number of controls) are indicated in each section. In the case of Real Time Cell Behavior (sec 4.15), a single technical repeat is sufficient to draw conclusions due to its high content (data was gathered for nine confinement structures every 30 minutes for 60 h). Cell passages 9-10 were used for all analyses.

Section	Parameter
Experimental Reliability (sec 4.10)	250 cells/mm^2
Proliferation and Cell Density (sec 4.11)	Sparse: 150 cells/mm^2 Intermediate and Dense: 250 cells/mm^2 Dense unconfined: ~1000 cells/mm^2
Path Lengths, All and Longest (sec 4.12)	150 cells/mm^2 250 cells/mm^2
Effect of Confined Cell Count on Neurite Length (sec 4.13)	150 cells/mm^2 250 cells/mm^2
Neurites Per Cell (sec 4.14)	150 cells/mm^2 250 cells/mm^2
Real Time Cell Behavior (sec 4.15)	150 cells/mm^2 in a single sample 9 structures analyzed Data collected every 30 minutes for 60 h

Table A.4.1: Experimental parameters and descriptions

A.4.4 Fluorescent Laminin Coating of 3D Printed Structures

Sterile PBS was cooled at 4°C for a minimum of 2 hours. 14 ml of cooled PBS was then added to a Slide-A-Lyzer Falcon tube under sterile conditions (Slide-A-Lyzer™ MINI Dialysis Devices, 3.5K MWCO, Thermo Cat. No. 88400). Two 500 μl aliquots of laminin (Sigma, L2020) were each applied to a Slide-A-Lyzer dialysis device, which were then placed in the Slide-A-Lyzer falcon tube and capped. Both falcon tubes were then stored at 4°C and PBS was replaced after 1 hour, 2 hours, and then prior to leaving overnight. This process was repeated a second time. Following dialysis, 100 μl of dialyzed laminin was diluted in 9.9 ml of sterile PBS, mixed, divided into 500 μl aliquots, then stored at -20°C. 50 μl of dialyzed laminin was reserved for labeling, 450 μl was stored at -20°C. Any remaining dialyzed laminin was stored separately at -20°C.

For labeling, 50 μl of dialyzed laminin was combined with a 50 μg vial of DyLight™ 550 NHS Ester (Thermo Cat. No. 62263) under sterile conditions, and the solution was incubated at 4°C for 2 days with gentle agitation twice daily. Labeled dialyzed laminin was then dialyzed in a fresh Slide-A-Lyzer™ device with pre-chilled PBS, following the same PBS change intervals as above, again for 2 days. The labeled dialyzed laminin was then combined with the 450 μl aliquot that was previously stored at -20°C to achieve a 1:9 labeled:unlabeled stock laminin solution. From this, a 10 μg/ml in PBS solution was prepared, with 500 µl aliquots stored at -20°C. Any remaining amount of 1:9 labeled:unlabeled stock laminin solution was stored at -20°C.

Fluorescent laminin was used to coat 3D printed microstructures in a manner similar to laminin described in sec. Microenvironment Preparation, A.4.2.

A.5 3D Printing

STL files were designed using Autodesk Inventor Professional 2023. Computer-Aided Design (CAD) models (STL files) of the structures were loaded into the DeScribe 2.6 software (Nanoscribe GmbH). The computer aided design structure was printed at 25X, NA = 0.8, Dip-in-lithography (DiLL mode) using a commercial laser direct writing device (Photonic Professional GT2, Nanoscribe GmbH) on a silanized 30 mm diameter coverslip (Epredia, #1.5). A laser power scaling factor of 100% (corresponding to ~66 mW) and a 50 mm/s printing speed were used as printing parameters. The structures were developed for 20 minutes in propylene glycol monomethyl ether acetate (PGMEA, Sigma-Aldrich, #484431-1L) followed by 2 minutes in isopropanol (Honeywell, Cat. 33539-2L). Structures are then stored in the dark at 4°C and used within two weeks.

While numerous printing parameters (e.g. laser power and writing speed) can be utilized to tune the Young's modulus of IP-Visio, Minnick et al. found that across a range of powers and speeds, the stiffness of IP-Visio was as low as ~40MPa and as high as ~280MPa[78]. These values are on the same order of magnitude as human bone (~100MPa)[101].

A.5.1 SEM

Samples were sputter-coated with an 80% gold, 20% palladium alloy (10 nm thickness layer, Leica ACE 600) and examined with a field-emission scanning electron microscope (JEOL JSM-7610F).

A.6 Raw Data Acquisition and Analysis

Each path (soma or neurite) was assigned a designation based on the definitions provided in section 4.7: edge cells were labeled as "edge," isolated cells as "free," and clustered cells as "other." The neurites associated with each cell were assigned the same designation. Additionally, each cell and its respective neurites were manually assigned a unique number. Both the unique number and the edge/free/other label were applied via the `Tag` → `Custom` dropdown menu in the Path Manager window and saved in the `PathName` column. The `PathID` value was automatically generated upon completion of a path (soma or neurite) in the image of interest. After compiling the paths for each cell, including somas and neurites, relevant details for each path were saved as outlined in table A.6.2. Data was collected via phase contrast microscopy and images were analyzed using SNT, a Fiji/ImageJ plug-in. Quantitative data obtained via

SNT was analyzed via Python. Further details about working with Fiji/SNT can be found in the online documentation: `https://imagej.net/plugins/snt/`; detailed information about swc files can be found here: `https://swc-specification.readthedocs.io/en/latest/swc.html#soma-representation`.

`Column Name`	**Description**
`PathID`	Unique identifier for each path.
`PathName`	The name or label assigned to each path.
`PathLength`	Length of the path.
`PathLengthUnits`	Units of measurement for path length.
`StartX`	Starting X coordinate of the path in 3D space.
`EndX`	Ending X coordinate of the path in 3D space.
`StartY`	Starting Y coordinate of the path in 3D space.
`EndY`	Ending Y coordinate of the path in 3D space.

Table A.6.2: CSV File Column Names and Their Descriptions (Restricted to those used for analysis herein).

A.7 Mann Whitney U test

The Mann-Whitney U test is a nonparametric statistical test that assesses whether there is a statistically significant difference between raw data belonging to independent groups. The Mann-Whitney U test was used to analyze the following datasets: 1) cell counts from three technical repeats, 2) median neurite lengths from independent groups of cells and 3) median neurite counts from independent groups of cells, therefore the requirement that the raw data being compared comes from independent datasets is satisfied. The Mann-Whitney U test works by ranking all the values from both groups together, from lowest to highest, and then comparing ranks rather than the raw data values themselves. Each value in the combined dataset is assigned a rank, and the test then sums the ranks for each group. Using rank sums removes any requirement that the data be normally distributed. More specifically, ranking data compares relative positions rather than raw values, eliminating the need for any assumption about how the data is distributed. The null hypothesis is that the rank sums do not differ significantly, while the alternative hypothesis is that the rank sums differ significantly. The Mann-Whitney U test is particularly useful when the data do not meet the assumptions of normality, as it does not rely on the assumption that the data follow a normal distribution. Relevant equations are provided below.

$$U_1 = R_1 - \frac{n_1(n_1+1)}{2} \tag{1}$$

$$U_2 = R_2 - \frac{n_2(n_2+1)}{2} \tag{2}$$

- U_1 and U_2 are the Mann-Whitney rank sum statistics for groups 1 and 2, respectively.
- R_1 and R_2 are the sums of ranks for groups 1 and 2, respectively.
- n_1 and n_2 are the sample sizes for groups 1 and 2, respectively.

$$U = \min(U_1, U_2) \tag{3}$$

$$E(U) = \frac{n_1 n_2}{2} \tag{4}$$

$$\sigma_U = \sqrt{\frac{n_1 n_2 (n_1 + n_2 + 1)}{12}} \tag{5}$$

$$Z = \frac{U - E(U)}{\sigma_U} \tag{6}$$

- U: The Mann-Whitney test statistic, representing the smaller of the two rank sum statistics.
- $E(U)$: Expected value of U.
- σ_U: Standard error of U.
- Z: Standardized test statistic for U, used to assess the significance of the test.

To find the p-value from Z:

- If the sample sizes n_1 and n_2 are large (typically $n_1, n_2 > 20$), the Z-value can be referenced directly against the standard normal distribution to obtain the p-value.
- For smaller sample sizes, a table of critical U-values for the Mann-Whitney test should be used to determine significance.

A.8 Use of Median and Confidence Interval

The median is a measure of central tendency that represents the middle value in a dataset when the values are ordered. When there is an odd number of data points, the median is the middle value; when there is an even number of data points, the median is the mean of the two middle values. Unlike the mean, the median is less affected by outliers, making it a useful indicator of the central point in skewed distributions.

A confidence interval (CI) provides a range of values within which the true population parameter, such as the median, will fall with a given level of confidence. For the median, calculating a confidence interval involves generating a distribution of medians through bootstrapping (described below): the original dataset is resampled (i.e. reconstructed) multiple times with replacement of a value immediately after it has been added to the resampled data set (this approach is commonly known as "resampling with replacement"). Next, a median is calculated for each resample. This process yields a set of medians that reflects the variability in an estimate of the population's true median. In a 95% confidence interval, the ranks within this set of medians which correspond to the 2.5% and 97.5% percentiles are then determined, representing the lower and upper bounds, respectively. For example, if 1,000 bootstrapped medians are generated, the lower bound rank is $0.025 \times 1000 = 25$ and the upper bound rank is $0.975 \times 1000 = 975$. The values at these positions in the sorted list of medians form the bounds of the 95% confidence interval around the median. This interval does not guarantee that the true population median lies within the bounds but rather reflects a 95% probability that it does, providing a measure of the reliability of our median estimate based on the sample data. Mathematical representations are as follows:

$$\mathrm{CI}_{\text{median}} = [X_L, X_U] \tag{7}$$

- X_L is the data value at the closest rank to $0.025 \times n$ and becomes the lower bound of the confidence interval,
- X_U is the data value at the closest rank to $0.975 \times n$ and becomes the upper bound of the confidence interval,
- n is the sample size.

If X_L or X_U do not fall on an exact data rank, they are approximated by selecting the closest ranked data points.

To enhance the calculation of confidence intervals, a technique called *bootstrapping* is used. Bootstrapping involves repeatedly resampling the data with replacement to create many "new" datasets of the same size from which we can estimate the desired parameter, such as the median. Each resample, in essence, provides a new view of the dataset, allowing us to observe how much the median varies across different random samples. The variation across these resampled medians then forms the basis for calculating a confidence interval, representing the range where the true population median is likely to lie.

A key aspect of bootstrapping is the number of *resamples*, which defines how many times the resampling process is repeated. More resamples generally provide a more stable and accurate estimate of the confidence interval, as it enables a more comprehensive exploration of possible sample variations. In each case in this investigation, 1,000 resamples were used to construct the interval.

Additionally, a *fixed random state* or seed value is often set to ensure that each run of the bootstrap calculation yields the same results. By using a fixed random state, the randomness of the resampling process is controlled, making the confidence interval reproducible. This is particularly valuable when verifying results or when consistency in the interval calculation is necessary across analyses. Overall, bootstrapping with multiple resamples and a fixed random state offers a robust approach to constructing confidence intervals for the median, especially when the data distribution is unknown or does not follow a typical normal distribution.

B Confined vs. External Neurite Lengths

In order to determine whether the neurite lengths observed by cells within the confinement structure are caused by virtue of the cells being confined, and not solely by any bias introduced into the experimental sample by the 3D printed confinement structure, cells both within the confinement structure and those external to the confinement structure were analyzed. Figure B.1 (i - iii) compares neurite lengths for cells under confinement and those external to the confinement structure. Median neurite lengths were measured for isolated, clustered, and edge labeled cells at 1 (i), 3 (ii), and 5 Days in Vitro (iii), with 95% confidence intervals provided in each case. A sample image (Fig. B.1, iv) highlights the distinction between confined and external cells: all cells outside the confinement structure can be given the same label (edge, isolated, clustered) as those within the confinement structure. Comparisons between confined and external cells, using the Mann-Whitney U test, consistently demonstrate shorter neurite lengths for isolated and clustered confined cells compared to their external counterparts ($p < 0.001$ for all days) with statistical significance. In addition, on days 1 and 5 in vitro, confined edge cells show shorter neurites with statistical significance (d1: $p < 0.01$, **; d5: $p < 0.001$, ***); on day 3 there is no statistically significant difference ("ns") between confined and external edge cells. These outcomes suggest that the observed suppression of neurite outgrowth can be attributed to the confinement imposed by the structure.

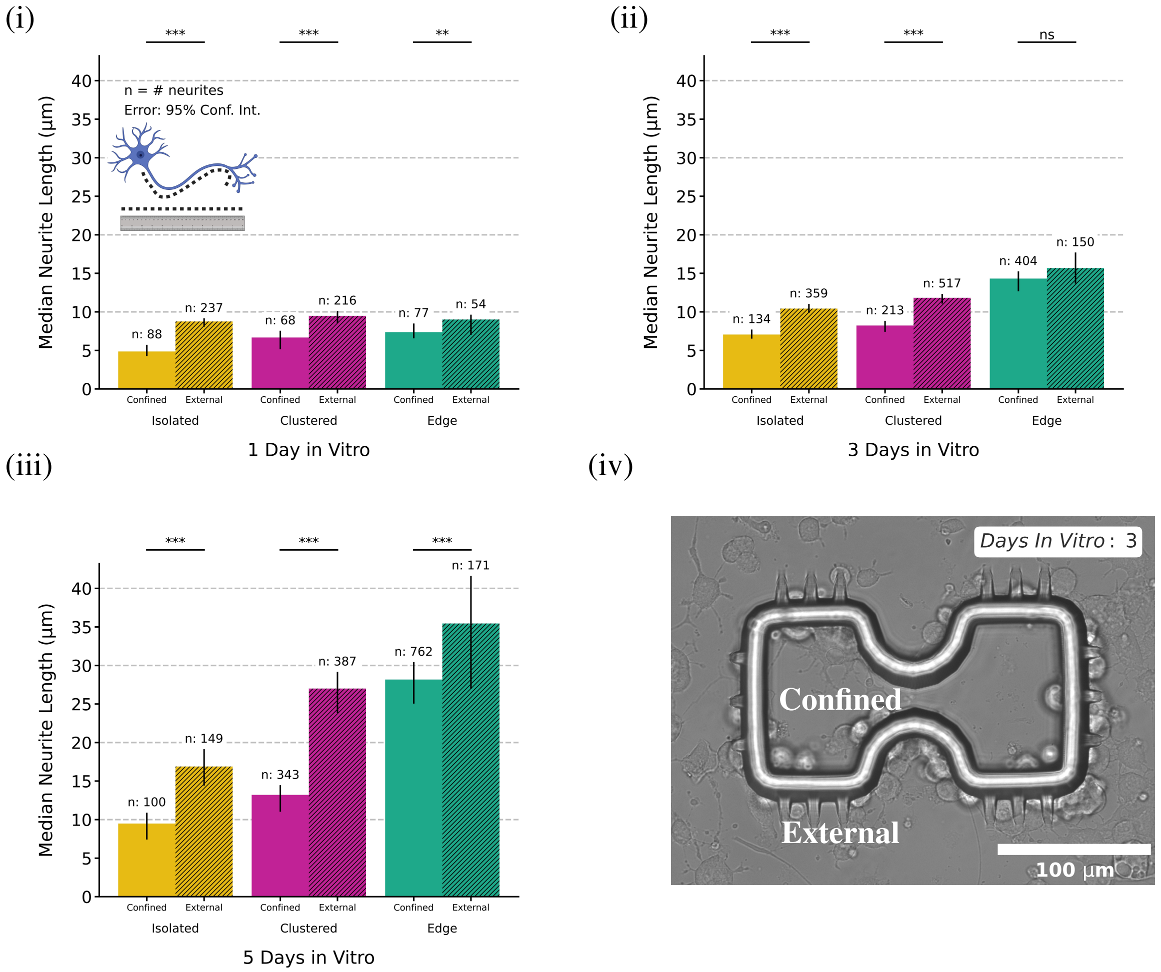

Figure B.1: Comparison of confined and external median neurite lengths for cell labels isolated, clustered and edge on 1 Day in Vitro (i), 3 Days in Vitro (ii), 5 Days in Vitro (iii), including a 95% confidence interval measurement in all cases, and a sample image indicating the locations of confined cells and external cells (iv). Confined-external pairs for all cell label groupings were compared using the Mann-Whitney U test. All plots on all days show a statistically significant difference for isolated confined-isolated unconfined and clustered confined-clustered unconfined ($p < 0.001$, denoted as ***). Edge confined-edge external comparisons are as follows: 1 Day in Vitro: $p < 0.01$, **; 3 Days in Vitro: ns; 5 Days in Vitro: $p < 0.001$, ***. Neuron graphic created in https://BioRender.com.

C Laminin Coating Heterogeneity

Fluorescence images and corresponding phase contrast images of two 3D printed hourglass structures coated with fluorescent laminin were obtained (Fig. C.1). While there are some fluorescent fragments observed in fig. C.1 (i), laminin does not appear to accumulate around the edge of the structure. Fig. C.1 (ii) at least suggests the structure and its surroundings otherwise contain few other particles which may cause autofluorescence. To perhaps capture greater detail, a second 3D printed structure was imaged both via fluorescence and phase contrast microscopy (Fig. C.1 (iii), (iv), respectively) and these images also do not show that laminin has accumulated at the structure edge; however some autofluorescence of foreign objects appears to have occurred. Outcomes demonstrated here could eliminate the possibility that the previously demonstrated PC12 preference for contact with the structure is explained by an abundance of laminin around the structure.

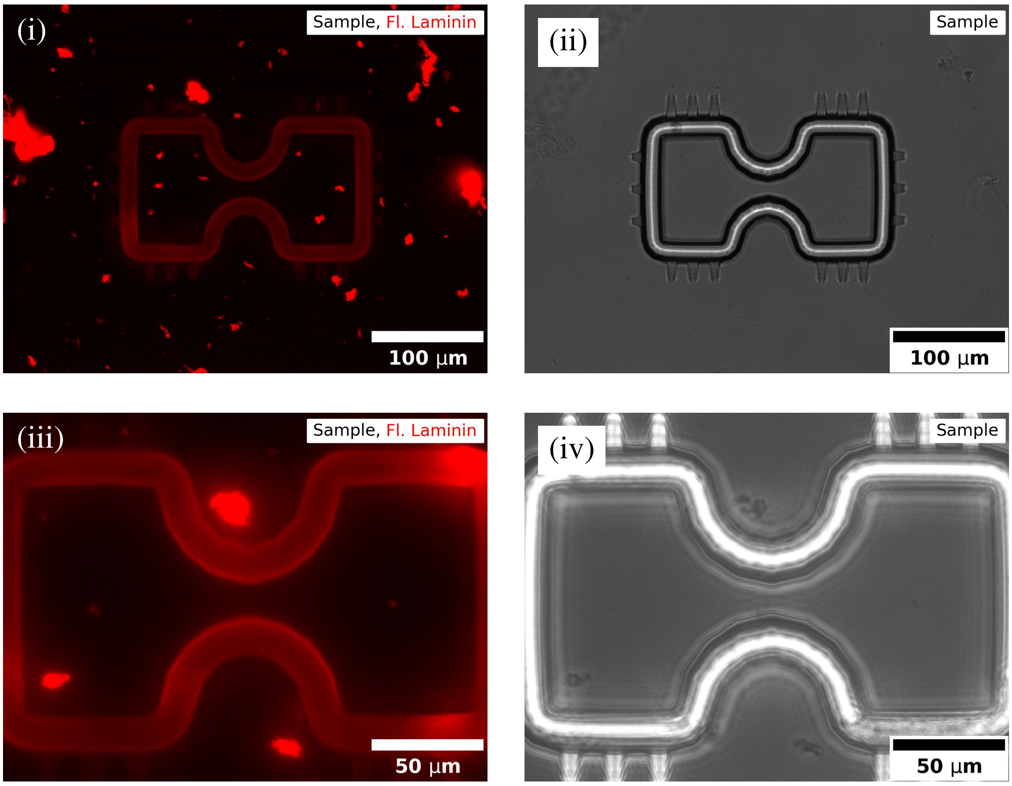

Figure C.1: Fluorescent image of a 3D-printed confinement structure after coating the surface and structure with fluorescent laminin (i), phase contrast image of the same structure (ii), fluorescent image of a second 3D-printed confinement structure after coating the surface and structure with fluorescent laminin (iii), phase contrast image of the second structure (iv). These images could eliminate the accumulation of laminin around the edge of the structure as a possible explanation for the demonstrated tendency of PC12 cells to seek or maintain contact with the structure.

Declaration of Independent Work and AI Assistance

This body of work was produced with the support of artificial intelligence (AI), namely Chat-GPT (version 3.5 and later). Chat GPT has been used here in the following ways: 1) to search for literature in multiple databases simultaneously, 2) to assist with the analysis of scientific literature via rapid summarization, 3) to teach Python and LateX, and guide the coding process by providing feedback on code and 4) assist with processing experimental data. Chat GPT's abilities and contributions were only used in a supportive role; at all times, the author remained the sole editor of all information appearing in this work.

Declaration

I hereby declare that I have written the submitted dissertation myself and have not used any sources or assistance other than those expressly designated by me. I hereby declare that I have not applied for an examination procedure at any other institution or that I have already used the dissertation in this or any other form elsewhere as an examination paper or submitted it to another faculty as a dissertation. I hereby declare that the dissertation may be checked for compliance with generally applicable scientific standards using electronic data processing programs.

Heidelberg, 8th May 2025

. . . .
Stephen L. Casale